BLIND PARAMETER ESTIMATION FOR DATA ACQUISITION IN DIGITAL COMMUNICATION SYSTEMS

A Dissertation

Presented to the Faculty of the Graduate School

of Cornell University

in Partial Fulfillment of the Requirements for the Degree of

Doctor of Philosophy

by

Wonzoo Chung

August 2002

BLIND PARAMETER ESTIMATION FOR DATA ACQUISITION IN DIGITAL COMMUNICATION SYSTEMS

Wonzoo Chung, Ph.D.

Cornell University 2002

This dissertation considers issues of blind parameter estimation for data acquisition in digital communication systems. Signal processing for data acquisition in digital communication systems mainly consists of synchronization, channel estimation, and equalization. While blind channel estimation and equalization techniques for linear modulation schemes have received intensive attention, neither blind (adaptive) synchronization for linear modulation nor blind equalization for non-linear modulation schemes have received nearly as much attention. We propose blind adaptive estimation schemes for several synchronization parameters for single and multi carrier systems, and study blind adaptive equalization for a particular non-linear modulation scheme.

The main approach we use in blind synchronization parameter estimation is dispersion minimization, which attempts to restore the dispersion free nature of the digital signals. We consider blind timing offset recovery based on dispersion minimization (chapter 2), carrier phase offset recovery based on dispersion minimization

(chapter 3), and carrier frequency offset recovery of multicarrier systems based on fourth power minimization as a variation of dispersion minimization (chapter 4). Due to the multimodality and the suboptimality of these approaches, performance analysis, for example, desirable and undesirable local minima, initialization strategies, and achieved MSE performance, is conducted for each application. Finally, the effect of a multipath channel on an FSK signal is analyzed and several blind adaptive schemes to mitigate the distortion due to a multipath channel are proposed.

Biographical Sketch

Wonzoo Chung was born in Seoul, Korea. He finished his B.S. in mathematics at Korea University, Seoul, Korea, and obtained Diplom Mathematiker at Universiät Regensburg, Germany in 1989 and 1992 respectively. Since 1997 he has been working toward the Ph.D degree in Electrical Engineering at Cornell University, Ithaca, NY, where he received M.S. degree at EE in 1999. His research interests are in the area of signal processing and digital communication.

To my fater,

Hongyoul Chung,

and

to my mother,

Youngsook Uie.

Acknowledgements

Like a tree, rooted in a ground, we stretch our hands towards mystical dark sky. Wind is coming and going, from gentle breeze to wild storm, swinging soul and body, and leaves us few choices but enjoying or enduring. Sometimes people call it fate, glowed by a single breeze and faded by a single chill. Here, if we could extend each of us from a tree to a forest, from a forest to millions of millions of forests, and far beyond, we might be able to see all joys and all sorrows of the world. There, we might be able to find holistic calmness, as they cancel out themselves and as we look down all the winds of the world as a wheel of cause and effect, extended from an isolated local tree. No need to say anything.

However, I am not there yet. With all the tides engraved in my heart, I would like to say about my debt of thank during 5 years at Cornell. This starts with my gratitude to the endless and limitless love and belief in me from my parents which have supported me during entire life.

First of all, I am truly thankful to the encounter with James (Prof. James P. Leblanc, currently with Lulea University of Technology, Sweden). At a branch point of life, I happened to meet a right person to open for me a trek reminding me of my nature. I hope I can do the same job for someone who lost in one's way someday.

Thanks to my colleagues, Raul Casas, Phil Schniter, Dornald Rick Brown, "Jai"

(Jaiganesh Balakrishnan, if you want to know his father's name too) Rick Martin, and finally Andy Klein, for letting and helping me develop and increase cultural capacity. Through the experiences with them I have lost something, which I no longer remember, and I have learned something, which I am so used now to not to be aware of. I enjoyed the fun with them which made possible such a perfect transition of mine as a cosmopolitan.

I am thankful to Prof. Lang Tong and Prof. Sheila Hemami for their time in reviewing this work and their helpful suggestions and encouragements. I want to express special thanks to Bill (Prof. William Sethares) for enlightening discussions, fierce arguments and helpful suggestions - not only about academic subjects. I am grateful for assistance from NSF Grant ECS-9811297, EEC-9872436, Applied Signal Technology, Fox Digital, Lucent Technologies, and NxtWave Communications. Thanks to beautiful Ithaca, your spring, summer, autumn, and winter. Lakes, maple trees, the willow tree in my backyard, nameless flowers and clouds I met, you gave me more than you think. Also, I deeply appreciate Dr. Justine Shin's support for my last year of Ph.D.

Finally, I thank my advisor Rick (Prof. C. Richard Johnson Jr.) for himself. Like a Zen master, the way he guided us was already educational enough for me and made my 5 years at Ithaca more than worthwhile; well guided enough to be confused again.

Table of Contents

List of Tables

List of Figures

Chapter 1

Introduction

1.1 Motivation

Driven by the digital revolution, the demand for being always connected at an ever higher data rate has accelerated recent dramatic growth of telecommunication systems. The analog communication systems of only a few decades ago have experienced a metamorphosis to sophisticated digital communication systems which use numerous modulation methods depending on the application and exploit various characters of digital communication signals resulting from intensive theoretical studies. Since the launch of the first digital cellular systems, currently expanding areas of digital communication systems can be categorized as: wireless internet over cellular systems (third generation cellular systems), digital broadcasting (such as high definition television (HDTV) and satellite radio), and "last mile" data communication technologies (ADSL, VDSL, wireless LAN, and emerging ultra wide band radio). In order to sustain a high data rate over harsh environments, these systems rely heavily on the power of digital signal processing. In fact, without the help of results in (adaptive) signal processing, the current achievements in modern communication systems would never have arrived this rapidly.

The first success was channel equalization. One of the main obstacles to data transmission is the frequency selective channel caused by multipath or other physical characteristics of the medium. Once the frequency selective channel is modelled as a time invariant linear impulse response, the problem is reduced to an identification and deconvolution problem. Existing techniques in adaptive signal processing such as Least Mean Squares (LMS) algorithm [Wid70] have been applied with great success [Luc65]. In order to avoid training sequences which are necessary for the LMS type algorithms but impede information rate, non data aided (blind) techniques to estimate or equalize the channel emerged [God80], [TA83], [TXK94]. Channel characterization has been applied for mobile environments and various estimation and equalization schemes based on diversity in the temporal domain (fractionally spaced equalization) [GW81], in the spatial domain (antenna array and SDMA [RFT98]), and in joint spatial-temporal space (space-time processing [PP97] and space-time coding [TSC98]) have been utilized. Another ground breaking application of digital signal processing for communication systems is multiuser detection [Ver86], which can be viewed as an extension of equalization to interference suppression in multiuser systems. Almost all possible combinations of the above digital processing methods have blossomed for various modulation schemes such as quadrature amplitude modulation (QAM), vestigial sideband (VSB), and orthogonal frequency division multiplexing (OFDM) in different multiuser access systems such as frequency division multiple access (FDMA), time division multiple access (TDMA), and code division multiple access (CDMA). Every available mathematical tool is deployed in order to push the performance as close to the theoretical limit of digital communication systems predicted by Shannon about five decades ago [Sha48].

However, unlike in the mathematical world, engineering in the real world is governed by another set of rules - economics, such as the law of diminishing returns [Sam70]. As gains due to the innovation from digital processing in the theoretical direction became saturated, several issues have risen that return attention to an old subject relatively overlooked by the digital processing community, namely the synchronization problems at the receiver front end where the digital segment meets the analog.

First of all, in order to satisfy both demands on higher data rate and spectral efficiency, accurate and robust synchronization becomes a critical prerequisite for further digital signal processing. Higher data rate under bandwidth constraints is usually achieved by a higher level constellation, bandwidth saving modulation schemes such as VSB, and reduction of training signals, which require acquisition of more optimized synchronization parameters. For example, the American standard for HDTV uses 8 to 16 level VSB signals with only 0.8% training sequences [Com00]. The receiver must operate under severe multipath channels with extremely long delay spread. In this system, conventional equalization schemes tolerating timing offset mismatch such as fractionally spaced equalization are not feasible due to excessive sample rate and equalization length. As a result, the equalization performance becomes highly sensitive to synchronization errors. Typically, blind equalization schemes implicitly assume reasonable synchronization performance, for which proper blind synchronization parameter estimation methods are required.

Secondly, the advent of OFDM systems has shifted the much of weight of receiver design from equalization to synchronization. OFDM systems transmit data over multiple carriers at different frequencies and simplify the equalizer structure by deploying a cyclic prefix at the cost of reduced data rate. Instead of inter symbol interface (ISI), OFDM systems must deal with loss of orthogonality of the subcarriers. Synchronization errors, especially frequency offset and phase noise, result in serious performance degradation to OFDM systems [PP99].

Finally, the need for low cost and highly integrated RF circuits creates a new task for digital signal processing in synchronization. Currently, analog components are the main obstacle for a cost effective receiver in comparison with the digital part which obeys Moore's law such that data density doubles each year. Recently, intensive research in the analog circuit community has been undertaken to improve this situation. Two remarkable approaches are architectural innovations driven by "homodyne" structures which directly convert radio frequency (RF) signals to baseband [Abi95], and inexpensive CMOS-based process technology for analog circuits [Abi99]. However, these cheaper and integrated solutions sacrifice the quality of RF processing and consequently require improved digital processing to compensate for the magnified analog impairments as well as provide more robust synchronization.

The desirable properties of synchronization algorithms to meet the requirements of these emerging challenges can be summarized as optimal (or accurate), robust (immune to distortions due to noise or time variation), and blind (non data aided). Blind synchronization not only increases the data rate, but also improves robustness, since reliable reference data is usually not feasible in the initial stage. The stance taken here is that adaptive blind estimation approaches, which have been studied intensively for channel estimation and equalization, would be good candidates for blind synchronization parameter estimation schemes.

This dissertation concerns blind parameter estimation issues in synchronization for QAM and OFDM systems and equalization for non-linearly modulated communication systems. The synchronization problem is treated as a blind adaptive parameter estimation problem, and existing blind adaptive approaches to linear equalization are modified for each synchronization parameter estimation problem. For the equalization issue in a non-linear modulation, the multipath effect on a non-linear modulation (Frequency Shift Keying) is modelled as a time varying linear channel, and blind adaptive equalization algorithms will be applied to mitigate the multipath effect.

1.2 Synchronization Review

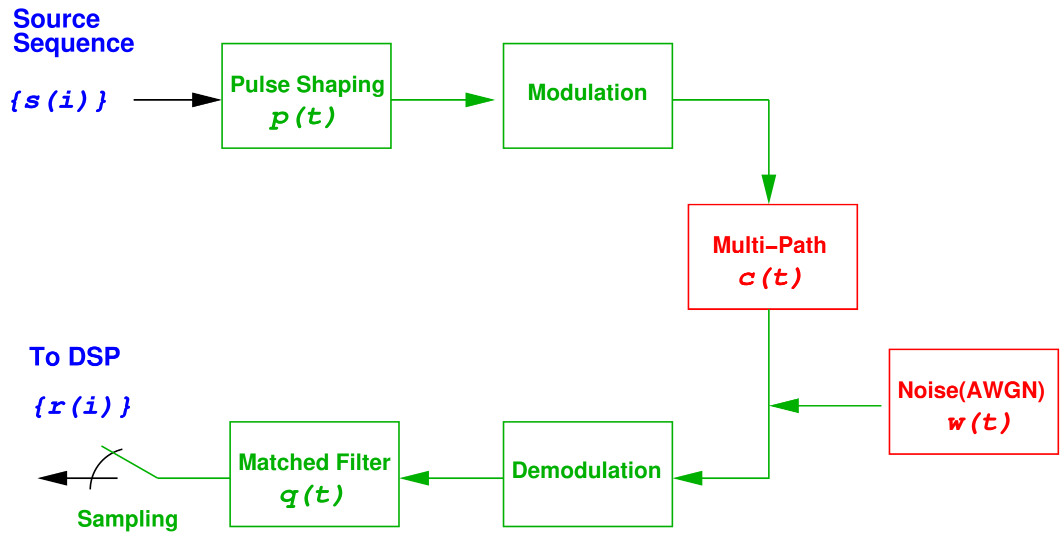

Figure 1.1: Communication system block diagram

In order to transmit digital data over an analog medium, an appropriate interface is needed. Synchronization concerns a proper (or optimal) interface match between the analog transmitter and the digital receiver. In this section we briefly review a linear modulation digital communication system focusing on significant synchronization parameters.

Consider a wireless communication system based on a linear modulation scheme as illustrated in Figure 1.1. As an example, we consider a quadrature amplitude modulation system. First, binary data are mapped to a complex number which is called a *symbol*, drawn from a finite set which is called a *constellation* or an *alphabet set*. Then, in each time duration T which is called the *symbol spacing* or *baud interval*, a particular pulse shape with different magnitude and phase corresponding to a symbol is generated. The train of pulses is modulated to radio frequency by multiplying with a high frequency sinusoid $\cos(2\pi f_c)$ where f_c is called the carrier frequency, and emitted through an antenna. As an electro-magnetic waveform, the radio frequency signal travels through air and is captured by a receiver.

The received signal is demodulated by $\cos(2\pi \hat{f}_c + \phi)$ and passed through a low pass filter (matched filter) which maximizes signal to noise ratio and is then sampled at $\hat{T} + \tau$. In the receiver, there are several problems to restore the transmitted symbols. First, although the carrier frequency f_c is known for most cases, the exact value of f_c is not attainable in general mainly due to implementation issues (imperfect oscillators). Since f_c is usually large, even a small difference between the exact carrier frequency f_c and the estimated one $\hat{f}_c$ can contribute significant distortion into the demodulated signals. Furthermore, since the modulator $\cos(2\pi f_c)$ and the demodulator $\cos(2\pi \hat{f}_c + \phi)$ are different physical entities, there is always an unknown phase offset ϕ. Similarly, in the sampling process, the exact sampling rate $1/T$ is not available in general, and is approximated by estimated sampling rate $1/\hat{T}$ with unknown timing offset τ. In the following we briefly summarize the effect of these parameter errors on the baseband signals.

- Carrier phase offset (ϕ) : For two dimensional constellations (such as QAM), carrier phase offsets cause a fixed rotation of the constellation proportional to ϕ, which impedes the decision process. For one dimensional constellations, carrier phase offset downgrades signal to noise ratio by weakening the signal component or introducing distortion (single side band case). This distortion can be modelled as a one tap channel, and proper modification of equalization techniques can be applied.

- Carrier frequency offset $(f_c - \hat{f}_c)$: In the presence of carrier frequency offset, a two dimensional constellation spins with a constant velocity proportional to the carrier frequency offset. One can view carrier frequency offset as a linearly time varying carrier phase offset. However, in an OFDM system the effect of carrier frequency offset is different from that of carrier phase offset, and degrades system performance seriously by destroying the orthogonality of the subcarriers.

- Timing phase offset (τ) : Since most communication systems are bandwidth constrained, the pulse conveying digital data has (theoretically) infinite time duration. Therefore, incorrect timing phase offset causes inter-symbol interference (ISI). Furthermore, excess bandwidth pulses are used in most systems for practical reasons. Proper timing should be set to minimize the undesirable effect of aliasing.

- Timing frequency offset $(1/T - 1/\hat{T})$: Timing frequency offset can be treated as a linearly time varying timing phase offset. Thus, tracking ability is required for a timing phase offset recovery algorithm.

In reality, due to the physical limitation of devices in both the receiver and transmitter, the described parameters possess a time varying nature as well as a random jitter driven by thermal noise. However, in this dissertation, we assume ideal circuitry so that synchronization problems can be characterized fully by the parameters described above. This simplifies synchronization into a set of deterministic estimation problems.

1.3 Methodology : Dispersion Minimization

Now consider the problem of estimating a parameter in communication systems in general. For an unknown deterministic parameter θ and an observation data vector $\mathbf{x}$, the optimal estimator, minimum variance unbiased (MVU) estimator, often cannot be found in practice, even if it exists and the probably density function (PDF) of $\mathbf{x}$ is known. As an alternative, maximum likelihood (ML) estimator can be used; this maximizes the parameterized PDF of $\mathbf{x}$ with respect to θ, $p(\mathbf{x};\theta)$, and is asymptotically optimal [Poo98]. However, in a communication system, the ML estimator is still extremely difficult to compute. Only for some simple cases, such as memoryless channels with additive white Gaussian noise, the ML estimator produces a manageable log likelihood function.

Mean Squared Error Criterion : On the other hand, given the signal processing benefits, the method of least squares (LS) is widely used and makes good physical sense for most problems of interest. Although no claims about optimality can be made, it is easy to implement and an adaptive solution is available. Figure 1.2 describes the generic scheme for a LS estimator. $s[n]$ denotes transmitted symbols which are considered purely deterministic. θ denotes the parameter of interest (which could be from the channel model or any of the synchronization parameters), and $f(\cdot,\theta)$ denotes the distortion function parameterized by θ (for example, for a channel parameter, $f(\cdot,\theta)$ denotes convolution with θ). The "perturbation" box represents the remaining impairments which the signal inevitably encounters during the transmission. It usually includes additive white Gaussian noise, non-linear

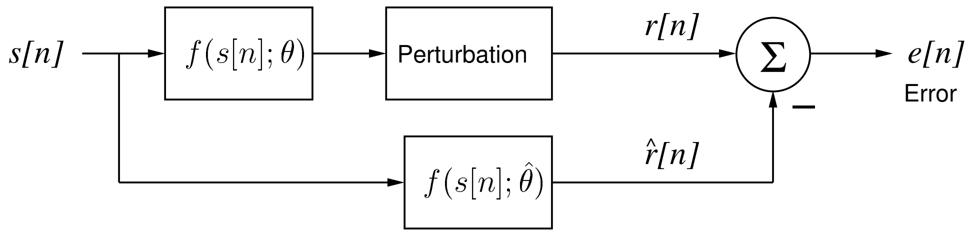

a) LS Estimation framework

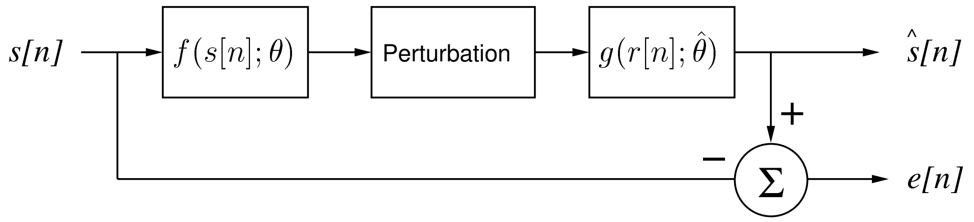

b) LS recovery framework

Figure 1.2: Least Squares Approach

distortions due to power amplifier, and multiplicative time-varying fading.

$r[n]$ is the received data in the presence of parameter θ. An estimate of θ is denoted by $\hat{\theta}$ and $\hat{r}[n]$ is data generated from $s[n]$, which depends on only $\hat{\theta}$. The least squares estimator (LSE) of θ chooses the $\hat{\theta}$ that makes $\hat{r}[n]$ close to the received data $r[n]$ in the LS error sense

$$\theta_{LS} = \arg\min_{\hat{\theta}} \sum_{n=0}^{N-1} |r[n] - \hat{r}[n]|^2, \tag{1.1}$$

where N is the size of the observed data. Once θ_{LS} is estimated, one can build a recovery device which undoes the effect of θ (as denoted by a function $g(\,\cdot\,;\hat{\theta})$ in Figure 1.2-b)) based on θ_{LS}. One can also apply the LS criterion to measure the performance of a recovery device. In this case one can view this estimation and recovery process as a one step process as depicted in Figure 1.2-b), where $g(\,\cdot\,;\hat{\theta})$

represents the recovery operation.

$$\theta_{LSS} = \arg\min_{\hat{\theta}} \sum_{n=0}^{N-1} |\hat{s}[n] - s[n]|^2 , \tag{1.2}$$

where θ_{LSS} can be called as a LS-solution. Instead of a finite size of observation data, one could you use infinite observation in order to obtain an "averaged" estimator over all possible $s[n]$. The resulting solution is called a minimum mean squared error (MMSE) estimator [Kay93], which is given by

$$\theta_{MMSE} = \arg\min_{\hat{\theta}} E\left\{|r[n] - \hat{r}[n]|^2\right\} , \tag{1.3}$$

Similarly, for the LS recovery scheme the MMSE solution is given by

$$\theta_{MMSES} = \arg\min_{\hat{\theta}} E\left\{|\hat{s}[n] - s[n]|^2\right\} . \tag{1.4}$$

The MMSE solution always exists and, furthermore, can be implemented in a simple adaptive algorithm (LMS) via stochastic gradient updates.

$$\theta_{k+1} = \theta_k - \mu \frac{\partial}{\partial\theta} |\hat{s}[n] - s[n]|^2 . \tag{1.5}$$

However, a significant drawback of the MMSE solution is that reference data is required in order to obtain the solution, e.g. in providing s to form $\hat{s} - s$ in (1.5). In the communication systems, a pseudo random sequence known to the receiver is periodically transmitted in order to train the equalizer, which results in degradation of the data rate.

Mean Dispersion Criterion : There is another approach which does not require reference data to obtain an estimate, although the solution might be less optimal in the MSE sense. The source signals in digital communication systems have a remarkable character in that they are drawn from a finite set of discrete elements. This property has not been exploited in the MMSE approach. Since each symbol is a point, in an ideal situation the received signal should not have any dispersion from the set of constellation points. In the presence of perturbations, minimization of dispersion can be used as a criterion to estimate a parameter. For example, for a constant modulus signal such as QPSK, $|s[n]|^2 = 1$, and we would want to choose $|\hat{s}[n]|^2$ to equal one as well. For QPSK, the minimum mean dispersion (MMD) solution is given by

$$\theta_{DM} = \arg\min_{\hat{\theta}} E\left\{ \left| |\hat{s}[n]|^2 - 1 \right|^2 \right\}. \tag{1.6}$$

This approach can be also extended for non constant modulus signals by penalizing the departure from the expected dispersion as $\gamma = E\left\{|s[n]|^4\right\} / E\left\{|s[n]|^2\right\}$. [JSE+98]

$$\theta_{DM} = \arg\min_{\hat{\theta}} E\left\{ \left| |\hat{s}[n]|^2 - \gamma \right|^2 \right\}. \tag{1.7}$$

This algorithm is not only blind but also can be implemented adaptively via a stochastic gradient algorithm,

$$\theta_{k+1} = \theta_k - \mu \frac{\partial}{\partial \theta} \left| |\hat{s}[n]|^2 - \gamma \right|^2. \tag{1.8}$$

This algorithm when applied for blind channel equalization is known as the Constant Modulus algorithm (CMA) [God80], [TA83], which is the most popular blind equalization in practice.

However, there are several drawbacks to this algorithm. First of all, the algorithm is inherently multimodal. Multimodality itself is not a vice, but the MMD solutions often show different performance and some of them might exhibit unacceptable performance. Second, even for the best solution among all MMD solutions, its MSE performance depends on the specific application. For the unconstrained linear estimation case (for example, fractionally spaced equalization), it has been shown that DM solutions are located near MMSE solutions so that DM solutions can be considered as good approximations of MMSE solutions [ZTJ98],[SJ00].

The multimodal nature of the DM approach typically necessitates application-dependent performance analysis. Characterization of the multimodal DM cost surface and the location of DM solutions are needed not only to justify the DM approach for a particular application, but also to provide a proper initialization strategy, assuring convergence to a local minimum with acceptable performance.

1.4 Outline of thesis

The signal processing for data acquisition in digital communication systems mainly consists of synchronization and channel estimation and equalization. While blind channel estimation and blind equalization techniques for linear modulation schemes have gained intensive attention, neither blind (adaptive) synchronization for linear modulation nor blind equalization for non-linear modulation schemes have received nearly as much attention. This dissertation focuses on blind adaptive synchronization parameter estimation for linearly modulated single carrier signals and OFDM signals, and blind adaptive equalization for a particular non-linear modulation scheme.

Chapter two considers blind timing phase offset recovery. Timing phase offset estimation issues with respect to minimizing the MSE of an equalizer output are introduced. A dispersion minimization algorithm is proposed as an approximation of MMSE timing offset in the presence of a one tap equalizer. The analysis of the dispersion minimization timing offset is conducted and its MSE performance is investigated. Part of this work has been published in [CBSJ01].

In chapter three, the performance of a blind adaptive approach for carrier phase offset recovery is investigated. The algorithm is based on minimization of dispersion of the projection of the real (or imaginary) part of the complex baseband signal. The stationary points of this algorithm are studied for a variety of source signals including digital VSB and QAM. Analysis of the performance and behavior of the algorithm in the realistic situation dealing with ISI or statistical dependencies between the in-phase and quadrature components is presented. The content of chapter three has been presented in [CSJ00].

In chapter four, a carrier frequency offset correction scheme for OFDM systems based on fourth order statistics is presented. The algorithm is developed to overcome the drawback of most existing blind carrier frequency offset recovery algorithms: the channel dependency of the performance. The condition that the global convergence of this algorithm to a unimodal solution is guaranteed is derived and most realistic OFDM systems are shown to satisfy the condition. Connections to other approaches such as Maximum Likelihood(ML) approximation and the Constant Modulus Algorithm (CMA), are presented. This work has been published as [CJ02].

In chapter five, we address issues in the equalization of non-linearly modulated signals (FSK) in the presence of a multipath channel. The effect of a multipath channel on FSK signals is modelled as a time-varying convolution, in contrast to the time invariant convolution multipath model in the linear modulation systems. We consider blind adaptive schemes in order to mitigate the distortion due to time varying channels in an average sense. The contents of chapter five have been published in [CMRJ00] and [CJR02].

Chapter six summarizes the result in this thesis and briefly discuss further extensions of this study.

1.5 Terminology and definitions

1.5.1 ℓ_p norm in a vector space

Here, we avoid rigorous definition of a norm in a vector space V, and introduce the ℓ_p and ℓ_∞ norms as a definition of notation.

- ℓ_p norm : For a given a vector $\mathbf{x}$ in a vector space V, the ℓ_p norm of $\mathbf{x}$, denoted by $\|\mathbf{x}\|_p$ is given by

$$\|\mathbf{x}\|_p = \sqrt[p]{\sum_k x_k^p} \tag{1.9}$$

- ℓ_∞ norm: Defined as a limit of ℓ_p, i.e.

$$\|\mathbf{x}\|_\infty = \lim_{p \to \infty} \|\mathbf{x}\|_p. \tag{1.10}$$

When the dimension of V is not finite, the ℓ_p norm does not exist; in other words, $\|\mathbf{x}\|_p$ can be unbounded for some $\mathbf{x} \in V$. In this dissertation, we assume that in the signal space we consider the ℓ_p norm (including the ℓ_∞ norm) always exists for all p. The most interesting ℓ_p norms for us are, the ℓ_2 norm, and the ℓ_4 norm and the ℓ_∞ norm. Specially, for the ℓ_2 norm we denote without subscript:

$$\|\mathbf{x}\| = \|\mathbf{x}\|_2. \tag{1.11}$$

Furthermore, for the ℓ_∞ norm

$$\|\mathbf{x}\|_\infty = \max\{|x_i|\}. \tag{1.12}$$

1.5.2 Kurtosis of a random variable

Consider a zero mean random variable s, i.e. $E\{s\} = 0$. *Kurtosis* is a normalized form of the fourth central moment of a distribution, which denotes the degree of peakedness of a distribution, also called the "excess" or "excess coefficient."

It has been shown that the kurtosis plays an important role in blind identification/equalization schemes based on higher-order statistics [BGR80],[Don81]. There are several definitions of kurtosis commonly encountered, including *Pearson kurtosis* (denoted by κ_s) and *Fisher kurtosis* (denoted by η_s) [AS72]. In this dissertation, the term "kurtosis" is taken to refer to the Pearson kurtosis.

- Kurtosis (Pearson Kurtosis)

$$\kappa_s = \frac{E\left\{|s|^4\right\}}{(E\left\{|s|^2\right\})^2}. \tag{1.13}$$

The kurtosis of a Gaussian random variable w is given by

$$\kappa_w = \begin{cases} 3 & \text{when } \{w\} \text{ is real} \\ 2 & \text{when } \{w\} \text{ is circular complex} \end{cases} \tag{1.14}$$

Fisher kurtosis is defined by the deviation from the Gaussian kurtosis, i.e.

- Fisher kurtosis

$$\eta_s = \kappa_s - \kappa_w. \tag{1.15}$$

A distribution with a high peak is called *leptokurtic* ($\eta_s > 0$), a flat-topped curve is called *platykurtic* ($\eta_s < 0$), and the normal distribution is called *mesokurtic* ($\eta_s = 0$). Since platykurtic is energy efficient, all communication source symbols are platykurtic. Table 1.1 lists kurtoses for a number of distributions.

1.5.3 Kurtosis of a vector

One can extend the concept of kurtosis defined for a random variable to a vector $\mathbf{x}$ in order to obtain a measure of the peakedness of the magnitudes of the vector taps.

Table 1.1: Kurtosis for selected distributions

Distribution	Pearson kurtosis κ_s	Fisher kurtosis η_s
Real Gaussian	3	0
Complex Gaussian	2	0
Binomial	$\frac{3pq(N-2)+1}{Npq}$	$\frac{1-6pq}{Npq}$
Exponential ($\lambda e^{-\lambda x}$)	9	6
BPSK	1	-2
8-PAM	1.76	-1.24
QPSK	1	-2
16-QAM	1.32	-1.68

- Kurtosis of a vector

$$\kappa_{\mathbf{x}} := \frac{\|\mathbf{x}\|_4^4}{\|\mathbf{x}\|^4}, \tag{1.16}$$

where $\|\cdot\|_4$ is the ℓ_4-norm defined as

$$\|\mathbf{x}\|_4 = \sqrt[4]{\sum_i |x_i|^4}. \tag{1.17}$$

The second moment and the fourth moment in the definition of kurtosis for a random variable in (1.13) are replaced by ℓ_2 norm and ℓ_4 norm respectively in (1.16). The following properties of the kurtosis of a finite length vector $\mathbf{x}$ show that $\kappa_{\mathbf{x}}$ represents the peakedness of $\mathbf{x}$.

i) Kurtosis of a vector is invariant under scalar multiplication

$$\kappa_{\mathbf{x}} = \kappa_{\alpha\mathbf{x}}. \tag{1.18}$$

ii) Kurtosis of a vector is upper bounded by 1 and lower bounded by $1/N$, where

N is the length of $\mathbf{x}$.

$$\frac{1}{N} \leq \kappa_{\mathbf{x}} \leq 1. \tag{1.19}$$

iii) $\kappa_{\mathbf{x}}$ has the maximum of 1 when $N-1$ of the N entries are zero and the minimum $1/N$ when all N entries have the same absolute value

Proof of *i)* is straightforward from the definition. Proof of *ii)* can be drawn from *iii)*. The proof of *iii)* is as the follow.

Suppose $\mathbf{x}$ is length N vector. Since $\kappa_{\mathbf{x}} = \kappa_{\alpha\mathbf{x}}$ for $\alpha > 0$, it is sufficient to find minima and maxima for $\|\mathbf{x}\|^2 = 1$. This is equivalent to finding minima and maxima of $\|\mathbf{x}\|_4^4$ under the constraint of $\|\mathbf{x}\|^2 = 1$. According to the Lagrange Multipliers method [TF88], the solutions of the following equation are the stationary points.

$$\frac{\partial}{\partial \mathbf{x}}\|\mathbf{x}\|_4^4 = \lambda \frac{\partial}{\partial \mathbf{x}}(\|\mathbf{x}\|_2^2 - 1) \tag{1.20}$$

$$\Rightarrow 2x_i(2\left|x_i\right|^2 - \lambda) = 0, \text{ for } \forall i. \tag{1.21}$$

This implies that all the stationary points have the form that the nonzero components have the same absolute value $\sqrt{\lambda/2}$. For a stationary point with M nonzero entries ($1 \leq M \leq N$), λ is given by $2/M$ from $\|\mathbf{x}\|^2 = 1$. Therefore, the kurtosis for a stationary point with M nonzero entries, $\mathbf{x}(M)$, is given by

$$\kappa_{\mathbf{x}(M)} = 1/M, \text{ for } M = 1, ..., N. \tag{1.22}$$

Thus, the maxima occurs when $M = 1$ and the minima occurs when $M = N$ ■

Figure 1.3 plots $\kappa_{\mathbf{x}}$ over 2-dimensional $\mathbf{x} = [x_1 \ x_2]^T$ on the unit circle S^1. For this 2-dimensional case one can clearly observe the relation between peakedness of $\mathbf{x}$ and $\kappa_{\mathbf{x}}$.

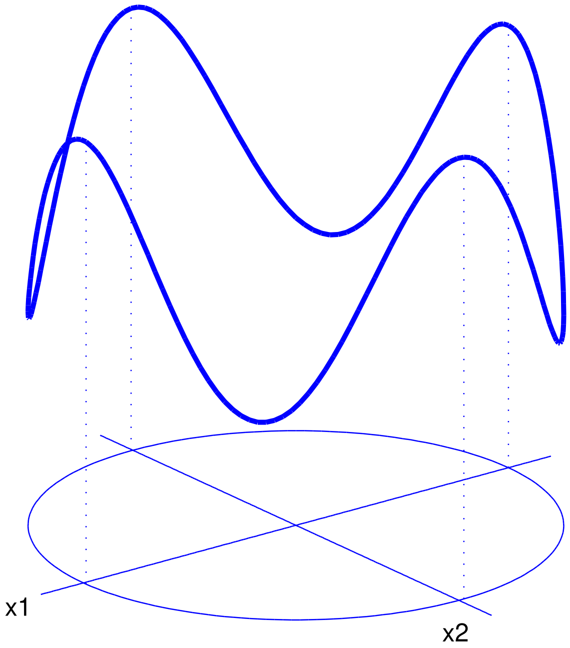

Figure 1.3: Kurtosis of $\mathbf{x}$ for $\mathbf{x} \in S^1$

Chapter 2

Timing phase offset recovery based on dispersion minimization

This chapter mainly concerns a timing phase offset recovery scheme which attempts to optimize the equalizer output MSE when the equalizer length is shorter than the ideal length. This timing offset estimation approach can be applied for jointly estimating timing offset and combining weights for multi-sensor systems. Among the existing timing recovery schemes, few are designed for optimizing equalizer output MSE and there is no blind scheme designed for a relatively short equalizer length. The proposed algorithm based on dispersion minimization is designed to minimize the MSE of a one tap equalizer output and exhibits reasonable performance for relatively short equalizers. The condition for unimodality of this algorithm for a single sensor system is investigated by studying its cost function. A geometric relationship between MMSE timing offset for a one tap equalizer and dispersion minimization timing offset is revealed. A heuristic argument for the MSE performance of the DM-timing is given.

2.1 Introduction

In most digital communication systems, digital sources are conveyed via excess bandwidth analog pulses which are designed to prevent aliasing from the sampled signals for a proper sampling offset in the absence of a multipath channel (Nyquist Criterion [Pro95]). Due to aliasing, the performance of the receiver with a symbol spaced equalizer is sensitive to the sampling offset, especially in the presence of multipath where the sampling offset perfectly eradicating aliasing does not exist in general. Furthermore, for the scenarios where multi-sensor outputs are combined in order to increase SNR, a proper sampling offset for each sensor can contribute to significant performance improvement [GLS96]. In both cases, estimation of an optimal timing offset is an important task, but the criterion for "optimality" is not obvious when timing offsets are determined in the synchronization stage. A natural approach is to minimize overall MSE performance of the detection device input, i.e. the MSE of a MMSE equalizer output [Kob71]. However, unfortunately, direct estimation of the timing offset minimizing overall MSE requires knowledge of the analog channel, in addition to the high computational complexity. Adaptive approaches based on training sequences or decisions from detection devices can be considered instead of direct computation, but coupling of timing offset and equalizer updates are considered undesirable for various reasons [God78]. Furthermore, since reliable reference or decision data might not be available in the initial acquisition, estimation of synchronization parameters such as timing offset could benefit from blind (non data aided) methods. On the other hand, in order to avoid the sensitivity of sampling offset in symbol spaced processing, sampling above the Nyquist rate of the analog pulses (so called fractionally sampling) has been proposed [GW81]. However, fractionally spaced sampling and equalization is not always feasible, especially when the additional hardware resource requirement cannot be met in practical situations. For example, in digital audio/video broadcasting the signals are often transmitted over a channel with delay spread too long to be equalized with a fractionally spaced equalizer with a restricted number of taps [Sch95]. Therefore, a desirable timing offset estimation scheme for a symbol spaced receiver would i) be blind, ii) not rely on equalizer output, and, at the same time, iii) optimize the MSE of the equalizer output.

Among the existing popular schemes for timing phase offset recovery, the output energy maximization (OEM) method is the one closest to satisfying the above three conditions. The algorithm finds a timing which maximizes the sampler output energy and consequently maximizes SNR. In [God78], it was shown that maximizing SNR is approximately equivalent to minimizing overall MSE of a receiver equipped with an infinite length equalizer. However, in practice equalizer length is usually shorter than the channel length and hence SNR maximization does not always agree with MSE minimization for a finite equalizer. Another blind approach in timing offset estimation schemes which do not rely on the equalizer output is to minimize dispersion of the sampler output signals. In [GLS96], Guglielmi et al. considered a dispersion minimization approach to jointly optimize the combiner weights and timing offsets of a pair of received signals from two sensors. Recently, for a single sensor case determining timing offset via dispersion minimization has been proposed in [CBSJ01].

In this chapter we study the dispersion minimization approach for timing recovery and focus on its MSE performance.

2.2 Problem Description

In this section we review the problem of timing offset in digital communication systems. Consider a digital baseband communication system in Figure 2.1, where the digital sources $\{s_i\}$ drawn from a finite alphabet set are converted to an analog signal $s(t)$ by convolving with the pulse shape function $g_T(t)$

$$s(t) = \sum_{i=-\infty}^{\infty} s_i g_T(t - iT), \tag{2.1}$$

where T is referred to as the symbol period. For practical reasons, the pulse g_T has excess bandwidth (i.e. the maximum frequency in g_T is larger than $1/T$), but, designed under the Nyquist pulse criterion[Pro95], it does not cause aliasing in the absence of timing offset and a multipath channel. In practice, the transmitted signal is subject to distortion due to multipath and noise. The multipath is characterized by a finite impulse response $m(t)$,

$$m(t) = \sum_{i=0}^{N-1} \rho_i \delta(t - \tau_i), \tag{2.2}$$

where τ_i and ρ_i denote the delay and the complex path gain of the i-th path, respectively. The noise is modelled as a wide sense stationary (w.s.s.) additive white Gaussian process $w(t)$ with variance σ_w^2 which is uncorrelated with the signal $s(t)$. At the receiver, the received signal is processed by a matched filter, $g_R(t)$, and the matched filter output $r(t)$ can be written as

$$r(t) = \sum_{i=-\infty}^{\infty} s_i c(t - iT) + w(t) \star g_R(t), \tag{2.3}$$

by defining an analog channel $c(t)$ by

$$c(t) = g_T(t) \star m(t) \star g_R(t), \tag{2.4}$$

where $\star$ denotes the convolution operator. The matched filter output is sampled

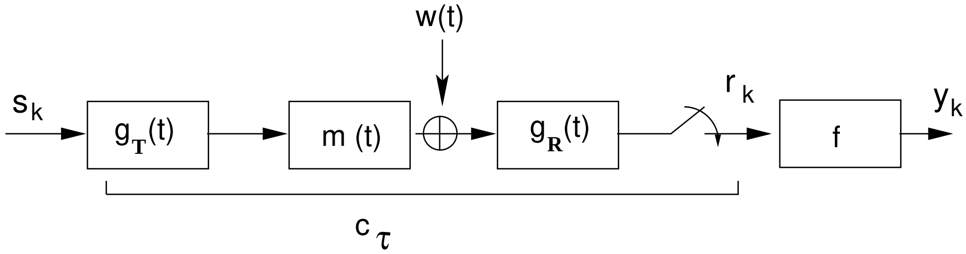

Figure 2.1: Digital Communication Systems Model

at the symbol rate $1/T$ with a timing offset τ $(0 \leq \tau < T)$.

$$r(kT+\tau) = \sum_{i=-\infty}^{\infty} s_i c((k-i)T+\tau) + w(t) \star g_R(t)|_{t=kT+\tau}. \tag{2.5}$$

Now, let us examine the effect of the timing offset on the sampled signals. Assume that $g_R(t)$ is symmetric $(g_R(t) = g_R(-t))$ and $g_R \star g_R$ satisfies the Nyquist pulse criterion (for example, a square root raised cosine filter [Pro95]). Then, the noise component $\{w(t) \star g_R(t)|_{t=kT+\tau}\}$, denoted by $\{w[k]\}$, is again a white Gaussian process with variance σ_w^2 independent from the choice of τ as shown in the following:

$$\begin{aligned} E\{w[k]w[k']\} &= \int_{-\infty}^{\infty}\int_{-\infty}^{\infty} g_R(kT+\tau-x)g_R(k'T+\tau-y)w(x)w(y)dxdy && (2.6)\\ &= \sigma_w^2 \int_{-\infty}^{\infty} g_R(kT+\tau-x)g_R(k'T+\tau-x)dx && (2.7)\\ &= \sigma_w^2 g_R \star g_R((k-k')T) = \sigma_w^2 \delta(k-k'). && (2.8)\end{aligned}$$

On the other hand, the signal component is dependent on the timing offset. By defining the sampled channel with respect to the sampling offset τ as a vector c_τ, i.e.

$$\mathrm{c}_\tau[k] := c(kT+\tau), \tag{2.9}$$

the sampled output can be written in a vector form

$$\mathrm{r} = \mathrm{c}_\tau \star \mathrm{s} + \mathrm{w}, \tag{2.10}$$

where s is a vector of the digital source data $\{s_i\}$. In the absence of multipath, $c_\tau[k]$ is given by

$$c_\tau[k] = g_T \star g_R(kT + \tau) = \delta(k + \tau), \tag{2.11}$$

and thus the correct timing offset $\tau = 0$ perfectly restores the digital data $\{s_k\}$. In the presence of multipath, c_τ cannot be reduced to a single non-zero tap in general. Furthermore, the aliasing due to excess bandwidth of $g_T \star g_R$ can deepen the spectral null of the sampled channel c_τ depending on the timing offset τ [Lyo75]. In this case, a timing offset determines a discrete time channel, and equalizer performance is limited by the resulting channel. Thus, timing offset in the presence of multipath should be determined jointly with the equalizer.

Consider a MMSE equalizer f_τ for a given channel c_τ with respect to a given timing τ. The optimal timing offset τ_{opt} is to minimize the MSE of the equalizer f_τ output, $y(\tau)$, in the presence of multipath channel, i.e.,

$$\tau_{opt} = \arg\min_\tau E\left\{(y_k(\tau) - s_k)^2\right\}. \tag{2.12}$$

This definition of timing offset optimality can be applied for a problem of combining multisensor inputs as illustrated in Figure 2.2. For an N antenna system, let $c^k_{\tau_k}$ be the sampled channel with respect to the sampling offset τ_k of the analog channel corresponding to the k-th antenna. The equalizer input is the sum of each sensor output multiplied by combining weight β_k, i.e.

$$r = \sum_{k=0}^{N-1} \beta_k c^k_{\tau_k} \star s + \sum_{k=0}^{N-1} \beta_k w_k, \tag{2.13}$$

where w_k is sampled noise from the k-th antenna. We assume $\{w_k\}$ are identically independent white Gaussian random variables with variance σ_w^2, and uncorrelated with the source s. In this case, the optimal timing offsets $\tau_0, ...\tau_{N-1}$ and combining weights $\beta_0, ..., \beta_{N-1}$ can be determined to minimize the MSE of the equalizer output y. By defining $\xi = (\tau_0, ..., \tau_{N-1}, \beta_0, ..., \beta_{N-1})$ as a vector of timing offsets and combining weights, and denoting the normalized resulting channel as

$$\mathrm{c}_\xi = \frac{1}{\sqrt{\sum_{l=0}^{N-1} \beta_l^2}} \sum_{k=0}^{N-1} \beta_k \mathrm{c}_{\tau_k}^k, \tag{2.14}$$

we have the same optimization problem for the multisensor combiner problem

$$\xi_{opt} = \arg\min_{\xi} E\left\{(y_k(\xi) - s_k)^2\right\}. \tag{2.15}$$

In this form, determining optimal timing offset or timing offsets and combining weights can be considered as a non-linear quadratic optimization problem over the channel vectors under a constraint imposed by the parameter $\{\tau\}$ or $\{\xi\}$. The difficulty of solving this problem is that the non-linear relation between the parameter τ (ξ) and the resulting channel c_τ (c_ξ) is extremely complicated. In the next section we will investigate the cost functions in (2.12) and (2.15) in more detail.

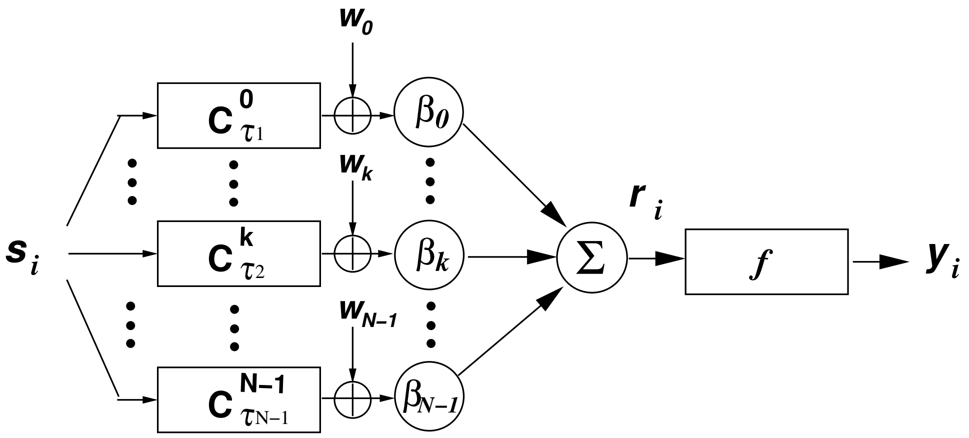

Figure 2.2: Timing offsets and combining weights for a multisensor combiner

2.3 Linear Equalizer output MSE and Timing

In this section we confine the equalizer $\mathbf{f}$ to be a linear equalizer. The output MSE of the MMSE linear equalizer for a particular timing offset τ will be written in terms of τ. We consider timing offsets for two extreme cases, a one tap equalizer and an infinite length equalizer, and numerically compare their performance for a finite length equalizer.

First, consider an N_f-tap MMSE linear equalizer $\mathbf{f}$ and its MSE. In order to deal with an infinite impulse response channel, we represent signals in the frequency domain. $C(\omega,\tau)$, $F(\omega)$, and $N(\omega)$ denote the frequency domain representation of the discrete time domain channel c_τ, the equalizer $\mathbf{f}$, and the noise $\{w(k)\}$ respectively. Setting $\lambda = \sigma_w^2/\sigma_s^2$ and assuming $\sigma_s^2 = 1$, the MMSE linear equalizer of length N_f for a given system delay d and timing offset τ is given by

$$\mathbf{f}_{MMSE} = (\mathbf{R}(\tau) + \lambda I)^{-1}\mathbf{p}(\tau), \tag{2.16}$$

where λ denotes noise to signal ratio (σ_w^2/σ_s^2) and the $N_f \times N_f$ matrix $R(\tau)$ and $N_f \times 1$ vector $\mathbf{p}(\tau)$ are given by

$$\mathbf{R}_{l,m}(\tau) = \frac{1}{2\pi}\int_{-\pi}^{\pi} |C(\omega,\tau)|^2 e^{-j(l-m)\omega} d\omega \tag{2.17}$$

$$\mathbf{p}(\tau) = [\mathrm{c}_\tau[0] \cdots \mathrm{c}_\tau[N_f - 1]]^H. \tag{2.18}$$

The minimum MSE of the equalizer output for length N_f is the MSE associated with $\mathbf{f}_{MMSE}$, and given by

$$MMSE(d,\tau,N_f) = 1 - \mathbf{p}(\tau)^H (R(\tau) + \lambda I)^{-1}\mathbf{p}(\tau). \tag{2.19}$$

In general, it is hard to express the MMSE in terms of τ in a closed form and to find a closed solution τ_{opt} which minimizes MMSE. Therefore, we consider two tractable extreme cases, $N_f = 1$ and $N_f = \infty$. From (2.16), we have

$$MMSE(d, \tau, N_f = 1) = 1 - \frac{|c[d]|^2}{||c_\tau||^2 + \lambda}, \tag{2.20}$$

$$MMSE(d, \tau, N_f = \infty) = \frac{1}{2\pi}\int_{-\pi}^{\pi} \frac{\lambda}{|C(\omega, \tau)|^2 + \lambda} d\omega. \tag{2.21}$$

(detailed derivation can be found in [Maz75].) Notice that in (2.21) the MMSE for an infinite length equalizer is in fact independent from the choice of the system delay d.

Similarly, for a decision feedback equalizer (DFE) one can derive a similar MMSE equation in terms of τ. For a DFE with finite length feed forward filter and feedback filter, the attainable MMSE in a closed form is hard to compute. When an infinite length feedback filter is assumed, the MMSE can be expressed in a relatively simple form for feed forward filter lengths $N_f = 1$ and $N_f = \infty$, as appeared in [Ari92] and [Sal73]

$$MMSE(d, \tau, N_f = 1) = 1 - \frac{|c[d]|^2}{\sum_{k=-\infty}^{d-1} |c[k]|^2 + \lambda}, \tag{2.22}$$

$$MMSE(d, \tau, N_f = \infty) = \exp\left\{\frac{1}{2\pi}\int_{-\pi}^{\pi} \ln \frac{\lambda}{|C(\omega, \tau)|^2 + \lambda} d\omega\right\}. \tag{2.23}$$

The similarity of MMSE formulas for the linear equalizer ((2.20), (2.21)) and the DFE ((2.22), (2.23)) suggest that the optimal timing for a MMSE linear equalizer can be used for a MMSE DFE without much loss in performance.

Now, we focus on the timing offset for a one tap linear equalizer. Since the delay term d appears only in $c_\tau[d]$ in $MMSE(d, \tau, N_f = 1)$, the attainable minimum MMSE with respect to the d is given by

$$\begin{aligned} MMSE(\tau, N_f = 1) &= \min_d MMSE(d, \tau, N_f = 1) && (2.24)\\ &= 1 - \max_d \frac{|c_\tau[d]|^2}{||c_\tau||^2 + \lambda} && (2.25)\\ &= 1 - \frac{||c_\tau||_\infty^2}{||c_\tau||^2 + \lambda}, && (2.26)\end{aligned}$$

where $||\cdot||_\infty$ denotes the ℓ_∞ norm. (Recall the definitions in Section 1.5.1) Finally, the optimal timing offset which minimizes the one tap equalizer MMSE is given by

$$\tau_{opt} = \max_{\tau} \frac{||\mathrm{c}_\tau||_\infty^2}{||\mathrm{c}_\tau||^2 + \lambda}. \tag{2.27}$$

Similarly, for the multisensor combiner case we have the same form

$$\xi_{opt} = \max_{\xi} \frac{||\mathrm{c}_\xi||_\infty^2}{||\mathrm{c}_\xi||^2 + \lambda}. \tag{2.28}$$

(For detailed derivation of (2.27) and (2.28) refer to Proof 2.A.1 in the appendix of this chapter).

We will call (2.27) and (2.28) the MMSE-timing function, and they provide a geometrical interpretation of the timing offset optimization for a one tap equalizer. Consider normalized c_τ,

$$\bar{\mathrm{c}}_\tau = \frac{\mathrm{c}_\tau}{||\mathrm{c}_\tau||}. \tag{2.29}$$

$\bar{\mathrm{c}}_\tau$ wanders around on N_c dimensional sphere as τ varies from $-1/2$ to $1/2$. Now τ_{opt} is set to choose the $\bar{\mathrm{c}}_\tau$ maximizing $||\bar{\mathrm{c}}_\tau||_\infty^2$, i.e. maximizing the largest magnitude of $\bar{\mathrm{c}}_\tau$. (See Figure 2.3). This implies that the timing offset optimized for a one tap equalizer attempts to minimize ISI by maximizing the magnitude of the tap corresponding to the system delay and, at the same time, suppressing other taps.

On the other hand, for the timing offset optimized for infinite length equalizers, [God78] proposed an approximation of (2.21) as the following

$$MMSE(\tau, N_f = \infty) \approx \frac{1}{||\mathrm{c}_\tau||^2 + \lambda}. \tag{2.30}$$

In this case, minimizing MMSE is equivalent to maximizing the channel power $||\mathrm{c}_\tau||^2$, and consequently just improving the signal to noise ratio, where the signal term includes ISI components.

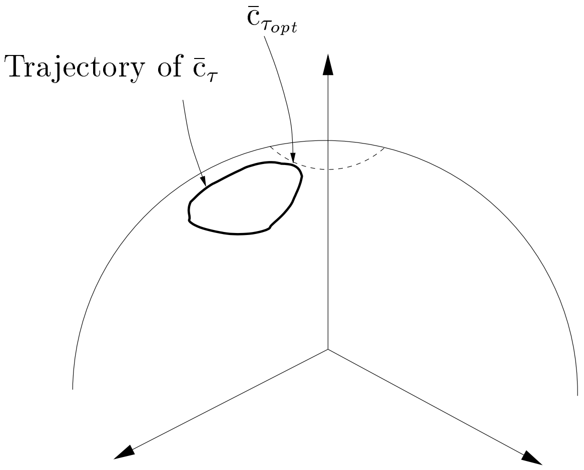

Figure 2.3: Geometrical interpretation of τ_{opt} for one tap equalizer

Apparently, there are significant differences in timing offsets optimized for one tap equalizers and infinite tap equalizers. In the following, we present a simulation example showing that the performance for short equalizers of the timing offset optimized for a single tap equalizer is superior to that optimized for an infinite length equalizer.

Example 2.1 In this example, first we consider an analog multipath channel

$$m(t) = \delta(t) + 0.6\delta(t - 1.4T) - 0.3\delta(t - 12.6T), \tag{2.31}$$

and a raised cosine pulse shaping filter with a roll-off factor $\alpha = 0.5$ and SNR=30dB. Numerical calculation shows that the optimal timing offsets for $N_f = 1$, $\tau_{N_f=1}$ and the optimal timing offset for $N_f = \infty$, $\tau_{N_f=\infty}$ are given by

$$\tau_{N_f=1} = 0.07, \quad \tau_{N_f=\infty} = 0.83 \tag{2.32}$$

(Matlab code simulating this example is provided in Section 2.B in the appendix of this chapter.) For these two timing offsets, Figure 2.4 plots the MSE of a) MMSE linear of equalizer length from 1 to 25, and b) MMSE DFE with feed back filter of fixed length 12 and feed forward equalizer length from 1 to 25. The optimal timing offset for each finite equalizer length has been calculated numerically and its MMSE equalizer MSE is depicted as a dotted line. In both cases, the timing optimized with respect to the norm in (2.26), $\tau_{Nf=1}$, produces better performance for short equalizers. Furthermore, notice that $\tau_{N_f=1}$ and $\tau_{N_f=\infty}$ optimized for the linear equalizer offer quite good MSE performance for the DFE equalizer.

In Figure 2.5 plots the averaged performance of $\tau_{N_f=1}$ and $\tau_{N_f=\infty}$ for random channels

$$m(t) = \sum_{k=0}^{5} \rho_k \delta(t - \tau_k), \tag{2.33}$$

where $\tau_k - tau_{k-1}$ is uniformly distributed over $[0, 4T]$ and ρ_k has random phase with exponential decayed magnitude ($e^{-\frac{\tau_k - \tau_0}{20}}$). For this class of channels, one can confirm that the MSE performance of $\tau_{N_f=1}$ is superior than that of $\tau_{N_f=\infty}$.

Since in practice the length of the symbol-spaced equalizer can never be long enough to remove all ISI, the timing offset optimized for the one tap equalizer is preferred. In Section 2.5 we will develop a blind scheme which approximates timing offsets optimized for a one tap equalizer. In the next section we will review some of existing timing recovery schemes focusing on blind approaches.

2.4 Conventional Approaches

There have been many approaches to timing phase offset recovery (for an early tutorial survey refer to [Fra80] and for texts see [MMF98], [MD97]). Here, we review a generalized version of a non-MMSE oriented approach (Mueller-Müller), a generic MSE approach, and an output energy maximization approach (Bandedge).

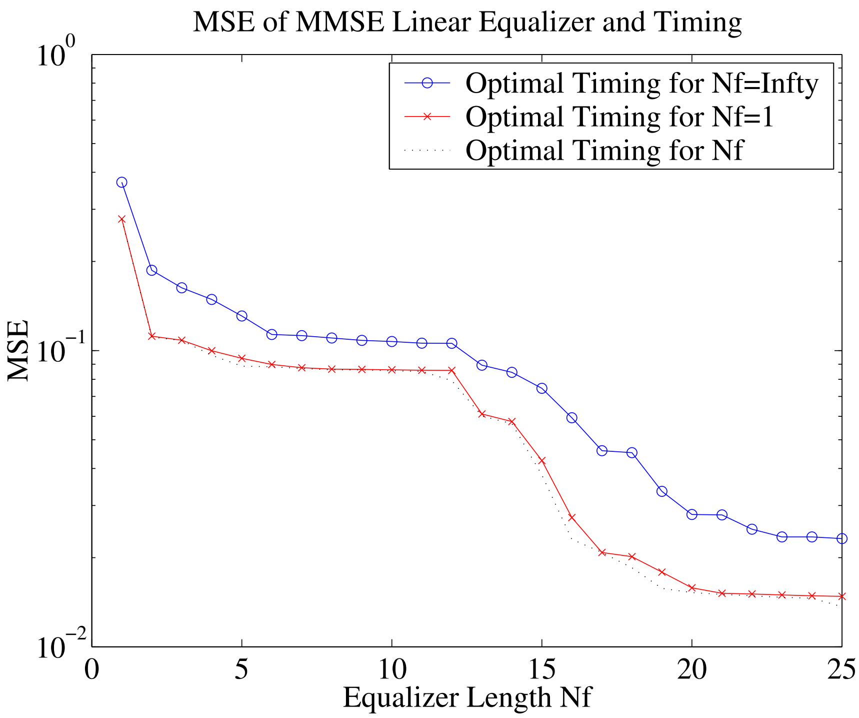

a) Linear Equalizer

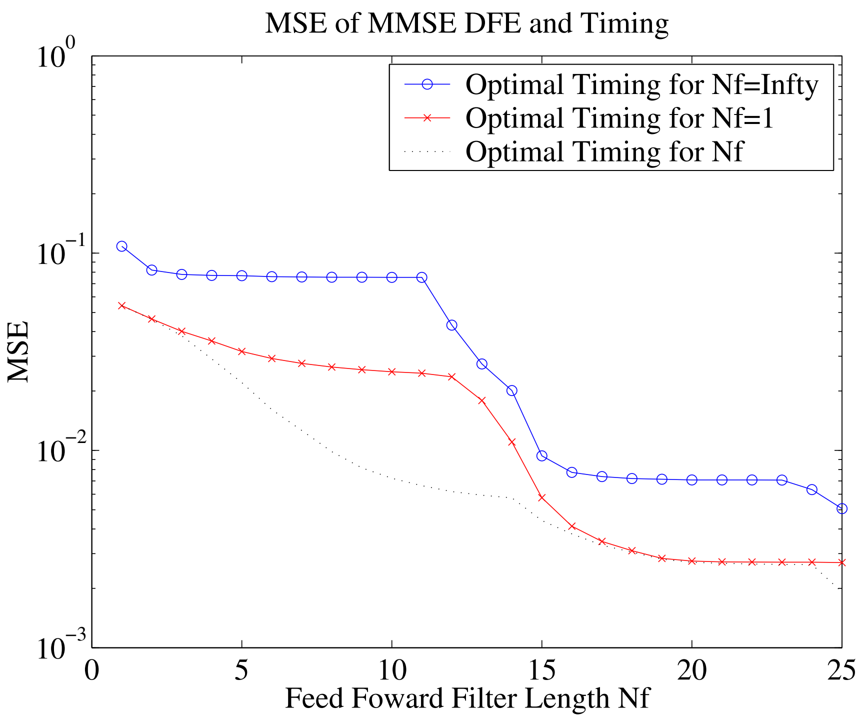

b) DFE with Feed back filter length 12

Figure 2.4: MMSE Equalizer output MSE and Timing offset

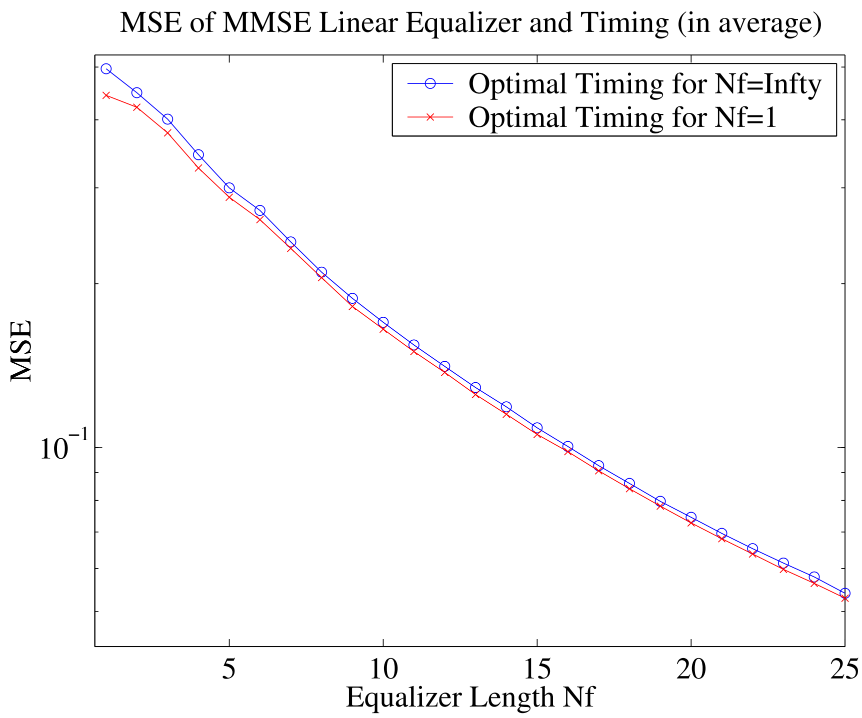

Figure 2.5: MMSE Equalizer output MSE and Timing offset: Averaged

2.4.1 Mueller and Müller Method

There is a class of timing recovery schemes which attempts to find a timing which maximizes the value of the largest tap (highest peak) of the resulting discrete time channel, i.e maximizing $\|c_\tau\|_\infty^2$ [MD97]. These approaches are based on the observation that the impulse response of the analog channel has a certain degree of symmetry near the peak. The peak is found by minimizing a cost function $f(\tau)$ consisting of a linear combination of a sampled impulse response,

$$f(\tau) = c_\tau^T u = \sum_i u_i c_\tau[i]. \tag{2.34}$$

for example,

$$f(\tau) = \frac{1}{2}c_\tau[-1] - \frac{1}{2}c_\tau[1] \tag{2.35}$$

However, direct access to the channel impulse response is not possible. Mueller Müller method [MM76] uses a decision directed method to construct $f(\tau)$.

- **Brief Summary:** For a given weight g, consider a weighted sum of sampled data y,

$$z = g^T y. \tag{2.36}$$

The goal is to set g such that $E\{z\} = f(\tau)$ with respect to an objective cost weight u. Since s is the only non-deterministic quantity, $E\{z\}$ can be written as

$$E\{z\} = \mathrm{c}_\tau^T E\{Sg\}, \tag{2.37}$$

where S is a Töplitz matrix generated from the source s. In order for $E\{z\}$ to be $f(\tau)$ we need $E\{Sg\} = u$. Assuming S is known, for example from decision feedback, one can find a least squares solution of g.

Apparently, for any realizable $f(\tau)$, the goal of this algorithm is to achieve maximized $\|\mathrm{c}_\tau\|_\infty$. In general, it is an intuitive approach especially when the multipath channel is mild, but there is no guarantee of the optimality in terms of equalizer output MSE in the presence of substantial multipath.

2.4.2 MSE approach

One straightforward approach is to find a timing offset which minimizes the MSE of the sampled output, i.e.

$$\tau_{opt} = \arg\min_\tau E\left\{\left|\sum_{i=-\infty}^{\infty} \mathrm{c}^2_{r_k - s_k}\right|\right\}. \tag{2.38}$$

The expectation in the above equation is reducible so that (2.38) becomes

$$\tau_{opt} = \arg\min_{\tau} \left(\|\mathrm{c}_\tau\|^2 - 2\|\mathrm{c}_\tau\|_\infty\right) \tag{2.39}$$

$$= \arg\min_{\tau} \left(\|\mathrm{c}_\tau\|^2(1 - 2\frac{\|\mathrm{c}_\tau\|_\infty}{\|\mathrm{c}_\tau\|^2})\right). \tag{2.40}$$

In comparison with the timing optimized for $MMSE(\tau, N_f = 1)$ in (2.27), this MMSE timing offset effectively assuming no equalization (i,e, $N_f = 0$) in (2.39) has a similar goal, maximizing $\|\mathrm{c}_\tau\|_\infty$ and, at the same time, minimizing $\|\mathrm{c}_\tau\|^2$. However, (2.40) does not contain a noise variance term. Therefore, the two timing offsets tend to agree for high SNR, but $MMSE(\tau, N_f = 1)$ is expected to exhibit superior performance for low SNR. Figure 2.6 shows that for high SNR the performance of the two timing offsets is identical, while for low SNR the timing offset optimized for $MMSE(\tau, N_f = 1)$ always achieves better MSE performance for all lengths of MMSE equalizer. This simulation is performed for the same channel considered in Example 2.1. The simulation result suggests that timing offset $MMSE(\tau, N_f = 0)$ can be used as an approximation of the one optimized for $MMSE(\tau, N_f = 1)$ when the noise is mild.

2.4.3 Bandedge Timing

In [God78], Godard showed numerically that the timing offset optimized to $MMSE(\tau, N_f = \infty)$ in (2.21) can be approximated by the one that maximizes the output energy, i.e.

$$\arg\min_{\tau} MMSE(\tau, N_f = \infty) = \arg\min_{\tau} \frac{1}{2\pi} \int_{-\pi}^{\pi} \frac{\lambda}{|C(\omega,\tau)|^2 + \lambda} d\omega \tag{2.41}$$

$$\approx \arg\min_{\tau} \frac{\lambda}{\frac{1}{2\pi}\int_{-\pi}^{\pi} |C(\omega,\tau)|^2 \, d\omega + \lambda} d\omega \tag{2.42}$$

$$= \arg\max_{\tau} \|\mathrm{c}_\tau\|^2. \tag{2.43}$$

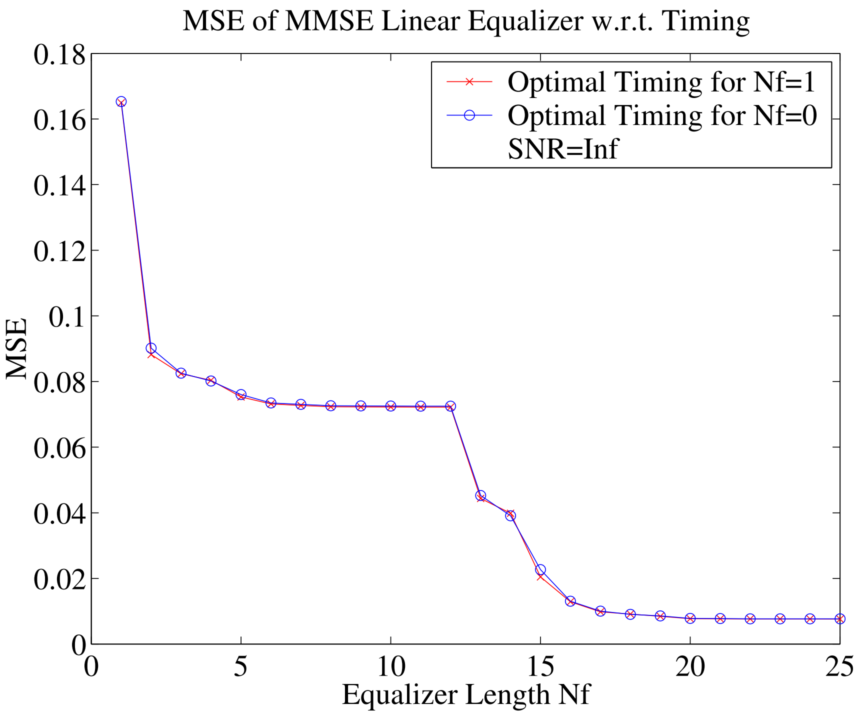

a) For SNR =inf

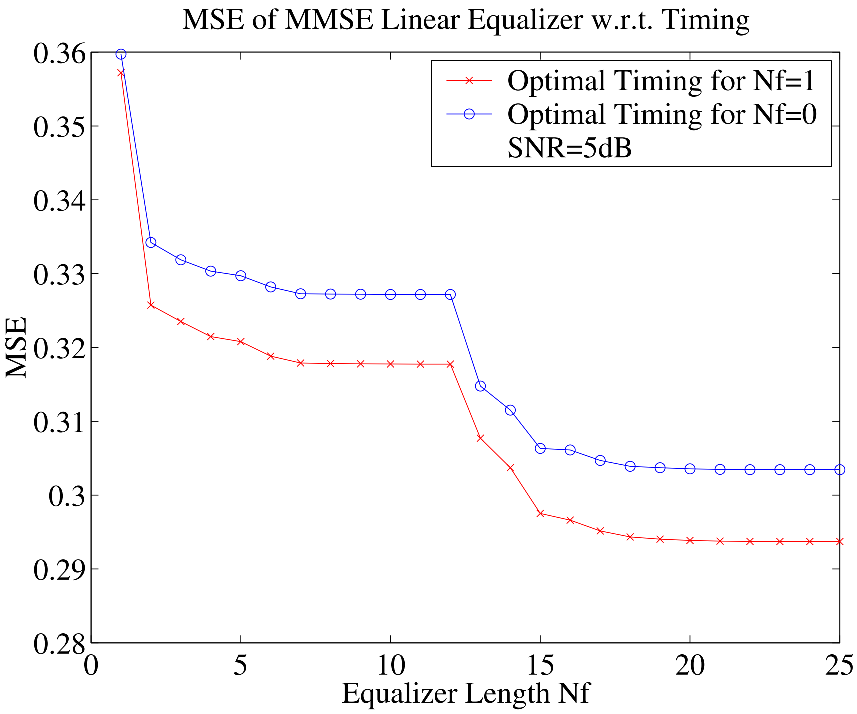

b) For SNR =5 dB

Figure 2.6: Performance of timing offsets: (2.27) v.s. (2.39)

Let $H(f)$ denote the frequency response of the analog channel. Usually, $H(f)$ has excess bandwidth spectrum, so $H(1/T) \neq 0$, but nonzero $H(f)$ does not occur above $f = 2/T$, i.e. $H(f) = 0$ for $f > 2/T$. In this case, from a Fourier series expansion of $\|c_\tau\|^2$, we have (for details refer to (2.66) in section 2.5.2)

$$\|c_\tau\|^2 = H \star H(0) + 2\,|H \star H(1/T)| \cos(2\pi\tau + \angle H \star H(1/T)) \tag{2.44}$$

$$\begin{aligned} &= \int |H(f)|^2 df \\ &\quad + 2\left|\int H(f)H^*(1/T - f)df\right| \cos(2\pi\tau + \angle \int H(f)H^*(1/T - f)df), \end{aligned} \tag{2.45}$$

where $\angle$ denotes the phase of a complex number. Therefore, to maximize $\|c_\tau\|^2$ by selecting the argument of $\cos(\cdot)$ such that $\cos(\cdot)$ is 1 results in

$$\tau = -\frac{1}{2\pi}\angle \int H(f)H^*(1/T - f)df, \tag{2.46}$$

The integration in (2.46) can be visualized as in Figure 2.7. As Figure 2.7 suggests

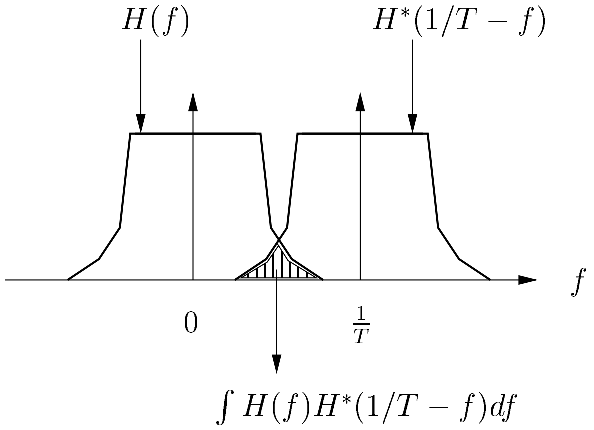

Figure 2.7: Bandedge Timing Information

the output energy maximization timing can be obtained by correlation of band edges of the analog domain channel. This implies that output energy maximization timing algorithm can be implemented in pass band unlike other schemes such as Mueller and Müller method or the MSE method.

2.5 Timing offset based on Dispersion Minimization

2.5.1 DM-timing Offsets

Instead of minimizing MSE, authors in [GLS96] and [CBSJ01] proposed minimizing the mean dispersion of the sampled signals by timing offset selection, given by

$$J(\tau) = E\left\{(|y_k(\tau)|^2 - \gamma)^2\right\}, \tag{2.47}$$

where γ is a constant corresponding to the source statistics. ($\gamma = E\,|s|^4 / E\,|s|^2$, for details refer to [JSE$^+$98].) The cost function is known as the Constant Modulus Algorithm (CMA) or constant modulus (CM) cost function and widely used for equalization. However, (2.47) approximates $MMSE(\tau, N_f = 0)$,

$$E\left\{|y_k(\tau) - s_k|^2\right\}, \tag{2.48}$$

and in order to approximate $MMSE(\tau, N_f = 1)$ with respect to a one tap equalizer α

$$E\left\{|\alpha r_k(\tau) - s_k|^2\right\}, \tag{2.49}$$

we need to minimize

$$J(\tau, \alpha) = E\left\{(|\alpha\, r_k(\tau)|^2 - \gamma)^2\right\}, \tag{2.50}$$

as illustrated in Figure 2.8. Using a stochastic gradient algorithm [TJL01] to minimize (2.50) by recursive selection of τ_k and α_k gives the DM-timing algorithm

$$\tau_{k+1} = \tau_k - \mu(|\alpha_k r_k(\tau_k)|^2 - \gamma)\ |\alpha_k|^2\, y_k(\tau_k)\ \frac{\partial r_k(\tau_k)}{\partial \tau_k} \tag{2.51}$$

$$\alpha_{k+1} = \alpha_k - \mu(|r_k(\tau_k)|^2 - \gamma)\ \alpha_k\, |r_k(\tau_k)|^2, \tag{2.52}$$

where $\partial r_k(\tau_k)/\partial\tau_k$ can be obtained numerically, when a closed form is not available.

Similarly, for a multisensor combiner system we have the same cost function,

$$J(\xi) = E\left\{(|y_k(\xi)|^2 - \gamma)^2\right\}, \tag{2.53}$$

and the same stochastic updates (Figure 2.9)

$$\xi_{k+1} \;=\; \xi_k - \mu(|y_k(\xi_k)|^2 - \gamma)\; y_k(\xi_k)\; \frac{\partial y_k(\xi_k)}{\partial \xi_k}. \tag{2.54}$$

Notice that for a multisensor combiner, a scalar equalizer f can be absorbed into combining weights by putting $\beta_k' = f\beta_k$. Thus, $J(\xi)$ can be seen as a function of only ξ.

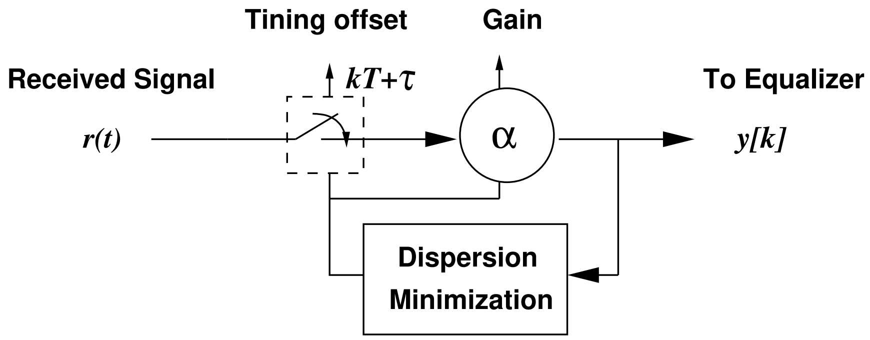

Figure 2.8: Dispersion Minimization Timing Offset

Expansion of the DM-cost function (2.50) provides detailed information on the DM timing offsets. Setting $\lambda = \sigma_w^2/\sigma_s^2$ and assuming $\sigma_s^2 = 1$, the DM cost function for a single antenna case (2.47) is given by the following (for the derivations including the multisensor combiner case, refer to Proof 2.A.2 in the appendix of this chapter.)

$$J(\tau,\alpha) = \alpha^4\left(\eta_s\|\mathrm{c}_\tau\|_4^4 + \kappa_w(\|\mathrm{c}_\tau\|^2+\lambda)^2\right) - 2\alpha^2(\kappa_s\|\mathrm{c}_\tau\|^2+\lambda) + \kappa_s^2, \tag{2.55}$$

where

$$\kappa_s = \frac{E\left\{|s|^4\right\}}{E\left\{|s|^2\right\}^2}, \qquad \kappa_w = \frac{E\left\{|w|^4\right\}}{E\left\{|w|^2\right\}^2}, \tag{2.56}$$

$$\eta_s = \kappa_w - \kappa_s, \tag{2.57}$$

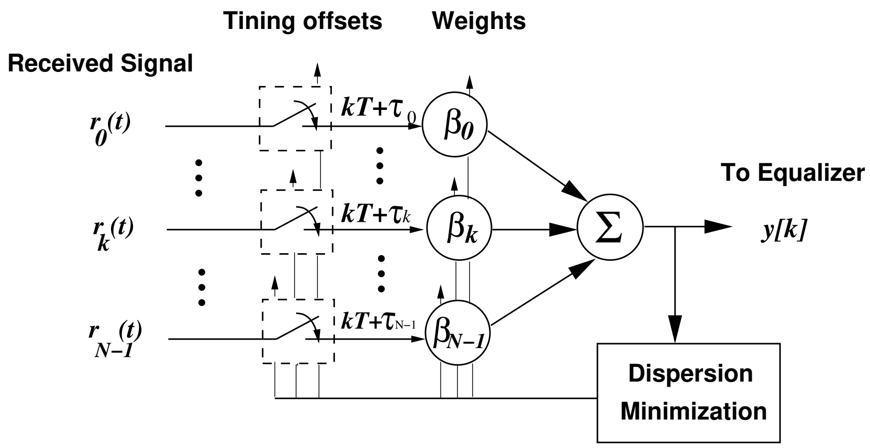

$$\zeta = (\tau_0, ..., \tau_{N-1}, \beta_0, ..., \beta_{N-1})$$

Figure 2.9: Dispersion Minimization Multisensor Combining

and $||\cdot||_4$ denotes the ℓ_4 norm.

Since the cost function (2.55) is a quadratic function of α, there exists a unique optimum α for each τ. Using this fact (2.55) can be written as a function of only τ, which provides the following intuition on the DM-timing offset.

Theorem 2.1 (DM-Minima) The DM-timing offset for a single sensor is given by

$$\tau_{DM} = \arg\max_{\tau} \frac{||\mathrm{c}_\tau||_4^2}{||\mathrm{c}_\tau||^2 + \lambda}, \tag{2.58}$$

and for a multisensor combiner is given by

$$\xi_{DM} = \arg\max_{\xi} \frac{||\mathrm{c}_\xi||_4^2}{||\mathrm{c}_\xi||^2 + \lambda}. \tag{2.59}$$

Proof: : Refer to Proof 2.A.3 in the appendix of this chapter.

There is a similarity between MMSE-timing and DM-timing. Recall the notation $\bar{\mathrm{c}}_\tau = \mathrm{c}_\tau / ||\mathrm{c}_\tau||$. In the absence of noise, the MMSE timing offset for a one tap equalizer is given by $\arg\max_\tau ||\bar{\mathrm{c}}_\tau||_\infty$, while DM-timing is $\arg\max_\tau ||\bar{\mathrm{c}}_\tau||_4$. Geometrically, the difference between these two timing offsets is only the norm (ℓ_4 or ℓ_∞) applied on a certain set on a unit sphere constrained by the range of τ, $\{\bar{c}_\tau\}_{-1/2<\tau<1/2}$. Figure 2.10 illustrates the difference between ℓ_∞ norm and ℓ_4 norm.

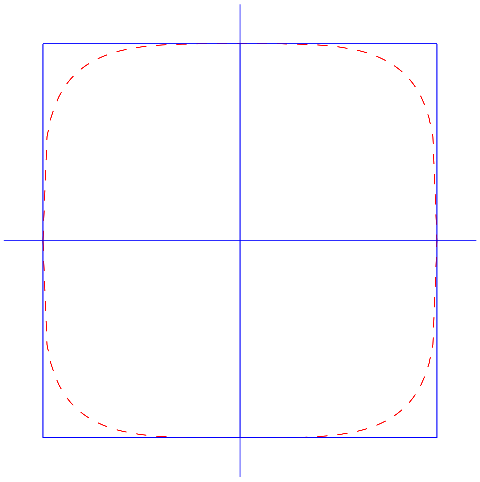

Figure 2.10: ℓ_∞ norm (solid) and ℓ_4 norm (dashed) in 2 dim.

2.5.2 Single sensor case: Cost function and Unimodality

For the single sensor case, we can further investigate how a given channel can effect the DM-timing offsets. This will enable us to set conditions under which the DM cost function bears a unique maximum, which seems to be satisfied in most practical situations. The result of this section implies the insensitivity of DM timing algorithm to the initial condition.

We define the following function in Theorem 2.1 as the *DM-timing cost*,

$$I(\tau) = \frac{||c_\tau||_4^2}{||c_\tau||^2 + \lambda}, \tag{2.60}$$

and the following analysis will be focused on this DM-timing cost and its unimodality instead of the DM-cost function.

Let $H(f)$ denote the Fourier transform of $c(t)$, the analog channel, and define

$$H_2 := H \star H, \quad H_4 := H \star H \star H \star H,$$

where $\star$ indicates the convolution operator. From the Fourier series expansion of $\|c_\tau\|^2$ and $\|c_\tau\|_4^4$ we have

$$\begin{aligned} \|c_\tau\|^2 &= \sum_{k=-\infty}^{\infty} c^2(t+kT) = \frac{1}{T}\sum_{k=-\infty}^{\infty} H_2(\frac{k}{T_s})e^{j2\pi\frac{kt}{T_s}}, & (2.61)\\ \|c_\tau\|_4^4 &= \sum_{k=-\infty}^{\infty} c^4(t+kT) = \frac{1}{T}\sum_{k=-\infty}^{\infty} H_4(\frac{k}{T_s})e^{j2\pi\frac{kt}{T_s}}. & (2.62)\end{aligned}$$

Assuming $T = 1$, since $c(t)$ is band limited, we have

$$\begin{aligned} H(f) &= 0 \quad \text{for } |f| > \tfrac{1}{T}\ , & (2.63)\\ H_2(f) &= 0 \quad \text{for } |f| > \tfrac{2}{T}\ , & (2.64)\\ H_4(f) &= 0 \quad \text{for } |f| > \tfrac{4}{T}\ , & (2.65)\end{aligned}$$

and from (2.61) and (2.62)

$$\begin{aligned} \|c_\tau\|^2 &= H_2(0) + 2\,|H_2(1)|\cos(2\pi\tau + \angle H_2(1)), & (2.66)\\ \|c_\tau\|_4^4 &= H_4(0) + 2\sum_{m=1}^{3}|H_4(m)|\cos(2m\pi\tau + \angle H_4(m)). & (2.67)\end{aligned}$$

The values of $\{H_2(k), H_4(m)\}$ are determined by the multipath channel $m(t)$ and pulse shaping filter $p(t)$. In practice, a commonly used pulse shaping filter is a raised cosine function, the spectrum of which is given by

$$X_{rc}(f) = \begin{cases} T, & 0 \le |f| \le (1-\alpha)/2T \\ \frac{T}{2}\left[1 + \cos(\frac{\pi T}{\alpha}(|f| - \frac{1-\alpha}{2T})\right], & \frac{1-\alpha}{2T} \le |f| \le \frac{1+\alpha}{2T} \\ 0, & |f| > \frac{1+\alpha}{2T} \end{cases} \qquad (2.68)$$

where α is called the roll-off factor which determines the excess bandwidth. A roll-off factor from 0.1 to 0.3 is commonly used in practice (for example [Com00], [HT01]).

For a multipath $m(t) = \sum_{i=0}^{N_c-1} \rho_i \delta(t-\tau_i)$, $H(f)$ is given by

$$H(f) = X_{rc}(f) \sum_{i=0}^{N_c-1} \rho_i e^{2\pi j \tau_i f}. \tag{2.69}$$

Furthermore, since the power of the received signal is adjusted to be normalized, we can assume that $\left|\rho_i e^{2\pi j \tau_i f}\right| \le 1$, without loss of much generality. Therefore,

$$\begin{aligned} |H(f)| &\le |X_{rc}(f)|, & (2.70)\\ |H_2(f)| &\le |X_{rc} \star X_{rc}(f)|, & (2.71)\\ |H_4(f)| &\le |X_{rc} \star X_{rc} \star X_{rc} \star X_{rc}(f)|. & (2.72) \end{aligned}$$

For a roll-off factor from 0.1 to 0.3, the tails of X_{rc} are quite small (Figure 2.11-a)), and consequently, the values $|H_4(2)|$,$|H_4(3)|$, and $|H_4(4)|$ are vanishingly small in comparison with other values such as $|H_4(0)|$ and $|H_4(1)|$, and thus ignorable (See Table 2.1 and Figure 2.11-b)).

In this case we have the following good approximation of $\|c_\tau\|_4^4$

$$\|c_\tau\|_4^4 \approx H_4(0) + 2\,|H_4(1)| \cos(2\pi\tau + \angle H_4(1)). \tag{2.73}$$

Using this approximation, we can simplify the DM-timing function, $I(\tau)$.

$$I(\tau) \approx \tilde{I}(\tau) := \frac{\sqrt{H_4(0) + 2\,|H_4(1)| \cos(2\pi\tau + \angle H_4(1))}}{H_2(0) + 2\,|H_2(1)| \cos(2\pi\tau + \angle H_2(1))}. \tag{2.74}$$

Although, the approximation $\tilde{I}(\tau)$ is still complicated in terms of computing a closed expression of τ_{DM}, at least we can study the unimodality of the DM-timing using $\tilde{I}(\tau)$.

Theorem 2.2 (Unimodality) First, let us denote

$$\begin{aligned} &G_2 = H_2(0) + \lambda, \quad G_4 = H_4(0), \\ &H_2 = 2\,|H_2(1)|, \quad H_4 = 2\,|H_4(1)|. \end{aligned} \tag{2.75}$$

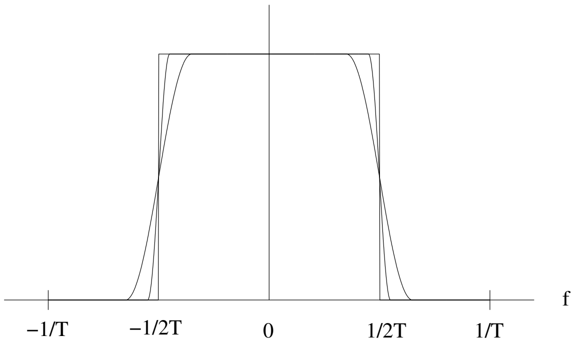

a) Raised cosines with roll-off factor $\alpha = 0$, 0.1, and 0.3.

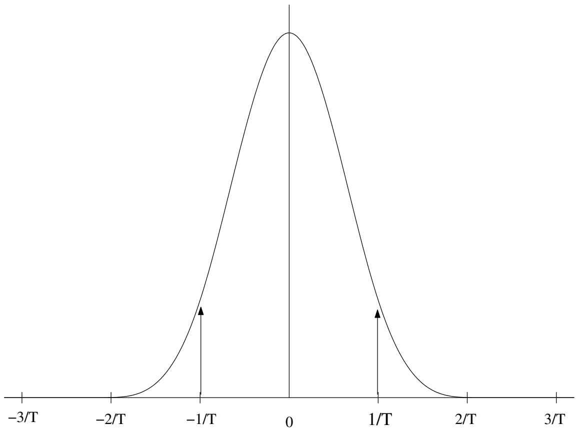

b) Spectrum of $X_{rc} \star X_{rc} \star X_{rc} \star X_{rc}(f)$ for $\alpha = 0.3$

Figure 2.11: Spectrum of Raised Cosine and its convolution

Then

$$\tilde{I}(\tau) = \frac{\sqrt{G_4 + H_4 \cos(2\pi\tau + \angle H_4(1))}}{G_2 + H_2 \cos(2\pi\tau + \angle H_2(1))} \tag{2.76}$$

is unimodal, i.e. has a unique maximum, when the following condition holds,

$$H_4 G_2 - 2H_2 G_4 > 5H_2 H_4. \tag{2.77}$$

Proof: Refer to Proof 2.A.4 in the appendix of this chapter.

Notice that the condition (2.77) in Theorem 2.2 can be satisfied when the tails, $H_2(1)$ and $H_4(1)$, decrease fast enough. In Table 2.1, one can verify that for small roll-off factors $\alpha \leq 0.3$ satisfies the condition (2.77), which implies that the DM-algorithm bears only one minimum regardless of the multipath channel.

Table 2.1: DM-timing function coefficients v.s. Roll-off factor of Raised Cosine(In the absence of a multipath channel)

Roll-off Factor	$\alpha = 0.1$	$\alpha = 0.3$	$\alpha = 0.5$	$\alpha = 1$
$H_2(0)$	0.9749	0.9249	0.8749	0.7499
$\lvert H_2(1)\rvert$	0.0124	0.0374	0.0624	0.1249
$H_4(0)$	0.6647	0.6512	0.6272	0.5411
$\lvert H_4(1)\rvert$	0.1675	0.1739	0.1849	0.2186
$\lvert H_4(2)\rvert$	1×10^{-5}	2×10^{-4}	0.0013	0.0106
$\lvert H_4(3)\rvert$	$\doteq 0$	$\doteq 0$	$\doteq 0$	1×10^{-5}
$H_4G_2 - 2H_2G_4 - 5H_2H_4$	0.2520	0.0945	-0.0633	-0.4876

In fact, the condition (2.77) given in Theorem 2.2 is a loose bound. A tighter bound can be found under slightly more complicated conditions.

Remark 2.1 The condition (2.77) in Theorem 2.2 can be replaced by the following set of conditions.

$$i) \quad H_4G_2 - 2.6H_2G_4 > H_2H_4, \tag{2.78}$$

$$ii) \quad H_4G_2 + H_2G_4 - H_2H_4 < 1, \tag{2.79}$$

$$iii) \quad \frac{H_4 + 2H2H4^2}{0.8 - H2H4} < G_4. \tag{2.80}$$

Proof: Refer to Proof 2.A.5 of the appendix of this chapter.

A numerical evaluation of the above conditions is listed in Table 2.2, which shows that roll-off factors up to $\alpha = 0.6$ satisfy the above unimodality conditions. From these numerical experiment, we can conclude that in most practical situations

Table 2.2: Evaluation of tighter bounds in Remark 2.1

Roll-off Factor	$\alpha = 0.1$	$\alpha = 0.3$	$\alpha = 0.6$	$\alpha = 1$
$H_4G_2 - 2.6H_2G_4 - H_2H_4 > 0$?	0.2752	0.1691	0.0298	-0.1324
$H_4G_2 - 2H_2G_4 - H_2H_4 < 1$?	0.3506	0.3925	0.4508	0.4884
$\frac{H_4+2H_2H_4^2}{0.8-H_2H_4} - G_4 < 0$?	0.2348	0.1786	0.0380	-0.2293

the DM-timing bears unique local minimum, and consequently the algorithm is insensitive to initialization, in spite of its blind nature. We conclude this section with an example where the DM-timing algorithm exhibits multimodal solutions.

Example 2.2 In Table 2.1 and Table 2.2, one discovers that for $\alpha = 1$ the conditions for unimodality are violated. This does not imply that the DM-timing function for any channel with roll-off factor $\alpha = 1$ has multimodal solutions. However, one can easily find an example, for example

$$m(t) = \delta(t) + 0.9\delta(t - 1.6T) - 0.8\delta(t - 4T), \tag{2.81}$$

with $\alpha = 1$. Figure 2.12 plots the DM-timing function $I(\tau) = \|\mathrm{c}_\tau\|_4^2/(\|\mathrm{c}_\tau\|^2 + \lambda)$ with a dashed line and the MMSE timing function $\|\mathrm{c}_\tau\|_\infty^2/(\|\mathrm{c}_\tau\|^2 + \lambda)$ with a solid line. Apparently, DM-timing has two local maxima at $\tau = 0.0571$ and $\tau = 0.6266$. In this example the global DM-solution $\tau = 0.0571$ exhibits inferior MSE performance relative to the other DM-timing offset (recall that $MMSE(\tau) = 1 - \|\mathrm{c}_\tau\|_\infty^2/(\|\mathrm{c}_\tau\|^2 + \lambda)$. The best MMSE timing offset is at neither DM-minima location.

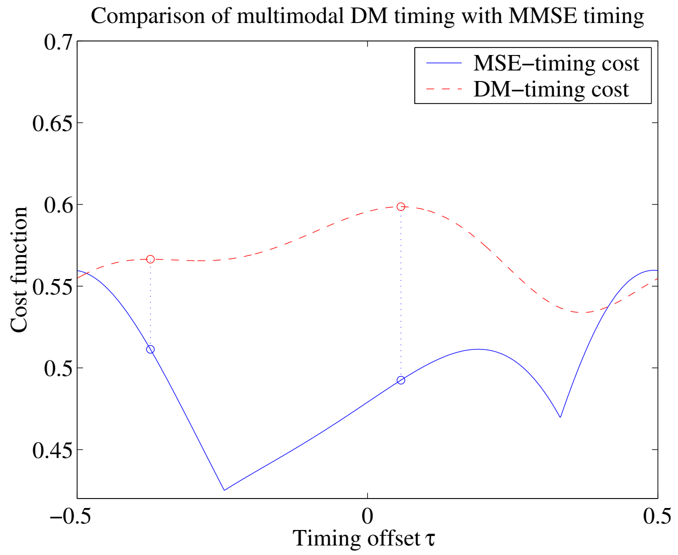

Figure 2.12: Example of DM-multimodal solutions

2.6 MSE performance of DM-timing

The MSE performance of the dispersion minimization approach has been intensively studied for the equalization applications under the assumption that perfect equalization is possible (such as in the fractionally spaced equalization scenario) [ZTJ98], [SJ00]. It has been shown that the dispersion minimization approach can achieve near MMSE performance when the achievable system response due to the equalizer is unconstrained. However, the results cannot be applied for the timing offset problem, since the channel vectors parameterized by timing offsets are constrained. In the next subsection, we will present a geometrical argument showing that one cannot establish a structural relationship between dispersion timing offset and its MSE performance.

2.6.1 Geometrical Approach : In the absence of noise

The geometrical implications of blind equalization approaches based on higher order statistics in terms of ℓ_2 and ℓ_4 and ℓ_∞ norms has been recognized by several authors [GT99], [Kun97]. The similarity between DM timing and MMSE timing characterized by the ℓ_4 norm and the ℓ_∞ norm can be viewed as a special case of the blind equalization problem. However, for the timing offset case the attainable system response c_τ is limited and consequently the geometrical approach based on the comparison of the ℓ_4 norm and the ℓ_∞ norm in order to obtain a MSE performance of DM timing is not successful.

Let $\mathcal{A}$ denote all attainable $\bar{\mathrm{c}}_\tau$ by the parameter τ, where $\bar{\mathrm{c}}_\tau = \mathrm{c}_\tau / ||\mathrm{c}_\tau||^2$. The MSE performance of DM-timing in the absence of noise is to compare the following two quantities:

$$||\bar{\mathrm{c}}_{DM}||_\infty^2 \text{ and } \max ||\bar{\mathrm{c}}||_\infty^2 \text{ with } \bar{\mathrm{c}} \in \mathcal{A}, \tag{2.82}$$

where

$$\bar{\mathrm{c}}_{DM} = \arg\max ||\bar{\mathrm{c}}||_4^2 \text{ with } \bar{\mathrm{c}} \in \mathcal{A}. \tag{2.83}$$

One could visualize $||\bar{\mathrm{c}}||_4$ as an approximation of $||\bar{\mathrm{c}}||_\infty$ and thus the maximum of the ℓ_4 norm is always located near the maximum of the ℓ_∞ norm. This is true when $N_c = 2$ as Figure 2.13 illustrates and the following example confirms, but in general it does not hold for higher dimensional cases.

Example 2.3 MSE of DM timing : 2-dimensional case

Suppose $\bar{c}_\tau \in S^1$, i.e. $\bar{c} = [c_\tau[1]\ c_\tau[2]]$ and $c_\tau^2[1] + c_\tau^2[2] = 1$. Since $\|x\|_4^2 > 0$ and $\|x\|_\infty^2 > 0$, we have $\|x\|_4^4 > \|x\|_\infty^4$ if and only if $\|x\|_4^2 > \|x\|_\infty^2$. Thus, we will show that $\|\bar{c}_{DM}\|_4^4 = \max \|\bar{c}\|_\infty^4$, i.e. for a given subset $\mathcal{A} \subset S^1$ and

$$\bar{c}_0 = \arg\max_{\bar{c} \in \mathcal{A}} \|\bar{c}\|_4^4, \tag{2.84}$$

we will show that

$$\bar{c}_0 = \arg\max_{\bar{c} \in \mathcal{A}} \|\bar{c}\|_\infty^4. \tag{2.85}$$

Suppose that $\bar{c}_1 \in \mathcal{A}$ is a maximum with respect to the ell_∞-norm, but $\bar{c}_1 \neq \bar{c}_0$, i.e. $\bar{c}_1$ is not a maximum with respect to the ℓ_4 norm. We denote $\bar{c}_0 = [x_0\ y_0]$ and $\bar{c}_1 = [x_1\ y_1]$. Without loss of generality, we can assume that $x_0^2 > y_0^2$, $x_1^2 > y_1^2$, and $x_1^2 = x_0^2 + \delta$ where $\delta > 0$, since $\bar{c}_0, \bar{c}_1 \in S^1$. Then,

$$x_1^4 + y_1^4 = (x_0^2 + \delta)^2 + (1 - (x_0^2 + \delta))^2 \tag{2.86}$$

$$= x_0^4 + y_0^4 + 2\delta(2x_0^2 - 1 + \delta). \tag{2.87}$$

Since $x_0^2 > y_0^2$ and $x_0^2 + y_0^2 = 1$, we have $x_0^2 > 1/2$, which implies that

$$\|\bar{c}_{\tau_1}\|_4^4 = x_1^4 + y_1^4 > x_0^4 + y_0^4 = \|\bar{c}_{\tau_0}\|_4^4. \tag{2.88}$$

This is contradictory to the assumption that $\bar{c}_0$ is maximum with respect to the ℓ_4 norm. Thus $\bar{c}_0 = \bar{c}_1$.

In order to study the MSE performance of DM-timing for a higher dimension we introduce the following conventions:

For a given c_τ, we define $\mathbf{x}$ component-wise

$$x_k = |c_\tau[k]|^2, \tag{2.89}$$

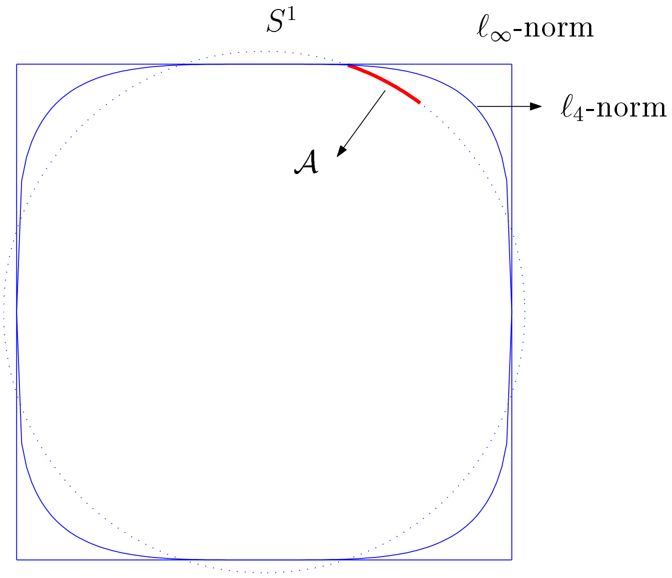

Figure 2.13: MSE performance of DM timing in 2 dim.

and let $\mathcal{A}$ denote the set of all attainable $\mathbf{x}$ by the parameter τ. Then,

$$\|\mathrm{c}_\tau\|_2 = \sum x_k, \tag{2.90}$$

$$\|\mathrm{c}_\tau\|_4 = \|\mathbf{x}\|_2, \tag{2.91}$$

$$\|\mathrm{c}_\tau\|_\infty = \|\mathbf{x}\|_\infty. \tag{2.92}$$

Now the problem of determining MSE performance DM-timing can be paraphrased as

$$\max_{\mathbf{x}\in\mathcal{A}} \|\mathbf{x}\|_\infty^2 \text{ and } \|\mathbf{x}_0\|_\infty^2 \text{ with } \sum_k x_k = 1, \tag{2.93}$$

where

$$\mathbf{x}_0 = \arg\max_{\mathbf{x}\in\mathcal{A}} \|\mathbf{x}\|^2 \text{ with } \sum_k x_k = 1. \tag{2.94}$$

Notice that $\sum_k x_k = 1$ and $x_k > 0$ for all k defines a hyper-plane, say $\mathcal{P}$. Let $\mathbf{n}$ denote the normal vector to the hyper-plane $\mathcal{P}$. Then, by defining

$$\mathbf{y} = \mathbf{x} - \mathbf{n}, \tag{2.95}$$

$\mathbf{y} \in \mathcal{P}$ and

$$\|\mathbf{x}\|^2 = \|\mathbf{n}\|^2 + \|\mathbf{y}\|^2. \tag{2.96}$$

This implies that ℓ_2-norm on the hyper plane $\mathcal{P}$ determines the $\mathbf{x}_0$ (see Figure 2.14-a))

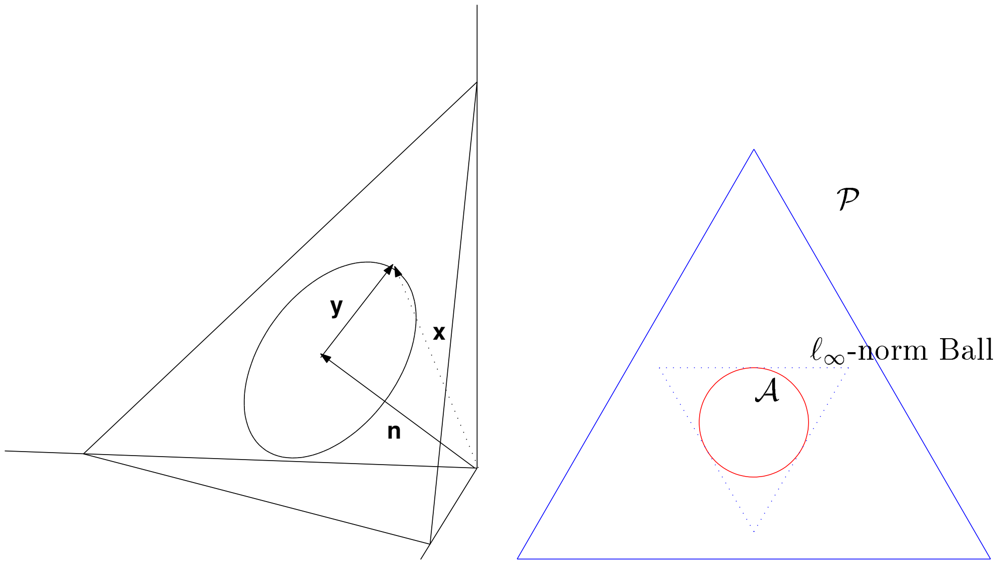

a) $\mathbf{x} = \mathbf{n} + \mathbf{y}$ in 3-dim. b) A particular $\mathcal{A}$ in 3-dim.

Figure 2.14: 3-dimensional example

Consider a 3-dimensional example as illustrated in Figure 2.14-b), where the attainable set $\mathcal{A}$ happens to be a circle on $\mathcal{P}$ centered at $\mathbf{n}$. In this case, $\|\mathbf{x}\|^2 = const.$ for all $\mathbf{x} \in \mathcal{A}$. However, on the other hand, an ℓ_∞ norm ball is drawn as a triangle, and $\|\mathbf{x}\|_\infty$ is not a constant. This example shows that there can be multiple *DM*-timings which exhibit different MSE performance. Another example we consider is illustrated in Figure 2.15. The attainable set $\mathcal{A}$ in this example has a unique DM-timing, but the DM-timing locates far from the MMSE-timing. Therefore, we can conclude that the MSE performance of DM-timing depends on the properties of $\mathcal{A}$, and the attempt to relate DM-timing and MMSE-timing based

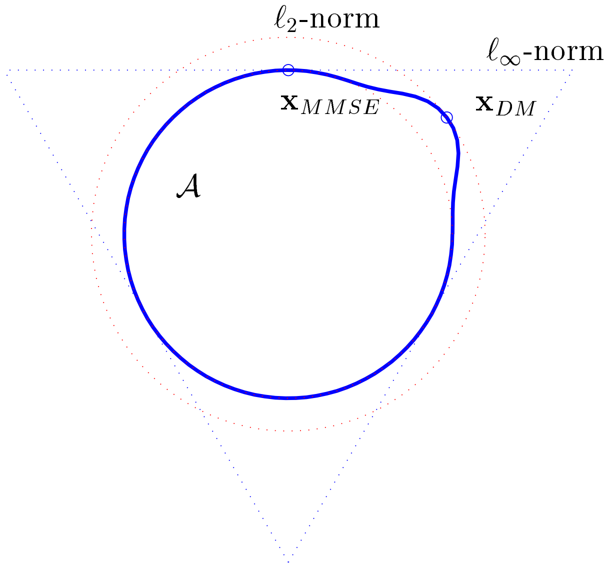

Figure 2.15: Unique DM-timing which does not optimize MSE

on the geometrical relationship between ℓ_4 and ℓ_∞ is futile. The following simulation experiment shows that we can find an undesirable $\mathcal{A}$ for a multipath channel which produces a DM-timing not optimized for MSE.

Example 2.4 Consider a single antenna case in the presence of a multipath channel

$$m(t) = \delta(t) + \delta(t - 3.4), \tag{2.97}$$

with a raised cosine pulse with roll-off factor $\alpha = 0.5$. In this example, DM-timing exhibits nearly the worst possible MSE performance. Figure 2.16 plots $||\bar{\mathrm{c}}_\tau||_\infty^4$ (solid line) and $||\bar{\mathrm{c}}_\tau||_4^4$ (dashed line). Recall that

$$MSE = 1 - ||\bar{\mathrm{c}}_\tau||_\infty^4. \tag{2.98}$$

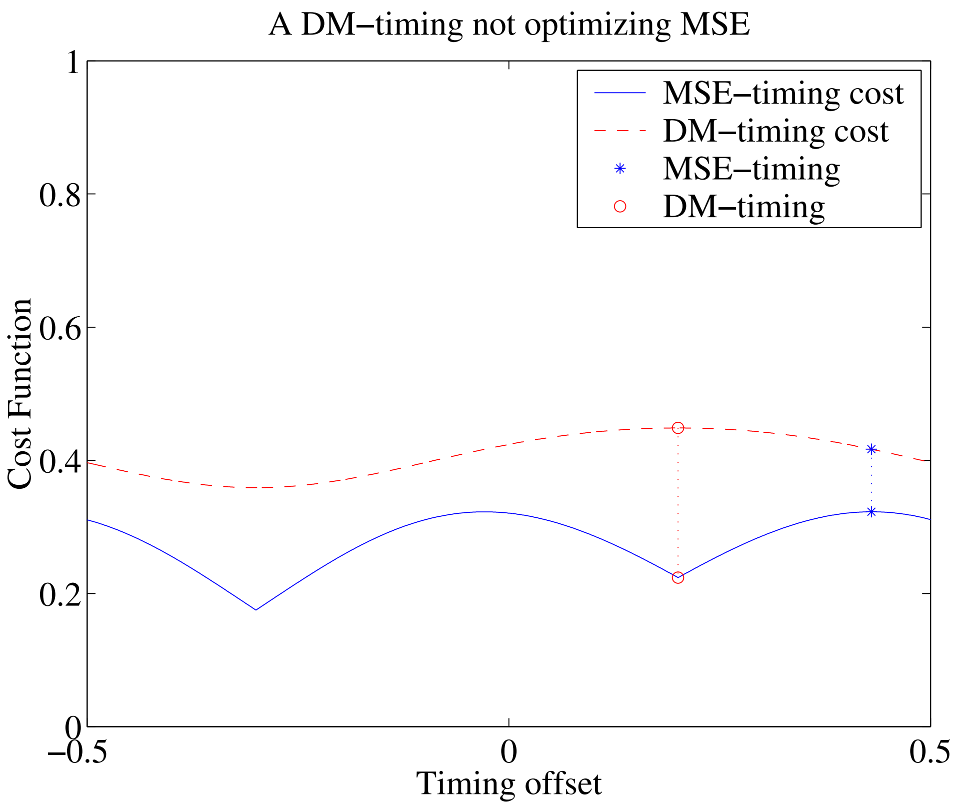

Figure 2.16: A DM-timing not optimizing MSE

2.6.2 Heuristic Approach : For the single sensor case

In the previous subsection, we have shown that DM-timing can have arbitrary MSE performance depending on the location and the shape of the set of all attainable channel responses, $\mathcal{A}$. The set $\mathcal{A}$ is mainly determined by the multipath channel $m(t)$ and the pulse shape $p(t)$ in the single sensor case. In this subsection we attempt to investigate the relation between the MSE performance of the DM timing offset and the severity of the given multipath channel; the more severe multipath is the poorer the DM timing offset performs.

Evaluation Method: Instead of direct MSE evaluation of DM-timing, we *locally* compare the two cost functions

$$\frac{\|\mathrm{c}_\tau\|_4^4}{(\|\mathrm{c}_\tau\|^2+\lambda)^2} \quad \text{and} \quad \frac{\|\mathrm{c}_\tau\|_\infty^4}{(\|\mathrm{c}_\tau\|^2+\lambda)^2}, \tag{2.99}$$

by comparing the location of local maxima of

$$\|\mathrm{c}_\tau\|_4^4 \quad \text{and} \quad \|\mathrm{c}_\tau\|_\infty^4. \tag{2.100}$$

A heuristic reason for this evaluation approach is; when the functions in (2.100) are the most influential term to produce the maxima of (2.99) (which is often true at least locally), closely located maxima of (2.100) imply closely located maxima of (2.99).

Furthermore, we assume that the pulse shape function $p(t)$ has small excess bandwidth tails so that we can use the approximation of $\|\mathrm{c}_\tau\|_4^4$ in (2.73)

$$\|\mathrm{c}_\tau\|_4^4 \approx H_4(0) + 2\,|H_4(1)|\cos(2\pi\tau\angle H_4(1)), \tag{2.101}$$

assuming the sample interval $T = 1$. (Recall that $H(f)$ is the frequency domain representation of the analog channel $c(t)$ given by a multipath $m(t)$ and a pulse shape function $p(t)$, and $H_4 = H \star H \star H \star H$.) Thus, the location of maximum of the $\|c_\tau\|_4^4$ is determined by $\angle H_4(1)$.

Case 1: Pure delay

First, as a simple example consider a pure delay channel, i.e. $m(t) = \delta(t - \tau_0)$. Since $c(t)$ is a raised cosine delayed by τ_0 , $\|c_\tau\|_\infty$ is maximized at $\tau = \tau_0$. On the other hand,

$$\begin{aligned} H(f) &= e^{-j2\pi\tau_0 f} P(f), && (2.102) \\ H_4(f) &= e^{-j2\pi\tau_0 f} P_4(f). && (2.103) \end{aligned}$$

where $P(f)$ denotes the Fourier transformation of $p(t)$ and $P_4(f) = P \star P \star P \star P$. In general, we denote

$$P_n(f) = \underbrace{P \star \cdots \star P}_{n \text{ times}} \tag{2.104}$$

Since $P(f)$ is real valued, the $\angle H_4(1)$ is given by $-2\pi\tau_0$ and maximum of $\|c_\tau\|_4^4$ is attained at $\tau = \tau_0$. In this pure delay case, $\|c_\tau\|_4^4$ and the $\|c_\tau\|_\infty^4$ have maxima at the same location $\tau = \tau_0$.

Before we investigate more general cases, we establish the following useful properties.

Lemma 2.1 Let τ_0 and τ_1 denote delays in the time domain and P is real and symmetric. Then

$$i) \quad \angle(e^{-j2\pi\tau_0 f} P(f) \star e^{-j2\pi\tau_1 f} P(f)) = -2\pi f \frac{\tau_0 + \tau_1}{2}, \tag{2.105}$$

$$ii) \quad \left| e^{-j2\pi\tau_0 f} P(f) \star e^{-j2\pi\tau_1 f} P(f) \right| \to P_2(f) \text{ as } |\tau_0 - \tau_1| \to 0, \tag{2.106}$$

$$iii) \quad \left| e^{-j2\pi\tau_0 f} P(f) \star e^{-j2\pi\tau_1 f} P(f) \right| \to 0 \text{ as } |\tau_0 - \tau_1| \to \infty. \tag{2.107}$$

Proof:

$$
\begin{aligned}
& e^{-j2\pi\tau_0 f}P(f) \star e^{-j2\pi\tau_1 f}P(f) \\
& = \int_{-1}^{f+1} e^{-j2\pi\tau_0 x}P(x)e^{-j2\pi\tau_1(f-x)}P(f-x)dx && (2.108)\\
& = e^{-j2\pi f\frac{\tau_0+\tau_1}{2}} \int_{-f/2-1}^{f/2+1} e^{-j2\pi x\frac{\tau_0-\tau_1}{2}} P(x-f/2)P(x+f/2)dx && (2.109)\\
& = e^{-j2\pi f\frac{\tau_0+\tau_1}{2}} \int_{-f/2-1}^{f/2+1} \cos\left(2\pi x\frac{\tau_0-\tau_1}{2}\right) P(x-f/2)P(x+f/2)dx. && (2.110)
\end{aligned}
$$

From (2.108) to (2.109), we have used the change of variable, $\mathbf{x} \mapsto x + f/2$. For (2.110), we have exploited that $\sin(2\pi x)P(x - f/2)P(x + f/2)$ is an anti-symmetric function, since $P(x - f/2)P(x + f/2)$ is symmetric. Property i) follows from the fact that the integration portion in (2.110) is real valued. Again, from (2.110) we have

$$
\begin{aligned}
& \lim_{|\tau_0-\tau_1|\to 0} \left|e^{-j2\pi\tau_0 f}P(f) \star e^{-j2\pi\tau_1 f}P(f)\right| \\
& = \lim_{|\tau_0-\tau_1|\to 0} \left| \int_{-f/2-1}^{f/2+1} \cos\left(2\pi x\frac{\tau_0-\tau_1}{2}\right) P(x-f/2)P(x+f/2)dx \right| && (2.111)\\
& = \left| \int_{-f/2-1}^{f/2+1} P(x-f/2)P(x+f/2)dx \right| && (2.112)\\
& = P_2(f), && (2.113)
\end{aligned}
$$

which proves ii). On the other hand, from (2.109) we have

$$
\begin{aligned}
& \lim_{|\tau_0-\tau_1|\to \infty} \left|e^{-j2\pi\tau_0 f}P(f) \star e^{-j2\pi\tau_1 f}P(f)\right| && (2.114)\\
& = \lim_{|\tau_0-\tau_1|\to \infty} \left| \int_{-f/2-1}^{f/2+1} e^{-j2\pi x\frac{\tau_0-\tau_1}{2}} P(x-f/2)P(x+f/2)dx \right| && (2.115)\\
& \le \lim_{|\tau_0-\tau_1|\to \infty} \left| \int_{-f/2-1}^{f/2+1} e^{-j2\pi x\frac{\tau_0-\tau_1}{2}} dx \right| && (2.116)\\
& = \lim_{|\tau_0-\tau_1|\to \infty} |(1+f/2)\mathrm{sinc}[(\tau_0-\tau_1)(1+f/2)]| && (2.117)\\
& = 0. && (2.118)
\end{aligned}
$$

which proves *iii*). ■

Case 2: Clustered channels

Assume that the multipath channel $m(t)$ given by

$$m(t) = \sum_{i=0}^{N-1} \rho_i \delta(t - \tau_i) \tag{2.119}$$

is clustered in the sense that $|\tau_i - \tau_j| \ll 1$ for all $i \neq j$. The analog channel $c(t)$ including pulse shape $p(t)$ is given by

$$c(t) = \sum_{i=0}^{N-1} \rho_i p(t - \tau_i). \tag{2.120}$$

Since the delays are clustered with a raised cosine $p(t)$ with roll-off factor α given by

$$p(t) = \mathrm{sinc}(t) \frac{\cos(\pi \alpha t)}{1 - 4\alpha^2 t^2}, \tag{2.121}$$

we can approximate $c(t)$ as

$$c(t) \approx \sum_{i=0}^{N-1} \rho_i \mathrm{sinc}(t - \tau_i) \tag{2.122}$$

for a small roll-off factor α and for the region $|t - \tau_i| \ll 1$ for all i. Furthermore, we can apply the approximation

$$\mathrm{sinc}(x) \approx 1 - \frac{\pi^2 x^2}{6} + \frac{\pi^4 x^4}{5!} - \cdots \approx 1 - \frac{\pi^2 x^2}{8} + \frac{\pi^4 x^4}{2^4 4!} - \cdots = \cos(\frac{\pi x}{2}) \tag{2.123}$$

for $|x| \ll 1$. Actually, this approximation is quite good for $|x| < 1$ (see Figure 2.17). Thus,

$$c(t) \approx \sum_{i=0}^{N-1} \rho_i \cos(\frac{\pi}{2} t - \frac{\pi}{2} \tau_i) \tag{2.124}$$

for $\tau_0 \leq t \leq \tau_{N-1}$. Notice that (2.124) implies that $c(t)$ is locally a sum of sinusoids with different magnitudes and phases. Since the cosines in (2.124) share the same frequency, $c(t)$ can be written as a cosine locally near $\tau_0 \leq t \leq \tau_{N-1}$. Let τ_c denote the phase term of the cosine which locally approximates $c(t)$, i.e.,

$$A\cos(\frac{\pi}{2}t - \tau_c) = \sum_{i=0}^{N-1} \rho_i \cos(\frac{\pi}{2}t - \frac{\pi}{2}\tau_i). \tag{2.125}$$

Then, $A\cos(\frac{\pi}{2}t - \tau_c)$ has a maximum at $t = 2\tau_0/\pi$, and locally $\mathrm{c}(t)$ has a maximum at the same location. Therefore,

$$\arg\max \|\mathrm{c}_\tau\|_\infty^4 \approx \frac{2}{\pi}\tau_0. \tag{2.126}$$

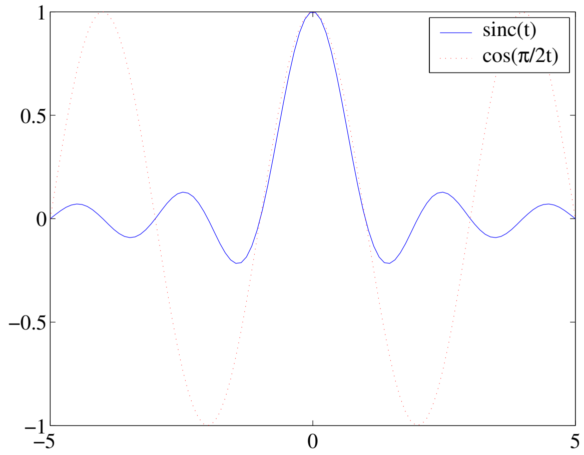

Figure 2.17: Cosine approximation for Sinc

On the other hand,

$$\begin{aligned} H_2(f) &= (\sum_{i=0}^{N-1} \rho_i e^{-j2\pi\tau_i f} P(f)) \star (\sum_{i=0}^{N-1} \rho_i e^{-j2\pi\tau_i f} P(f)) && (2.127)\\ &= \sum_{i=0}^{N-1} \rho_i^2 e^{-j2\pi\tau_i f} P_2(f) + \sum_{i\neq j} e^{-j2\pi\tau_i f} P(f) \star e^{-j2\pi\tau_j f} P(f) && (2.128)\\ &\approx \sum_{i=0}^{N-1} \rho_i^2 e^{-j2\pi\tau_i f} P_2(f) + \sum_{i\neq j} \rho_i\rho_j e^{-j2\pi f\frac{\tau_i+\tau_j}{2}} P_2(f) && (2.129)\\ &= (\sum_{i=0}^{N-1} \rho_i e^{-j\pi\tau_i f})^2 P_2(f). && (2.130) \end{aligned}$$

where in (2.129) we have used property *ii*) of Lemma 2.1 given the assumption that the multipath channel is clustered. Similarly, since P_2 is again real and symmetric, after applying Lemma 2.1 we have

$$H_4(f) \approx (\sum_{i=0}^{N-1} \rho_i e^{-j\frac{\pi}{2}\tau_i f})^4 P_4(f), \tag{2.131}$$

and consequently,

$$\angle H_4(1) \approx 4\angle(\sum_{i=0}^{N-1} \rho_i e^{-j\frac{\pi}{2}\tau_i}). \tag{2.132}$$

From the relation

$$\sum_{i=0}^{N-1} \rho_i e^{-j\frac{\pi}{2}\tau_i} = \sum_{i=0}^{N-1} \rho_i \cos(-\frac{\pi}{2}\tau_i) + j\sum_{i=0}^{N-1} \sin(-\frac{\pi}{2}\tau_i), \tag{2.133}$$

we see a connection between (2.132) and (2.124) by letting $t = 0$ in (2.124). Thus, we have

$$\sum_{i=0}^{N-1} \rho_i e^{-j\frac{\pi}{2}\tau_i} \quad = \quad A e^{-j\tau_c}, \tag{2.134}$$

$$\angle(\sum_{i=0}^{N-1} \rho_i e^{-j\frac{\pi}{2}\tau_i}) \quad = \quad -\tau_c. \tag{2.135}$$

Therefore,

$$\arg\max \|\mathrm{c}_\tau\|_4^4 \approx -\frac{4}{2\pi}\angle H_4(1) = \frac{2}{\pi}\tau_c. \tag{2.136}$$

Finally, for clustered channels, we can say

$$\arg\max \|\mathrm{c}_\tau\|_4^4 \approx \arg\max \|\mathrm{c}_\tau\|_\infty^4. \tag{2.137}$$

Simulation results suggest that this approximation is applicable as long as all $\{\tau_k\}$ are located within one symbol interval (Refer to Example 2.5 and Figure 2.19).

Case 3: Sparse channels

Now let assume the multipath $m(t) = \sum_i \rho_i \delta(t - \tau_i)$ is sparse in the sense that

$$|\tau_i - \tau_j| \gg 1 \text{ for all } i \neq j. \tag{2.138}$$

Without loss of generality, we assume that ρ_0 is the maximum multipath magnitude and $\rho_0 = 1$. The analog channel is given by $c(t) = \sum_i \rho_i p(t-\tau_i)$. Since the multipath is sparse, near the highest peak $t = \tau_0$ the contribution from the tails of other peaks can be ignored, i.e. locally at $t = \tau_0$

$$\mathrm{c}(t) \approx p(t - \tau_0). \tag{2.139}$$

Thus, we have

$$\arg\max \|\mathrm{c}_\tau\|_\infty^4 \approx \tau_0. \tag{2.140}$$

On the other hand,

$$\begin{aligned}
H_2(f) &= (\sum_{i=0}^{N-1} \rho_i e^{-j2\pi\tau_i f} P(f)) \star (\sum_{i=0}^{N-1} \rho_i e^{-j2\pi\tau_i f} P(f)) && (2.141)\\
&= \sum_{i=0}^{N-1} \rho_i^2 e^{-j2\pi\tau_i f} P_2(f) + \sum_{i \neq j} e^{-j2\pi\tau_i f} P(f) \star e^{-j2\pi\tau_j f} P(f) && (2.142)\\
&\approx \sum_{i=0}^{N-1} \rho_i^2 e^{-j2\pi\tau_i f} P_2(f) && (2.143)\\
&= \sum_{i=0}^{N-1} \rho_i^2 e^{-j2\pi\tau_i f} P_2(f). && (2.144)
\end{aligned}$$

where in (2.143) we have used property *iii*) of Lemma 2.1 given the assumption that the multipath channel is sparse. Similarly, we have

$$H_4(f) \approx \sum_{i=0}^{N-1} \rho_i^4 e^{-j2\pi\tau_i f} P_4(f), \tag{2.145}$$

and consequently,

$$\angle H_4(1) \approx \angle \sum_{i=0}^{N-1} \rho_i^4 e^{-j2\pi\tau_i}. \tag{2.146}$$

Notice that in the calculation of $\arg\max \|c_\tau\|_\infty^4$, we were able to ignore the terms $\rho_k e^{-j2\pi\tau_k}$ for $k \neq 0$. However, in (2.146) for the calculation of $\arg\max \|c_\tau\|_4^4$, we are directly facing the interference due to those terms, although their contribution has diminished by a power of 4 (recall that $\rho_k \leq 1$). One can see the relation between $\|c_\tau\|_\infty^4$ and $\|c_\tau\|_4^4$ via $H_{2^n}(1)$ when $\rho_k < 1$ for $k \neq 0$. For example,

$$H_{2^n}(f) \approx \sum_{i=0}^{N-1} \rho_i^{2^n} e^{-j2\pi\tau_i f} P_{2^n}(f), \tag{2.147}$$

$$\angle H_{2^n}(1) \approx \angle \sum_{i=0}^{N-1} \rho_i^{2^n} e^{-j2\pi\tau_i}. \tag{2.148}$$

As $n \to \infty$, $\rho_k^{2^n} \to 0$ for $k \neq 0$. The only surviving term is $e^{-j2\pi\tau_0}$, which implies $\lim_{n\to\infty} \arg\max \|c_\tau\|_{2^n} = \arg\max \|c_\tau\|_\infty$, as we expected.

The main implication of (2.146) is that the MSE performance of DM-timing is sensitive to the severity of the multipath channel and the distribution of $\{\tau_k\}$. Assuming a randomly distributed $\{\tau_k\}$, we approximately bound the deviation of $\arg\max \|c_\tau\|_4^4$ from $\arg\max \|c_\tau\|_\infty^4$ by comparing the second largest multipath tap, say ρ_1, with the most undesirable τ_1. Without loss of generality, we assume $\tau_0 = 1$ and $e^{-j2\pi\tau_1} = e^{j\frac{pi}{2}}$. Then,

$$|\angle H_4(1)| \lessapprox \angle(1 + \rho_1^4 e^{j\frac{\pi}{2}}) \tag{2.149}$$

$$= \tan^{-1}(\rho_1^4). \tag{2.150}$$

Finally, we have,

$$\left|\arg\max \|c_\tau\|_4^4\right| \lessapprox \frac{1}{2\pi} \tan^{-1}(\rho_1^4), \text{ while } \arg\max \|c_\tau\|_\infty^4 = 0. \tag{2.151}$$

Figure 2.18 illustrates the tap magnitude ρ vs. the bound given in (2.151) In the worst case, (when $\rho_1 = 1$), we have

$$\left|\arg\max \|c_\tau\|_4^4\right| \lessapprox \frac{1}{8}, \tag{2.152}$$

which gives a reference for the bound of the deviation of DM-timing from MMSE-timing (1/8 is 25% of the timing offset range $|\tau| < 1/2$). Unfortunately, the bound of the deviation of $\arg\max \|c_\tau\|_4^4$ from $\arg\max \|c_\tau\|_\infty^4$ does not hold any particular implication on its MSE performance. However, still we can make the following conclusions from this thought experiment type investigation: *i*) DM-timing tends to locate near MMSE-timing, and *ii*) severe multipath tends to degrade MSE performance of DM-timing proportional to the fourth power of the multipath tap magnitude.

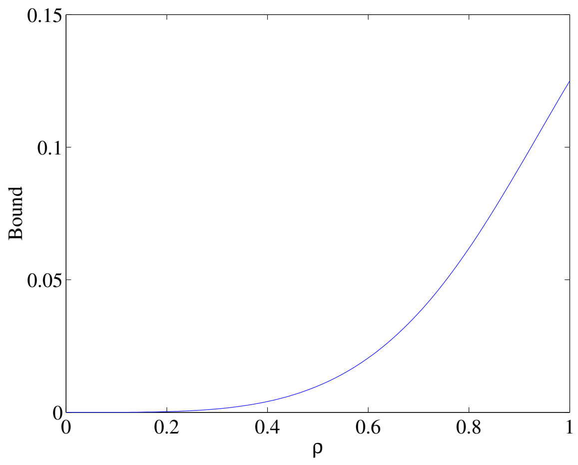

Figure 2.18: Bound of $|\arg\max \|c_\tau\|_4^4|$

Example 2.5 Consider a severe multipath channel

$$m(t) = \delta(t) + 0.8\delta(t-0.4) + \delta(t-0.8), \tag{2.153}$$

with a raised cosine pulse function with roll-off factor $\alpha = 0.3$. Figure 2.19-a) compares $\|c_\tau\|_4^4$ and $\|c_\tau\|_\infty^4$. In this plot, one can confirm that $\|c_\tau\|_4^4$ is a good approximate of $\|c_\tau\|_\infty^4$ especially near local maxima. Figure 2.19-b) shows the DM-timing cost $\|c_\tau\|_4^4/(\|c_\tau\|^2+\lambda)^2$ and MSE timing cost $\|c_\tau\|_\infty^4/(\|c_\tau\|^2+\lambda)^2$. Notice the similarity between Figure a) and Figure b), which validates the approach of comparing the ℓ_4 norm and the ℓ_∞ norm proposed in this subsection.

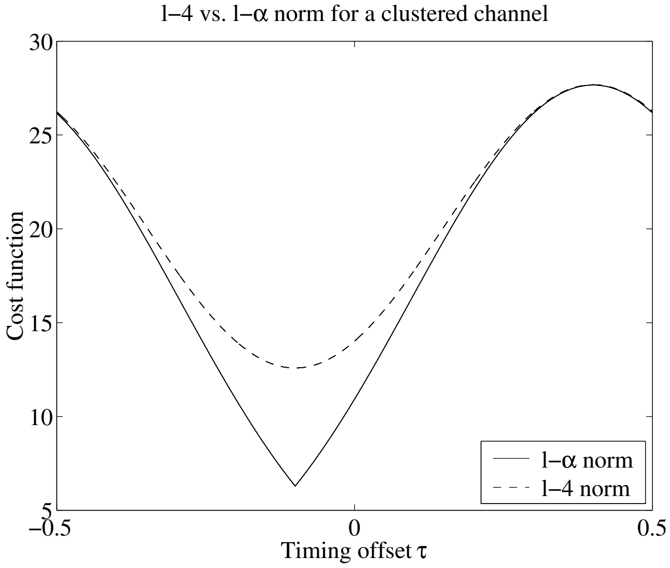

a) The ℓ_4 norm and the ℓ_∞ norm

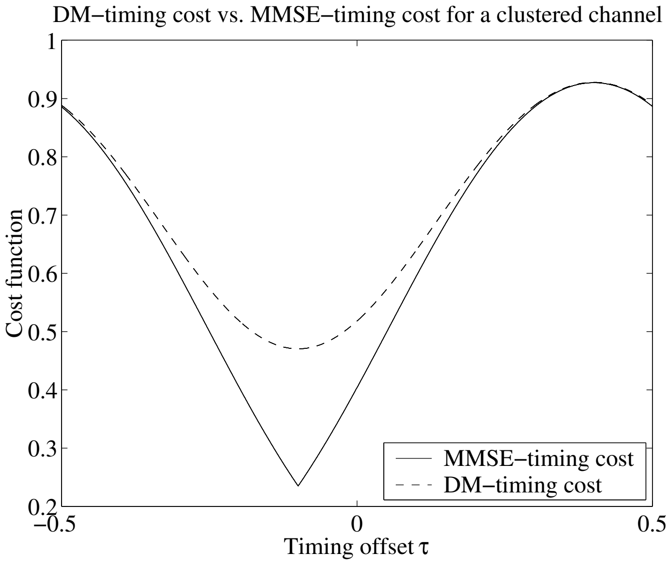

b) DM-timing and MMSE-timing costs

Figure 2.19: DM-timing and MSE-timing for a clustered channel

2.7 Conclusion

We have formulated the timing phase offset recovery problem as a channel optimization in the presence of a finite length equalizer with respect to the MSE of the equalizer output. The problem of optimally combining multisensor outputs with optimized timing offsets can also be formulated in the same framework. We studied a blind adaptive approach based on dispersion minimization in order to achieve such optimality of the timing offset. Geometrical understanding of dispersion minimization is presented in comparison with an MMSE approach. Focused on the single sensor case, the issue of unimodality of the DM-solution has been addressed. MSE performance of DM-timing has been indirectly investigated by bounding the deviation of the DM solution from a MMSE solution. We showed that for clustered multipath channels the deviation is small regardless of severity of multipath, while for sparse channels the deviation is relative to the severity of the multipath; the more severe the multipath is, the poorer MSE performance.

Appendix for Chapter 2

2.A Proofs

Proof 2.A.1 (of (2.28) : MMSE combiner parameters)

Suppose that the output of each antenna r_k is combined with weighting vector β and then equalized by a single tap equalizer f. The MSE of a multisensor combiner with respect to delay d is given by

$$MSE(\xi, f) = E\left\{\left|\sum_{m=-\infty}^{\infty}\sum_{k=0}^{N-1} f\beta_k \mathrm{c}_{\tau_k}^k[m]s_m + \sum_{k=0}^{N-1} f\beta_k \mathrm{w}_k - s_d\right|^2\right\} \tag{2.154}$$

$$\begin{aligned} &= \sigma_s^2\left|f\sum_{k=0}^{N-1}\beta_k \mathrm{c}_{\tau_k}^k[d] - 1\right|^2 + \sigma_s^2\sum_{m\neq d}\left|\sum_{k=0}^{N-1} f\beta_k \mathrm{c}_{\tau_k}^k[m]\right|^2 \\ &+ \sigma_w^2\,|f|^2\sum_{k=0}^{N-1}|\beta_k|^2 . \end{aligned} \tag{2.155}$$

Setting $\lambda = \sigma_w^2/\sigma_s^2$ and assuming $\sigma_s^2 = 1$ as usual,

$$\frac{\partial}{\partial f}MSE(\xi, f) = 2f^*\left(\sum_{m=-\infty}^{\infty}\left|\sum_{k=0}^{N-1}\beta_k \mathrm{c}_{\tau_k}^k[m]\right|^2 + \lambda\sum_{k=0}^{N-1}|\beta_k|^2\right) - 2\sum_{k=0}^{N-1}\mathrm{c}_{\tau_k}^k[d]. \tag{2.156}$$

Recall that

$$\mathrm{c}_\xi = \frac{1}{\sum_{k=0}^{N-1}|\beta_k|^2}\sum_{k=0}^{N-1}\beta_k \mathrm{c}_{\tau_k}^k .$$

Thus

$$f_{opt} = \frac{\mathrm{c}_\xi^*[d]}{||\mathrm{c}_\xi||^2 + \lambda}, \tag{2.157}$$

$$MMSE(\xi, Nf = 1) = 1 - \frac{|\mathrm{c}_\xi[d]|^2}{||\mathrm{c}_\xi||^2 + \lambda}. \tag{2.158}$$

Therefore,

$$\xi_{opt} = \arg\max_{\xi}\frac{|\mathrm{c}_\xi[d]|^2}{||\mathrm{c}_\xi||^2 + \lambda}. \tag{2.159}$$

■

Proof 2.A.2 (of (2.55) : Expansion of DM-cost function)

We will derive the cost function for a multisensor combiner case first. Then the single antenna case follows as a special case. For a given parameter set $\xi = (\tau_0, ..., \tau_{N-1}, \beta_0, ..., \beta_{N-1})$, denote $\mathrm{h} = \sum_{k=0}^{N-1} \beta_k \mathrm{c}_{\tau_k}^k$. Then the cost function (2.55) is written as

$$\begin{aligned} J(\xi) &= E\left\{\left(\left|\mathrm{h}^T s + \sum_{k=0}^{N-1} w_k \beta_k\right|^2 - \gamma\right)^2\right\} \\ &= E(\left|\mathrm{h}^T s\right|^4) + 4E\left\{\left|\mathrm{h}^T \mathrm{s}\right|^2 \left|\sum w_k \beta_k\right|^2\right\} \\ &+ E\left\{((\mathrm{h}^T \mathrm{s})^*)^2 (\sum_{k=0}^{N-1} w_k \beta_k)^2\right\} + E\left\{(\mathrm{h}^T \mathrm{s})^2 (\sum_{k=0}^{N-1} w_k^* \beta_k^*)^2\right\} \\ &+ E\left\{\left|\sum_{k=0}^{N-1} w_k \beta_k\right|^4\right\} - 2\gamma E\left\{\left|\mathrm{h}^T s + \sum_{k=0}^{N-1} w_k \beta_k\right|^2\right\} + \gamma^2. \end{aligned} \tag{2.160}$$

First, from the fact $\{s_i\}$ is i.i.d.

$$E(\left|\mathrm{h}^T \mathrm{s}\right|^4) = m_4 \sum_i \left|\mathrm{h}_i\right|^4 + 2m_2^2 \sum_{i \neq j} \left|h_i\right|^2 \left|h_j\right|^2 + \left|E(s_n^2)\right|^2 \sum_{i \neq j} h_i^2 (h_j^*)^2, \tag{2.161}$$

where m_2 is the second moment and m_4 is the fourth moment. Since we assume $\{s\}$ is circular when it is complex,

$$\left|E(s_n^2)\right|^2 \sum_{i \neq j} h_i^2 (h_j^*)^2 = \begin{cases} 0 & \text{complex case} \\ m_2^2 \sum_{i \neq j} h_i^2 h_j^2 & \text{real case} \end{cases}. \tag{2.162}$$

Therefore,

$$E(\left|h^T s\right|^4) = m_4 \sum_i \left|\mathrm{h}_i\right|^4 + \kappa_w m_2^2 \sum_{i \neq j} \left|h_i\right|^2 \left|h_j\right|^2 \tag{2.163}$$

$$= m_4 \|\mathrm{h}\|_4^4 + \kappa_w m_2^2 (\|\mathrm{h}\|^4 - \|\mathrm{h}\|_4^4) \tag{2.164}$$

$$= \eta_s m_2^2 \|\mathrm{h}\|_4^4 + \kappa_w m_2^2 \|\mathrm{h}\|^4. \tag{2.165}$$

On the other hand,

$$E\left\{((\mathrm{h}^T\mathrm{s}))^2(w_n^*\sum_{k=0}^{N-1}\beta_k^*)^2\right\} = E\left\{(\mathrm{h}^T\mathrm{s})^2\right\}E\left\{(w_n^*\sum_{k=0}^{N-1}\beta_k^*)^2\right\} \tag{2.166}$$

$$= E(s^2)E(w_k^*)^2\sum_i h_i^2\sum_k(\beta_k^*)^2. \tag{2.167}$$

Similarly,

$$E(s^2)E(w_k^*)^2\sum_i h_i^2\sum_k(\beta_k^*)^2 = \begin{cases} 0 & \text{complex case} \\ m_2\sigma_w^2\|\mathrm{h}\|^2\sum_k|\beta_k|^2 & \text{real case}\end{cases}. \tag{2.168}$$

Now, the cost function can be written as

$$\begin{aligned} J(\xi) =& \eta_s m_2^2\|\mathrm{h}\|_4^4 + \kappa_w m_2^2\|\mathrm{h}\|^4 + 2\kappa_w m_2\sigma_w^2\|\mathrm{h}\|^2\sum_k|\beta_k|^2 + E|w|^4\left(\sum_k|\beta_k|^2\right)^2 \\ &- 2\gamma m_2(\|\mathrm{h}\|^2 + \sigma_w^2\sum_k|\beta_k|^2) + \gamma^2. \end{aligned}$$

Since $\sigma_s^2 = 1$, $m_2 = 1$ and $\gamma = \kappa_s$, and $\lambda = \sigma_w^2$. Furthermore, from the definition of kurtosis κ_w,

$$E\left\{|w|^4\right\} = \kappa_w(E\left\{|w|^2\right\})^2 = \kappa_w\lambda^2. \tag{2.169}$$

Thus,

$$\begin{aligned} J(\xi) =& \eta_s\|\mathrm{h}\|_4^4 + \kappa_w\|\mathrm{h}\|^4 + 2\kappa_w\lambda\|\mathrm{h}\|^2\sum_k|\beta_k|^2 + \kappa_w\lambda^2\left(\sum_k|\beta_k|^2\right)^2 \\ &- 2\kappa_s(\|\mathrm{h}\|^2 + \lambda\sum_k|\beta_k|^2) + \kappa_s^2. \end{aligned} \tag{2.170}$$

For a single sensor case, the above cost function turns into the following

$$\begin{aligned} J(\tau,\alpha) =& \eta_s\|\alpha\mathrm{c}_\tau\|_4^4 + \kappa_w\|\alpha\mathrm{c}_\tau\|^4 + 2\kappa_w\lambda\|\alpha\mathrm{c}_\tau\|^2\alpha^2 + \kappa_w\lambda^2\alpha^4 \\ &- \kappa_s(\|\alpha\mathrm{c}_\tau\|^2 + \lambda\alpha^2) + \kappa_s^2 \end{aligned} \tag{2.171}$$

$$= \alpha^4\left(\eta_s\|\mathrm{c}_\tau\|_4^4 + \kappa_w(\|\mathrm{c}_\tau\|^2+\lambda)^2\right) - 2\alpha^2(\kappa_s\|\mathrm{c}_\tau\|^2 + \lambda) + \kappa_s^2, \tag{2.172}$$

which is (2.55). ■

Proof 2.A.3 (of Theorem 2.1)

Consider the multisensor combiner case first. From (2.170) in Proof 2.A.2, the DM-cost function jointly with a scalar equalizer can be written as

$$\begin{aligned}
J(\xi,\alpha) =& \alpha^4\eta_s\|\mathrm{h}\|_4^4 + \alpha^4\kappa_w\|\mathrm{h}\|^4 + 2\alpha^4\kappa_w\lambda\|\mathrm{h}\|^2\sum_k|\beta_k|^2 + \alpha^4\kappa_w\lambda^2\left(\sum_k|\beta_k|^2\right)^2 \\
&- 2\kappa_s\alpha^2(\|\mathrm{h}\|^2+\lambda\sum_k|\beta_k|^2) + \kappa_s^2 \\
=& \alpha^4\left(\eta_s\|\mathrm{h}\|_4^4 + \kappa_w\left(\|\mathrm{h}\|^2+\lambda\sum_k|\beta_k|^2\right)^2\right) \\
&- 2\kappa_s\alpha^2(\|\mathrm{h}\|^2+\lambda\sum_k|\beta_k|^2) + \kappa_s^2.
\end{aligned} \tag{2.173}$$

Recall that $\mathrm{h} = \sum_k \mathrm{c}_{\tau_k}^k$. Since the cost function is a quadratic of α^2,

$$\alpha_{opt}^2 = \kappa_s\frac{\|\mathrm{h}\|^2+\lambda\sum_k|\beta_k|^2}{\eta_s\|\mathrm{h}\|_4^4+\kappa_w\left(\|\mathrm{h}\|^2+\lambda\sum_k|\beta_k|^2\right)^2}. \tag{2.174}$$

Now J can be written with respect to α_{opt}^2

$$\begin{aligned}
J(\xi,\alpha_{opt}) &= \kappa_s^2-\kappa_s^2\frac{\left(\|\mathrm{h}\|^2+\lambda\sum_k|\beta_k|^2\right)^2}{\eta_s\|\mathrm{h}\|_4^4+\kappa_w\left(\|\mathrm{h}\|^2+\lambda\sum_k|\beta_k|^2\right)^2} && (2.175)\\
&= \kappa_s^2-\kappa_s^2\frac{1}{\kappa_w+\eta_s\left(\dfrac{\|\mathrm{h}\|_4^2}{\|\mathrm{h}\|^2+\lambda\sum_k|\beta_k|^2}\right)^2}. && (2.176)
\end{aligned}$$

From the definition $\mathrm{c}_\xi = \frac{1}{\sum_k|\beta_k|^2}\sum_k \mathrm{c}_{\tau_k}^k$, the only non-constant term in $J(\xi,\alpha_{opt})$ can be written as

$$\frac{\|\mathrm{h}\|_4^2}{\|\mathrm{h}\|^2+\lambda\sum_k|\beta_k|^2} = \frac{\|\mathrm{c}_\xi\|_4^2}{\|\mathrm{c}_\xi\|^2+\lambda}. \tag{2.177}$$

We assume a proper power normalization in the receiver so that most taps of c_ξ are less than 1 (because physical channels are attenuating) and consequently $\|\mathrm{c}_\xi\|_4 \leq \|\mathrm{c}_\xi\|$. Since η_s is negative, minimizing $J(\xi,\alpha_{opt})$ is same as maximizing the only non-constant term. Thus,

$$\xi_{opt} = \arg\max_\xi \frac{\|\mathrm{c}_\xi\|_4^2}{\|\mathrm{c}_\xi\|^2+\lambda}. \tag{2.178}$$

For the single sensor case is a special case of the above proof. ■

Proof 2.A.4 (of Theorem 2.2)

We use the following substitution

$$x = 2\pi\tau + \angle H_4(1), \quad 0 \le x \le 2\pi, \tag{2.179}$$

so that we have

$$\tilde{I}(x) = \frac{\sqrt{H_4 \cos(x) + G_4}}{H_2 \cos(x+\phi) + G_2}, \tag{2.180}$$

where $\phi = \angle H_2(1) - \angle H_4(1)$. Furthermore, we denote

$$K(x) = H_4 \cos(x) + G_4, \tag{2.181}$$

$$Q(x) = H_2 \cos(x+\phi) + G_2. \tag{2.182}$$

Since $\tilde{I}(x) > 0$, the unimodality of $\tilde{I}(x)$ is equivalent to that of $\tilde{I}^2(x)$. Notice that $\tilde{I}(x)$ (and thus $\tilde{I}^2(x)$ too) is a bounded function and $\tilde{I}^2(0) = \tilde{I}^2(2\pi)$. This implies that the number of minima should be same as the number of maxima. Therefore, it is sufficient to show that the derivative of $\tilde{I}^2(x)$ has only two roots, one of which is the maximum and the other one is the minimum. Consider the derivative

$$\frac{d}{dx}\tilde{I}^2(x) = \frac{K'(x)Q(x) - 2K(x)Q'(x)}{Q^3(x)}. \tag{2.183}$$

Because $Q(x) > 0$, it is enough to show that the numerator in (2.183) has only two roots. We can expand the numerator of (2.183) as

$$\begin{aligned} & K'(x)Q(x) - 2K(x)Q'(x) \\ & = 2H_2K(x)\sin(x+\phi) - H_4Q(x)\sin x \\ & = [\sin\phi 2H_2K(x)]\cos x - [H_4Q(x) - \cos\phi 2H_2K(x)]\sin x. \end{aligned} \tag{2.184}$$

We want to apply the following trigonometry identity to the above equation.

$$A\cos x + B\sin x = \sqrt{A^2+B^2}\sin(x + \tan^{-1}\frac{A}{B}). \tag{2.185}$$

In order to do that, we need to check that the coefficient terms of $\sin x$ and $\cos x$ in (2.184) are non-zero for some x.

First, observe that

$$\begin{aligned} &H_4Q(x) - \cos\phi 2H_2K(x) \\ &\qquad = H_4(G2 + H2\cos(x+\phi)) - \cos\phi 2H_2(G_4 + H_4\cos(x)) \\ &\qquad = G_2H_4 - H_2H_4\cos x\cos\phi - H_2H_4\sin x\sin\phi - 2H_2G_4\cos\phi \\ &\qquad = G_2H_4 - 2H_2G_4\cos\phi - H_2H_4\cos(x-\phi) \\ &\qquad \geq G_2H_4 - 2H_2G_4 - H_2H_4 \\ &\qquad > 0. \end{aligned} \tag{2.186}$$

where in the last step we have used the condition (2.77).

Second, when $\sin\phi = 0$, then (2.184) collapses into the following sinusoid

$$\tilde{I}^2(x) = -[H_4Q(x) - \cos\phi 2H_2K(x)]\sin x, \tag{2.187}$$

and has only two roots, since the coefficient is non-zero from (2.186). Therefore, we can assume $\sin\phi \neq 0$, which guarantees for all $x \in [0, 2\pi]$ either

$$\begin{gathered} \sin\phi 2H_2K(x) > 0, \\ \text{or} \\ \sin\phi 2H_2K(x) < 0. \end{gathered} \tag{2.188}$$

Now, we have

$$\tilde{I}^2(x) = \left(\sqrt{(H_4Q(x))^2 - 4\cos\phi H_2H_4Q(x)K(x) + (2H_2K(x))^2}\right)\sin(x - \varphi(x)), \tag{2.189}$$

where

$$\varphi(x) = \tan^{-1}\frac{\sin\phi 2H_2K(x)}{H_4Q(x) - \cos\phi 2H_2K(x)}. \tag{2.190}$$

Since the coefficient of the sin term in (2.189) is non-zero, it is sufficient to show that the sin term,

$$\sin(x - \varphi(x)), \tag{2.191}$$

has only two roots for $0 \leq x < 2\pi$ in order to prove the theorem. Notice that $\varphi(x)$ is a continuous function of $\cos(x)$ and $\cos(x + \phi)$, thus

$$\varphi(0) = \varphi(2\pi). \tag{2.192}$$

When $x - \varphi(x)$ increases strictly monotonically for $0 \leq x \leq 2\pi$, i.e.,

$$\frac{d}{dx}(x - \varphi(x)) > 0, \tag{2.193}$$

then

$$-\varphi(0) \leq x - \varphi(x) \leq 2\pi - \varphi(0), \tag{2.194}$$

and $\cos(x - \varphi(x))$ has only two roots, since

$$\frac{d}{dx}\cos(x - \varphi(x)) = -\sin(x - \varphi(x))\frac{d}{dx}(x - \varphi(x)). \tag{2.195}$$

Therefore, we need to show that

$$\frac{d}{dx}(x - \varphi(x)) > 0, \quad \text{or} \quad \frac{d}{dx}\,\varphi(x) < 1. \tag{2.196}$$

We will show that $\left|\frac{d}{dx}\,\varphi(x)\right| < 1$. Using the fact

$$\frac{d}{dx}\tan^{-1}(x) = 1/(1 + x^2), \tag{2.197}$$

we have

$$\left|\frac{d}{dx}\,\varphi(x)\right| = \left|\frac{\sin\phi 2H_2H_4(H_4Q(x)\sin(x) - H_2K(x)\sin(x+\phi))}{(H_4Q(x))^2 + (H_2K(x))^2 - 2\cos\phi(H_4Q(x))(2H_2K(x))}\right| \tag{2.198}$$

$$\leq \frac{2H_2H_4\left|H_4Q(x)\sin(x) - H_2K(x)\sin(x+\phi)\right|}{\sqrt{((H_4Q(x))^2 + (2H_2K(x))^2)^2 - (2(H_4Q(x))(2H_2K(x)))^2}} \tag{2.199}$$

$$= \frac{2H_2H_4\,|H_4Q(x)\sin(x) - H_2K(x)\sin(x+\phi)|}{(H_4Q(x))^2 - (2H_2K(x))^2} \tag{2.200}$$

$$\leq \frac{2H_2H_4(H_4Q(x) + H_2K(x))}{(H_4Q(x))^2 - (2H_2K(x))^2} \tag{2.201}$$

$$\leq \frac{2H_2H_4}{H_4Q(x) - 2H_2K(x)} \tag{2.202}$$

$$< \frac{2H_2H_4}{2H_2H_4} = 1. \tag{2.203}$$

From (2.202) to (2.203), we used the following inequality from the condition in (2.77).

$$H_4Q(x) - 2H_2K(x) = H_4H_2\cos(x+\phi) + H_4G_2 - 2H_2H_4\cos(x) - 2H_2G_4 \tag{2.204}$$

$$\geq H_4H_2 + H_4G_2 + 2H_2H_4 - 2H_2G4 \tag{2.205}$$

$$> 2H_2H_4. \tag{2.206}$$

From (2.198) to (2.199), we utilized the following inequality

$$\left|\frac{\sin\phi}{a - b\cos\phi}\right| \leq \frac{1}{\sqrt{a^2-b^2}}, \tag{2.207}$$

proof of which is given by the following. Consider

$$\frac{d}{d\phi}\frac{\sin\phi}{a-b\cos\phi} = \frac{a\cos\phi - b}{(a-b\cos\phi)^2}. \tag{2.208}$$

Therefore, $\cos\phi = b/a$ is the maxima of $\sin(\phi)/(a - b\cos\phi)$. Hence

$$\left|\frac{\sin\phi}{a - b\cos\phi}\right| \leq \frac{\sqrt{1-\frac{b^2}{a^2}}}{a - \frac{b^2}{a}} = \frac{1}{\sqrt{a^2-b^2}}. \tag{2.209}$$

■

Proof 2.A.5 (of Remark 2.1)

All the arguments before (2.198) in Proof 2.A.4 are valid under the conditions in Remark 2.1. In particular, (2.186) in Proof 2.A.4 is valid under condition *i*) in

Remark 2.1. Therefore, we resume analysis with (2.198) using the tighter conditions provided in Remark 2.1.

$$
\begin{aligned}
&\left|\frac{d}{dx}\,\varphi(x)\right| \\
&= 2H_2H_4\left|\sin\phi\frac{(G_2H_4-2H_2G_4\cos\phi)\sin(x)-H_2G_4\sin(x-\phi)+H_2H_4\sin\phi}{(H_4Q(x)-\cos\phi 2H_2K(x))^2+4H_2^2K^2(x)}\right| && (2.210)\\
&\le 2H_2H_4\left|\sin\phi\frac{(G_2H_4-2H_2G_4\cos\phi)\sin(x)-H_2G_4\sin(x-\phi)+H_2H_4\sin\phi}{(H_4Q(x)-\cos\phi 2H_2K(x))^2}\right| && (2.211)\\
&= 2H_2H_4\left|\sin\phi\frac{(G_2H_4-2H_2G_4\cos\phi)\sin(x)-H_2G_4\sin(x-\phi)+H_2H_4\sin\phi}{(G_2H_4-2H_2G_4\cos\phi-H_2H_4\cos(x-\phi))^2}\right| && (2.212)\\
&\le 2H_2H_4\left|\sin\phi\frac{(G_2H_4-H_2H_4-2H_2G_4\cos\phi)+H_2G_4+2H_2H_4}{(G_2H_4-H_2H_4-2H_2G_4\cos\phi)^2}\right| && (2.213)\\
&\le 2H_2H_4\left|\sin\phi\frac{1+H_2G_4+2H_2H_4}{(G_2H_4-H_2H_4-2H_2G_4\cos\phi)}\right| && (2.214)\\
&\le 2H_2H_4\frac{1+H_2G_4+2H_2H_4}{\sqrt{(G_2H_4-H_2H_4)^2-4H_2^2G_4^2}} && (2.215)\\
&\le 2H_2H_4\frac{1+H_2G_4+2H_2H_4}{\sqrt{2.76H_2^2G_4^2}} && (2.216)\\
&< \frac{5}{4}\,\frac{H_4+H_2H_4G_4+2H_2H_4^2}{G_4} && (2.217)\\
&< \frac{5}{4}\,\frac{G_4(0.8-H_2H_4)+H_2H_4G_4}{G_4} && (2.218)\\
&= 1.
\end{aligned}
$$

Again we have shown that $\left|\frac{d}{dx}\varphi(x)\right| < 1$. In (2.214), we used the following inequality from the condition $ii)$ in Remark 2.1.

$$
G_2H_4 - H_2H_4 - 2H_2G_4\cos\phi \le G_2H_4 - H_2H_4 + 2H_2G_4 < 1. \tag{2.219}
$$

For (2.215), we utilized the following inequality in Proof 2.A.4

$$
\left|\frac{\sin\phi}{a-b\cos\phi}\right| \le \frac{1}{\sqrt{a^2-b^2}}. \tag{2.220}
$$

From (2.216) to (2.218), we used $H_2 + 2H_2H_4^2 < G_4(0.8 - H_2H_4)$ from condition *iii*) in Remark 2.1. ■

2.B Matlab Code

This appendix contains the Matlab code used to generate simulation results reported in Example 2.1 and Figure 2.4.

```
%
%  MSE of MMSE Equalizer and Timing
%
Function []= examp21()


SNR=30;                 % SNR
lambda=10^(-SNR/10);
L=100;                  % Oversampling Rate
[c,t]=chngen(-6,19,L,[0 1.4 12.6 ],[1 0.6 -0.3],.5);
       % Generating Analog Channel raised cosine alpha =0.5


for k=1:L;
bc=c(k:L:length(c));                % Sampled channel at tau=(k-1)/L
Joem(k)=sum(bc.^2);                 % Output Energy Maximzaiton cost
Jmm(k)=max(bc.^2)/(sum(bc.^2)+lambda); % MMSE_Nf=1 cost
end


[dum tauoem]=max(Joem);   % OEM timing index
```

```
[dum taumm1]=max(Jmm);    % MMSE timing index
Tau_NF_1  =(tauoem-1)/L  % OEM timing
Tau_NF_inf=(taumm1-1)/L  % MMSE timing
coem=c(tauoem:L:length(c)); % The channel sampled at the OEM timing
cmm1=c(taumm1:L:length(c)); % The channel sampled at the MMSE timing
Lb=12;                    % Length of Feedback filter for DFE
Nf=1:1:25;                % Length of Feedforward filter

for k=1:length(Nf);       % For loop for calculation of MSE
oemmse(k)=est_mmse(coem,Nf(k),SNR);
mm1mse(k)=est_mmse(cmm1,Nf(k),SNR);
doemmse(k)=dfe_est(coem, Nf(k), Lb, lambda);
dmm1mse(k)=dfe_est(cmm1, Nf(k), Lb, lambda);
end                       % End of for loop

bestmse=zeros(1,length(Nf));
dbestmse=zeros(1,length(Nf));

for k=1:length(Nf);       % For loop for best MSE timing
  tmp1=zeros(1,L);
  tmp2=zeros(1,L);
    for kk=1:L
      bc=c(kk:L:length(c));
      tmp1(kk)= est_mmse(bc,Nf(k),SNR);
      tmp2(kk)=dfe_est(bc,Nf(k),Lb,lambda);
```

```
    end
  bestmse(k)=min(tmp1);
  dbestmse(k)=min(tmp2);
end  % End of for loop

figure(1)
plot(Nf,oemmse,'-o')
hold on
     plot(Nf,(mm1mse),'r-x')
     plot(Nf, bestmse, ':k')
hold off
legend('Optimal Timing for Nf=Infty', ...
       'Optimal Timing for Nf=1', ...
       'Optimal Timing for Nf')
title('MSE of MMSE Linear Equalizer and Timing')
     xlabel('Equalizer Length Nf')
     ylabel('MSE')

figure(2)
plot(Nf,doemmse,'-o')
hold on
     plot(Nf,dmm1mse,'r-x')
     plot(Nf,dbestmse,':k')
hold off
title('MSE of MMSE DFE and Timing')
```

```
     xlabel('Feed Foward Filter Length Nf')
     ylabel('MSE')
legend('Optimal Timing for Nf=Infty', ...
       'Optimal Timing for Nf=1', ...
       'Optimal Timing for Nf')


Function mmse=est_mmse(c,Nf,SNR);
% Estimate MMSE given channel  c
% baud spaced equalizer length Nf
% and SNR
c=c(:);
Nc=length(c);
Nh=Nf+Nc-1;
lambda= 10^(-SNR/10);
C=convmtx(c,Nf);
A=C*pinv(C'*C+lambda*eye(Nf))*C';
nmse=1-diag(A);
[nmmse delay]=min(nmse);
mmse=nmmse;


Function [c,t]=chngen(tw1, tw2,L,act,acc,alpha);
%  c=(tw1 tw2,L,act,acc,alpha);
%  Generating Oversampled channel of
```

```
%  an analog mutipath channel specified act and acc
%  with respect to a rasied cosine pulse shape.
%  tw1 tw2:   Time window, assuming Ts=1
%  L:    Oversampling factor, assuming Ts=1
%  act:  Analog channel time
%  acc:  Analog Channel Coefficients
%  alpha: roll off factor
t=(tw1:1/L:tw2) ;
c=zeros(size(t));

for k=1:length(act)
     [dummy indx]= min(abs(t-act(k)));
     dct(k)=t(indx);
     c=c+rcos(t-t(indx),alpha)*acc(k);
end



Function y=rcos(t,alpha);
% [y]=rcos(t,alpha);
%
% This function generates a Raise Cosine Pulse with
% roll off factore alpha on time t
  y=sinc(t);
if alpha > 0
 I=find((1-4*alpha^2.*t.^2));
```

```
 J=find((1-4*alpha^2.*t.^2)==0);
y(I)=y(I).*cos(pi*alpha*t(I))./(1-4*alpha^2.*t(I).^2);
y(J)=y(J).*sin(pi*alpha*t(J))./(8*alpha*t(J));
end
```

Chapter 3

Carrier phase offset correction based on dispersion minimization

This chapter presents an analysis of the performance and behavior of a blind adaptive carrier phase offset recovery scheme based on Dispersion Minimization (DM). The algorithm, called here the DM-derotator, is a kind of simple equalizer that attempts to correct just for carrier phase offset by minimizing the dispersion of the projection of the real part of the (complex) data signal. The recent application of this algorithm to digital broadcast signals motivates our analysis. This chapter classifies the stationary points of the DM-derotator for a variety of source signals including digital VSB and QAM, and discusses initialization strategies. The analysis is extended to a variety of situations including (*i*) its behavior in the presence of Inter Symbol Interference, (*ii*) its behavior when there are statistical dependencies between the in-phase and quadrature components, and (*iii*) its tracking ability.

3.1 Introduction

In modern communication systems, the demand for high data rates over band-limited channels suggests a preference for blind equalization over training sequence-based equalization schemes. However, blind equalization schemes exhibit a residual phase ambiguity [JSE+98], [TXK94] and cannot correct the phase distortion in the received signal due to a band-limited channel or carrier phase mismatch between the transceiver and the receiver [Pro95]. For two dimensional constellations, this phase offset causes a rotation of the equalizer output, which hinders the switch to decision directed (DD) adaptation. Furthermore, for VSB signals, which has been chosen for digital High Definition TV (HDTV) in the United States [Com00], the residual phase offset introduces undesirable distortion to the equalizer input signals and can degrade equalizer performance (Section 3.3-B).

Several blind algorithms based on the decision directed approach have been proposed in [MMF98],[Mac98]. However, reliable decision feedback (which assures convergence of a decision directed algorithm) is not always available, especially at the synchronization stage. A blind adaptive carrier phase offset correction algorithm, which does not rely on decision feedback, has been mentioned by S. Bellini in [Hay94](Chapter 2) and independently proposed in [CSJ00] and [TCE+01]. This algorithm minimizes the dispersion of the real component of the received signal in contrast to the MSE-based minimization of decision feedback schemes. The method can be used either before or after equalization as required by the system. Section 3.2 introduces the DM-derotator and analyzes its local minima and local maxima by studying the cost function in an ideal situation. In section 3.3, the DM-derotator is detailed for QAM and VSB sources, and several examples are given. Section 3.4 studies the behavior of the DM-derotator in less ideal situations, i.e. in the presence of inter symbol interference (ISI) and when there is statistical dependency between the in-phase and quadrature components. In section 3.5, the tracking ability of the DM-derotator is investigated using a first order approximation of a linearly time varying phase offset. The final section concludes.

3.2 DM-Derotator

This section describes a blind phase correction algorithm based on dispersion minimization. The analysis requires certain assumptions under which the cost function of the algorithm can be derived and its stationary points classified. Cases which violate these assumptions are studied in section 3.4. A variant of the algorithm, which utilizes a single complex tap is also considered at the end of this section.

3.2.1 DM-Derotator Algorithm

Suppose that a complex random sequence $\{s\}$ drawn from a finite constellation with known statistical properties suffers from an unknown constant phase offset Φ in the presence of white complex Gaussian noise $\{w\}$. Consider the measured output

$$y = se^{i\Phi} + w.$$

In order to estimate Φ and directly remove this offset, consider the single tap derotator shown in Figure 3.1, where ϕ represents an estimate of Φ, and the arrow represents a way of iteratively updating ϕ. This can be viewed as the problem of equalizing a scalar channel, but conventional blind equalization techniques are not feasible due to their phase ambiguity [JSE+98], [TXK94]. Instead, we focus on the projection of the real part of the received signal y.

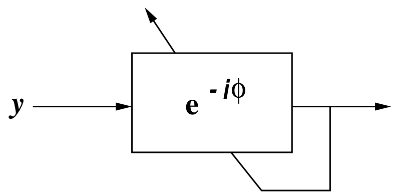

Figure 3.1: One Tap Derotator

In the absence of noise and ISI, and if ϕ were exactly equal to Φ, then the projection of y onto the real axis would consist of a collection of points at the (real part of the) symbol values defined by the constellation from which s is drawn. In the presence of noise and ISI, the projection will consist of a number of clusters centered at these symbol values. When ϕ is somewhat different from Φ, the clusters widen. Thus, a sensible criterion for estimating Φ is to try and minimize the dispersion of the projection of the constellation onto the real axis. Formally, consider the cost function, which is named the *Dispersion Minimization Derotator* (DMD) cost function,

$$J = E\left\{(\Re(ye^{-i\phi})^2 - \gamma)^2\right\}, \tag{3.1}$$

where γ (which shall be referred to as the DMD constant) is a real constant and $\Re(\cdot)$ denotes the real projection operator (i.e. $\Re(a+bi) = a$). For many signal constellations, the ϕ that minimizes $J(\phi)$ will be equal to Φ, but for some signal constellations the dispersion can be made even smaller by projecting onto a line other than the real axis. For example, section 3.4.2 shows that the V29 signal constellation minimizes $J(\phi)$ when $\phi = \Phi + \frac{\pi}{4}$.

Using a stochastic gradient algorithm [TJL01] to minimize (3.1) gives the DM-derotator algorithm

$$\phi_{k+1} = \phi_k - \mu\ (\Re(ye^{-i\phi_k})^2 - \gamma)\ \Re(ye^{-i\phi_k})\ \Im(ye^{-i\phi_k}), \tag{3.2}$$

which exploits the fact that $\frac{\partial}{\partial\phi}\Re(ye^{-i\phi_k}) = -\Im(ye^{-i\phi_k})$, where $\Im(\cdot)$ denotes projection onto the imaginary axis, i.e., $\Im(a+bi) = b$.

The application of this algorithm to QAM signals has been suggested by S. Bellini which can be found in [Hay94], and simulations in [SCG91] indicate good performance even in the presence of large phase offsets. The application to VSB signals is considered in [CSJ00] and [TCE$^+$01]. Together, these studies motivate a more complete analysis.

3.2.2 Terminology and Assumptions

One of the most revealing ways to understand the behavior of an algorithm such as (3.2) is to study the cost function (or error surface) over which the algorithm evolves. In order to describe the cost function efficiently, some terminology is required.

For a random sequence $\{s\}$, let m_2 and m_4 denote the second moment and the fourth moment, i.e.

$$m_2 := E\left\{|s|^2\right\}, \quad m_4 := E\left\{|s|^4\right\}. \tag{3.3}$$

Furthermore, let $\{s_R\}$ and $\{s_I\}$ denote the real part and the imaginary part of the sequence $\{s\}$ respectively.

$$s_R = \Re(s), \quad s_I = \Im(s).$$

The DM-derotator cost function (3.1) will be studied based on the following assumptions, which are commonly accepted as appropriate for communication systems.

Assumption 3.1

i) $\{s_R\}$ and $\{s_I\}$ are zero-mean and sub-Gaussian, i.e. their kurtoses, κ_{s_R} and κ_{s_I}, are each less than 3.

ii) The noise $\{w\}$ is complex circular white Gaussian.

iii) The source $\{s\}$ and the noise $\{w\}$ are independent.

3.2.3 Analysis of the Cost Function in an Ideal Scenario

A variety of constellation sets are used in communication systems to transmit information, and the transmitted signals usually suffer from multipath interference. Depending on the constellation and the multipath channel, the statistical properties of the received signals change, and the DM-derotator cost function may behave differently. Since an exhaustive study of the cost function for each situation would be impractical, this section considers a class of ideal situations which simplify the analysis. Certain non-ideal situations of practical significance will be treated separately in the following sections. The assumptions required in this section are:

Assumption 3.2 (Ideal Situation)

i) The second cross-moment is separable, i.e,

$$E\left\{{s_R}^2{s_I}^2\right\} = E\left\{{s_R}^2\right\}E\left\{{s_I}^2\right\}. \tag{3.4}$$

ii) Most cross-moments vanish,

$$E\left\{{s_R}^k{s_I}^m\right\} = 0,\ \text{if } k \neq 2,\ m \neq 2 \text{ and } 0 < k, m \leq 3. \tag{3.5}$$

iii) The variance of the real and imaginary parts of the signal are the same,

$$E\left\{{s_R}^2\right\} = E\left\{{s_I}^2\right\}. \tag{3.6}$$

In the absence of ISI, most common constellations (such as n^2-QAM and VSB signals) satisfy the above assumptions (e.g. see Proof 3.A.1 in appendix to this chapter). Under these assumptions, the DM-derotator cost function has well defined maxima and minima.

Property 3.1 (Stationary Points of the DMD) Under Assumption 3.1 and 3.2, the DMD cost function has the following stationary points:

$$\begin{aligned} &\text{Local Minima:} \quad \theta = 0, \pi/2, \pi, 3\pi/2, \text{ and } 2\pi. \\ &\text{Local Maxima:} \quad \theta = \pm \sin^{-1}\sqrt{\frac{\eta_{s_R}}{\eta_{s_R}+\eta_{s_I}}}. \end{aligned} \tag{3.7}$$

Proof: The cost function (3.1) can be rewritten as

$$J(\theta) \quad = \quad E\left\{(\Re(se^{i\theta}+\omega e^{-i\phi})^2-\gamma)^2\right\}.$$

Because ω is complex circular Gaussian, its statistics are the same as those of $\omega e^{-i\phi}$. Hence, we have

$$J(\theta) \quad = \quad m_{R4}\cos^4\theta + m_{I4}\sin^4\theta + \frac{3m_2^2}{2}\sin^2 2\theta - 2\gamma(m_2+\sigma^2)+\sigma_4+\gamma^2,$$

where $\sigma^2 = E\left\{\Re(w)^2\right\}$, $\sigma_4 = E\left\{\Re(w)^4\right\}$, $m_2 = E\left\{{s_R}^2\right\} = E\left\{{s_I}^2\right\}$, $m_{R4} = E\left\{{s_R}^4\right\}$, and $m_{I4} = E\left\{{s_I}^4\right\}$. The derivative of J is

$$\frac{\partial}{\partial\theta}J \quad = \quad -2m_2^2(\eta_{s_R}+\eta_{s_I})\sin 2\theta\left\{\sin^2\theta - \frac{\eta_{s_R}}{\eta_{s_R}+\eta_{s_I}}\right\}.$$

Since $\eta_{s_R}, \eta_{s_I} > 0$, the stationary points of J occur at θ for which $\sin 2\theta = 0$ and $\sin\theta = \pm\sqrt{\eta_{s_R}/(\eta_{s_R}+\eta_{s_I})}$. The second derivative of J is given as

$$\frac{\partial^2}{\partial\theta^2}J \quad = \quad -4m_2^2(\eta_{s_R}+\eta_{s_I})\cos 2\theta\left\{\sin^2\theta - \frac{\eta_s}{\eta_{s_R}+\eta_{s_I}}\right\} - 2m_2^2(\eta_{s_R}+\eta_{s_I})\sin^2 2\theta.$$

Notice that for the stationary points $\left\{\theta | \sin^2\theta = \eta_{s_R}/(\eta_{s_R}+\eta_{s_I})\right\}$ the second derivative (3.8) is always negative. This shows that they are local maxima, and consequently that $\{\theta | \sin 2\theta = 0\}$ are local minima. ■

Remark: Observe that the local minima of the DMD cost function are points to which, on average, the DM-derotator algorithm will converge.

The analysis shows that the algorithm yields a desired local minimum at $\theta = 0$, however, with a possible ambiguity of 90°. For some sources (such as n^2-QAM) this ambiguity is irrelevant, but for other source signals (such as VSB) it may cause undesirable local minima. Furthermore, like a CMA equalizer [JSE+98], the performance of this algorithm is dependent on the kurtosis of the source. Notice that as $\eta_{s_R}, \eta_{s_I} \to 0$, the cost function becomes flat, which implies that the performance of the DM-derotator degrades as the source approaches Gaussian.

Equation (3.8) shows that the DMD constant γ contributes only to the constant term in the cost function, and hence it does not change the dynamics of the cost function. Thus, γ can be arbitrarily chosen. In practice, γ should be chosen to minimize the excess mean squared error, but in subsequent sections γ will be set to 0 to further simplify the analysis.

3.2.4 DMD Without Norm Constraint

The DM-derotator, by adjusting only the value of ϕ in $e^{i\phi}$, essentially constrains the magnitude of the tap to unity. This causes the update term to require the calculation of trigonometric functions , which involves some implementation complexity. This constraint can be relaxed by using a single complex tap update with the cost function

$$J(\mathrm{f}) = E\left\{(\Re(y\mathrm{f}^*)^2 - \gamma)^2\right\}, \tag{3.8}$$

which leads to the stochastic descent algorithm

$$\mathrm{f}_{k+1} = \mathrm{f}_k + \mu\ (\Re(y\mathrm{f}_k^*)^2 - \gamma)\ \Re(y\mathrm{f}_k^*)y. \tag{3.9}$$

The DMD constant γ must now be adjusted to keep the power gain of the derotator at unity. In conventional CMA equalizers, setting $\gamma = m_4/m_2$ achieves unity output power [JSE+98]. For the DM-derotator, γ can be set to either $\gamma = m_{R4}/m_2$ or $\gamma = m_{I4}/m_2$. When $\kappa_{s_R} \neq \kappa_{s_I}$, i.e. the real and the imaginary parts are not statistically symmetric, the choice of γ from the above two is roughly equivalent to setting a preference between the real and the imaginary directions. This will be clarified later.

Since the gradient system is identical regardless of the choice of the coordinate system, the cost function can be analyzed in polar coordinates by letting f $= re^{i\theta}$. Then, we have

$$\begin{aligned} J(re^{i\theta}) =& m_{R4}r^4\cos^4\theta + m_{I4}r^4\sin^4\theta + \frac{3m_2^2r^4}{2}\sin^2 2\theta + 3r^4\sigma^2 \\ & - 2r^2\gamma(m_2+\sigma^2) + \gamma^2, \end{aligned} \tag{3.10}$$

$$\frac{\partial}{\partial\theta}J = - 2m_2^2r^4(\eta_{s_R}+\eta_{s_I})\sin 2\theta\left\{\sin^2\theta - \frac{\eta_{s_R}}{\eta_{s_R}+\eta_{s_I}}\right\}, \tag{3.11}$$

$$\frac{\partial}{\partial r}J = 4r\left[r^2m_2^2\left(\kappa_{s_R}\cos^4\theta + \kappa_{s_I}\sin^4\theta + \frac{3}{2}\sin^2 2\theta + 3\frac{\sigma^2}{m_2^2}\right) - \gamma(m_2+\sigma^2)\right]. \tag{3.12}$$

Notice that in the angular direction θ, the cost function has the same local minima and local maxima as in Property 3.1. In the radial direction r, there is a local maximum at $r = 0$ and a minima surface at

$$r^2 = \frac{\gamma(1+\sigma^2/m_2)}{m_2(\kappa_{s_R}\cos^4\theta + \kappa_{s_I}\sin^4\theta + \frac{3}{2}\sin^2 2\theta + 3\sigma^2/m_2^2)}. \tag{3.13}$$

By letting $\gamma = \kappa_{s_R}m_2 = m_{R4}/m_2$ (provided that the real part is the reference direction), we can specify radial values for each local minimum given in Property 3.1. Assuming $m_2^2 = 1$ (i.e., a normalized source)

$$r^2 = \begin{cases} \kappa_{s_R}\dfrac{1+\sigma^2}{\kappa_{s_R}+3\sigma^2} & \text{for } \theta = 0,\ \pi. \\[2ex] \kappa_{s_R}\dfrac{1+\sigma^2}{\kappa_{s_I}+3\sigma^2} & \text{for } \theta = \pi/2,\ 3\pi/2. \end{cases}$$

Notice that in the absence of noise ($\sigma^2 = 0$), r^2 is given by

$$r^2 = \begin{cases} 1 & \text{for } \theta = 0,\ \pi. \\ \dfrac{\kappa_{s_R}}{\kappa_{s_I}} & \text{for } \theta = \pi/2,\ 3\pi/2. \end{cases} \tag{3.14}$$

Thus, the gain at $\theta = 0$, and at $\theta = \pi$, is unity as desired, while the gain at $\theta = \pi/2$, and at $3\pi/2$, is the ratio of the kurtoses between the real and the imaginary parts. The different values of r for different local minima can be used to discern the (possibly undesirable) convergence to the local minima at $\theta = \pi/2$, $\theta = 3\pi/2$ by monitoring $||\mathrm{f}||^2$ as shown in Example 3.3.2.

3.3 Examples

3.3.1 For n^2-QAM signals

For an n^2-QAM source, the real and the imaginary components are independent with identical distributions. Thus, in the absence of ISI, the received n^2-QAM signal satisfies Assumption 3.2. With the DMD constant $\gamma = 0$, the cost function in (3.8) simplifies to

$$J = \frac{m_2^2}{2}\eta_s \sin^2 2\theta + m_4 + 3\sigma^2, \tag{3.15}$$

which is plotted in Figure 3.2 as a function of the kurtosis of the source. Notice that the cost surface is symmetric about $\pi/2$ due to the statistical homogeneity of the real and the imaginary components of the QAM signal.

3.3.2 For digital VSB signals

For digital VSB sources, the real component is an independent and identically distributed (i.i.d.) PAM source and the complex component is generated by the discrete

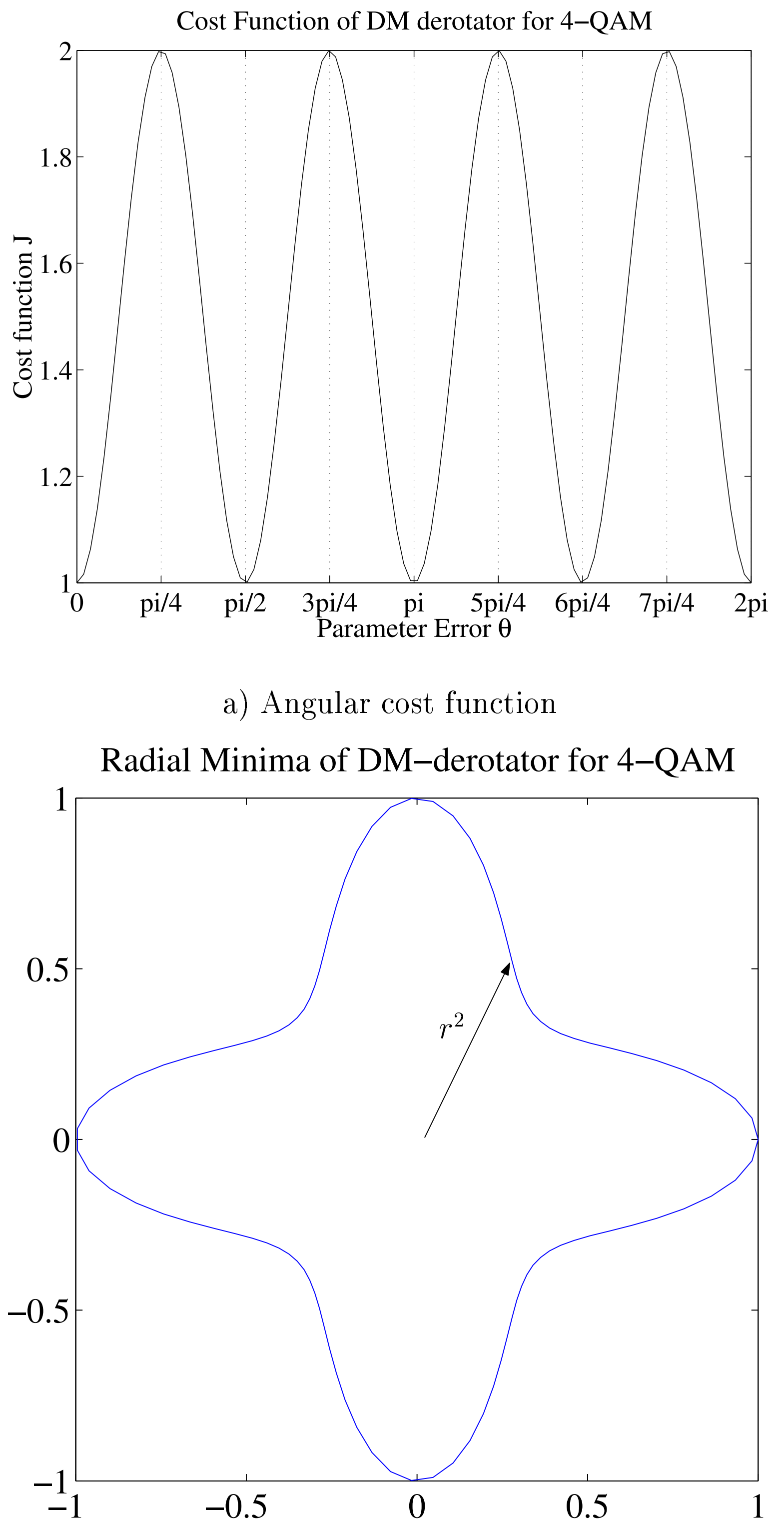

a) Angular cost function

b) Radial Minima

Figure 3.2: The Cost function of DM-derotator for 4-QAM

Hilbert transform of the real component [Pro95], i.e.

$$y[k] = s_R[k]\cos\phi + s_I[k]\sin\phi,$$

and

$$s_I[k] = \sum_{n=-\infty}^{\infty} h[n]s_R[k-n], \tag{3.16}$$

where $h[k]$ is the discrete Hilbert transform filter given explicitly in (3.40) of Proof 3.A.1 in the appendix to this chapter. The relation between the output sequence $\{y_k\}$ and the source sequence $\{s_k\}$ is represented by a non-casual IIR linear system

$$\mathrm{y} = (\cos\phi + \sin\phi\,\mathrm{h}) \star \mathrm{s},$$

where s, y, and h denote the sequence of source, output and Hilbert transform filters in vector form, $\star$ denotes the convolution operator, and the time indices have been suppressed for notational simplicity. Since $\mathrm{h}^{-1} = -\mathrm{h}$, the phase offset can be corrected by a non-casual IIR filter based on

$$(\cos\phi + \sin\phi\,\mathrm{h})^{-1} = \cos\phi - \sin\phi\,\mathrm{h}.$$

When ISI is present channel responses are incorporated in (3.17) to give

$$\mathrm{y} = (\cos\phi\,\mathrm{c}_R + \sin\phi\,\mathrm{h} \star c_I) \star \mathrm{s},$$

where c_R and c_I denote the FIR channel responses of the real and the imaginary parts respectively. Thus, a blind equalization algorithm not only attempts to equalize the channel response, but also attempts to compensate for the phase distortion by approximating the phase offset inversion filter (3.17). While this may seem desirable, in practice this phase correction property of the equalizer can be a liability. First of all, a large number of taps are utilized to compensate for what is in reality a single parameter distortion. Too many taps will inevitably degrade the steady state performance of the equalizer and slow convergence. Second, features of the required equalizer impulse response such as sparsity cannot be exploited due to the influence of the Hilbert transform filter. This can be significant in applications such as HDTV where long equalizers are used [ECHS00]. Finally, for a decision feedback equalizer (DFE), the convolution of the Hilbert transform filter with the channel will tend to increase the magnitude of the DFE taps and may result in increased error propagation. Therefore, blind phase recovery before equalization is highly desirable for digital VSB signals.

Although the real component $\{s_R\}$ and the imaginary component $\{s_I\}$ of digital VSB signals are statistically dependent, due to the anti-symmetry of the discrete Hilbert transform filter and the i.i.d. property of the real component, they satisfy all conditions in Assumption 3.2 in the absence of ISI. Furthermore, the kurtosis of the imaginary component is given by

$$\kappa_{s_I} = 2 + \frac{\kappa_{s_R}}{3}.$$

(A proof of the above statements regarding the statistical properties of the digital VSB signal is given in Proof 3.A.1 in the appendix of this chapter.) Consequently,

$$\sqrt{\frac{\eta_{s_R}}{\eta_{s_R} + \eta_{s_I}}} = \frac{\sqrt{3}}{2}. \tag{3.17}$$

This asymmetry of source statistics between the real and the imaginary components induces an asymmetry in the cost function as shown in Figure 3.3. For digital VSB signals, $0°$ and $180°$ are desirable local minima (the resulting output is s_R), while $90°$ and $270°$ are not desirable minima (the resulting output is s_I). These minima interspersed with local maxima which occur at $60°$, $120°$, $240°$, and $300°$ from $\sin\theta = \pm\sqrt{3}/2$ as described in Property 3.1. The convergence to the undesirable local minima can be detected by monitoring the norm of DMD as described in (3.14). The ratio of the two squared norms at different local minima is given from (3.14) as

$$\frac{||\mathrm{f}||^2_{\theta=0^\circ}}{||\mathrm{f}||^2_{\theta=90^\circ}} = \frac{3\kappa_{s_R} + 9\sigma^2}{\kappa_{s_R} + 6 + 9\sigma^2}. \tag{3.18}$$

For 8-VSB signals, which are used in the American HDTV standard [Com00], $\kappa_{s_R} \approx 1.762$. For SNR from infinity to 10dB, the above ratio is approximately 0.69. On the other hand, the squared norm of a desirable local minima, $||\mathrm{f}||^2_{\theta=0^\circ}$ is quite close to 1 above 10dB SNR. Therefore, in most practical situations (e.g. with SNR larger than 10dB) it is possible to distinguish the desirable from the undesirable local minima. Once detected, an undesirable minimum can be used to direct a reinitialization of the algorithm via a simple rotation.

3.4 DMD in the Presence of Non-idealities

A received signal suffering from ISI, or one generated from a source with an inherent In-phase/Quadrature dependency may violate the conditions in Assumption 3.2. Since the DM-derotator can be applied after blind equalization for QAM, ISI may not be a significant obstacle. However, for VSB signals, ISI can degrade the performance of a DM-derotator. Consequently, this section studies the effect of ISI on the DM-derotator when applied to VSB signals before equalization.

3.4.1 VSB under Inter Symbol Interference

In the presence of ISI, VSB signals in general fail to satisfy all conditions in Assumption 3.2. For example, let the complex sequence $\{r\}$ arise from a VSB signal as in (3.17),

$$r := \mathrm{c}_R \star s_R + j\mathrm{c}_I \star s_I. \tag{3.19}$$

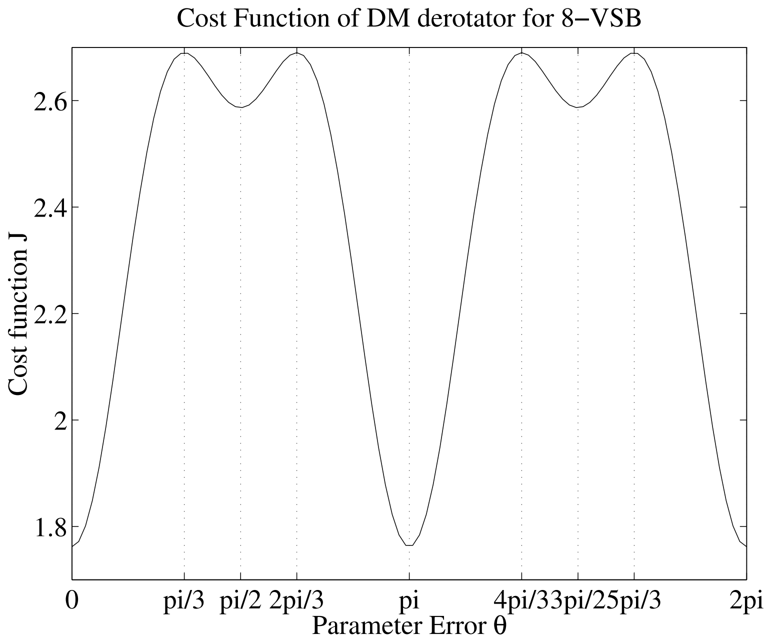

a) Angular cost function

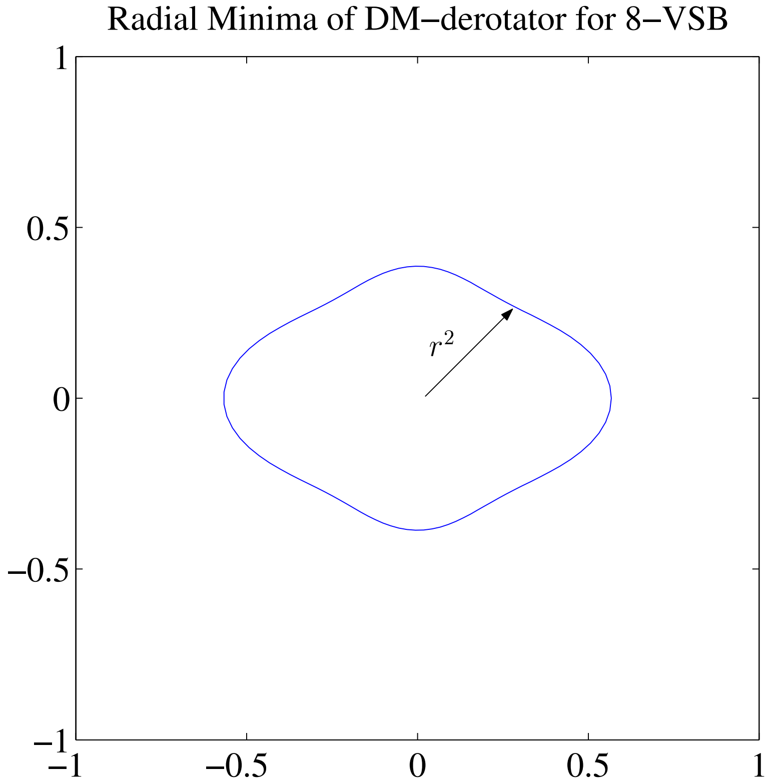

b) Radial Minima

Figure 3.3: The Cost function of DM-derotator for 8-VSB

Due to the ISI channel, $E\{r_R r_I\}$ contains the cross terms $c_R[k]c_I[k']E\{s_R[k]s_I[k']\}$. The same argument used in Proof 3.A.1 in the appendix of this chapter shows that

$$E\{s_R[k]s_I[k']\} = h[k-k']E\{{s_R}^2\}, \tag{3.20}$$

which does not vanish unless $k-k'$ is even. In this situation, the DMD cost function becomes too complicated to analyze. To succinctly observe the change of dynamics in the cost function in the presence of ISI, assume that conditions i) and ii) of Assumption 3.2 still hold, but that the third is violated, i.e. $E\{{r_R}^2\} \neq E\{{r_I}^2\}$. (Observe also that these assumptions also cover the case of multipath channels that have small $\{r_R^k r_I^m\}$ $(m, l \neq 2)$ terms and $E\{r_R^2 r_I^2\} \approx E\{r_R^2\}E\{r_I^2\}$.)

Let m_{R2} and m_{I2} denote $E\{{r_R}^2\}$ and $E\{{r_I}^2\}$ respectively, and define their ratio as ρ,

$$\rho := \frac{m_{I2}}{m_{R2}}, \quad \text{i.e., } m_{I2} = \rho m_{R2}.$$

Then the DMD cost function (3.8) in the presence of ISI can be written as

$$J_{ISI} \quad = \quad m_{R4}\cos^4\theta + m_{I4}\sin^4\theta + \frac{3}{2}\rho m_{R2}^2\sin^2 2\theta + C.$$

where C denotes a constant term. The derivative of this cost function is given by

$$\frac{\partial}{\partial\theta}J_{ISI} = -2m_{R2}^2(6\rho - \kappa_{r_I}\rho^2 - \kappa_{r_R})\sin 2\theta\left\{\sin^2\theta - \frac{3\rho - \kappa_{r_R}}{6\rho - \kappa_{r_I}\rho^2 - \kappa_{r_R}}\right\}.$$

Recall that κ_{r_R} and κ_{r_I} are the kurtosis of $\mathrm{c}_R \star s_R$ and $\mathrm{c}_I \star s_I$ respectively. As shown in Proof 3.A.1 in the appendix of this chapter, κ_{r_R} and κ_{r_I} are given by

$$\kappa_{r_R} = 3 - \kappa_{\mathrm{c}_R}\eta_{s_R}, \;\; \kappa_{r_I} = 3 - \kappa_{\mathrm{c}_I}\eta_{s_I}, \tag{3.21}$$

where

$$\kappa_{\mathrm{c}_R} := \frac{\sum \mathrm{c}_R^4[n]}{(\sum c_R^2[n])^2}, \quad \kappa_{\mathrm{c}_I} := \frac{\sum \mathrm{c}_I^4[n]}{(\sum c_I^2[n])^2}. \tag{3.22}$$

From

$$\sum \frac{\mathrm{c}^4[n]}{(\sum \mathrm{c}^2[n])^2} = \frac{\sum \mathrm{c}^4[n]}{\sum \mathrm{c}^4[n] + \sum_{n \neq n'} c^2[n]c^2[n']} \leq 1, \tag{3.23}$$

κ_{c_R} and κ_{c_I} are less than 1 and decrease as the severity of channel multipath increases. Therefore, κ_{r_R} and κ_{r_I} are larger than the original κ_{s_R} and κ_{s_I} in the presence of an ISI channel.

Notice that the dynamic system described by (3.21) changes depending on the choice of ρ in (3.21), and consequently the cost function (3.21) may have a different pattern of local minima and local maxima. All the possible stationary points of the cost function (3.21) can be classified based on ρ as the following (details are provided in Proof 3.A.2 in the appendix of this chapter).

i) For $0 < \rho < \frac{\kappa_{r_R}}{3}$ (Figure 3.4-a)),

$$\begin{aligned} &\text{Local minima:} \quad \theta = \pi/2, 3\pi/2. \\ &\text{Local maxima:} \quad \theta = 0, \pi. \end{aligned} \tag{3.24}$$

ii) For $\frac{\kappa_{r_R}}{3} < \rho < \frac{3}{\kappa_{r_I}}$ (Figure 3.4-b)),

$$\begin{aligned} &\text{Local minima:} \quad \theta = 0, \pi/2, \pi, 3\pi/2. \\ &\text{Local maxima:} \quad \theta = \pm \sin^{-1}\sqrt{\tfrac{3\rho - \kappa_{r_R}}{6\rho - \kappa_{r_I}\rho^2 - \kappa_{r_R}}}. \end{aligned} \tag{3.25}$$

iii) For $\rho > \frac{3}{\kappa_{r_I}}$ (Figure 3.4-c)),

$$\begin{aligned} &\text{Local minima:} \quad \theta = 0, \pi. \\ &\text{Local maxima:} \quad \theta = \pi/2, 3\pi/2. \end{aligned} \tag{3.26}$$

Figure 3.4 illustrates the changing J_{ISI} for an 8-VSB signal passing through a power mismatched inphase and quadrature channel, i.e.

$$\mathrm{c}_R = 1, \quad \mathrm{c}_I = \sqrt{\rho}. \tag{3.27}$$

In this case

$$\frac{\kappa_{r_R}}{3} \approx 0.573, \frac{3}{\kappa_{r_I}} \approx 1.166. \tag{3.28}$$

The only circumstances where the DM-derotator fails to converge to the desired local minima occurs within case i). The critical bound on ρ for this event is

$$\rho_c := \frac{\kappa_{r_R}}{3} = 1 - \kappa_{c_R}\frac{\eta_{s_R}}{3}, \tag{3.29}$$

which can be close to 1 as the received signals suffer from severe multipath due to decreasing κ_{c_R}. For example, for 8-VSB signals and an ISI-free channel (i.e., $\kappa_{c_R} = 1$), $\rho_c = 0.5873$. However, multipath interference can increase ρ_c. For instance, the three tap channel $\mathrm{c} = [1,\ 0.7,\ 0.5]$ increases ρ_c to 0.8225.

The DM-derotator without norm constraint behaves in a similar fashion, though exact bounds are more complicated. When ρ becomes small, the norm of the (undesirable) local minima in case i) becomes large in order to compensate for the relatively small power of the imaginary component. Comparing this to the ISI-free case in Example 3.3.2, where the norm of undesirable local minima shrinks, it is clear that monitoring the norm of the DM-derotator parameter is not helpful in the presence of severe ISI when there are significant power differences between the real and the imaginary components. However, even in the undesirable case, $\rho < \rho_c$, the DM-derotator converges to a solution exactly 90° off from the correct phase offset. Hence modest system "intelligence," such as monitoring the cluster variance of the decision device output and introducing 90° shift to the derotator, can be readily applied to overcome the convergence to undesirable local minima.

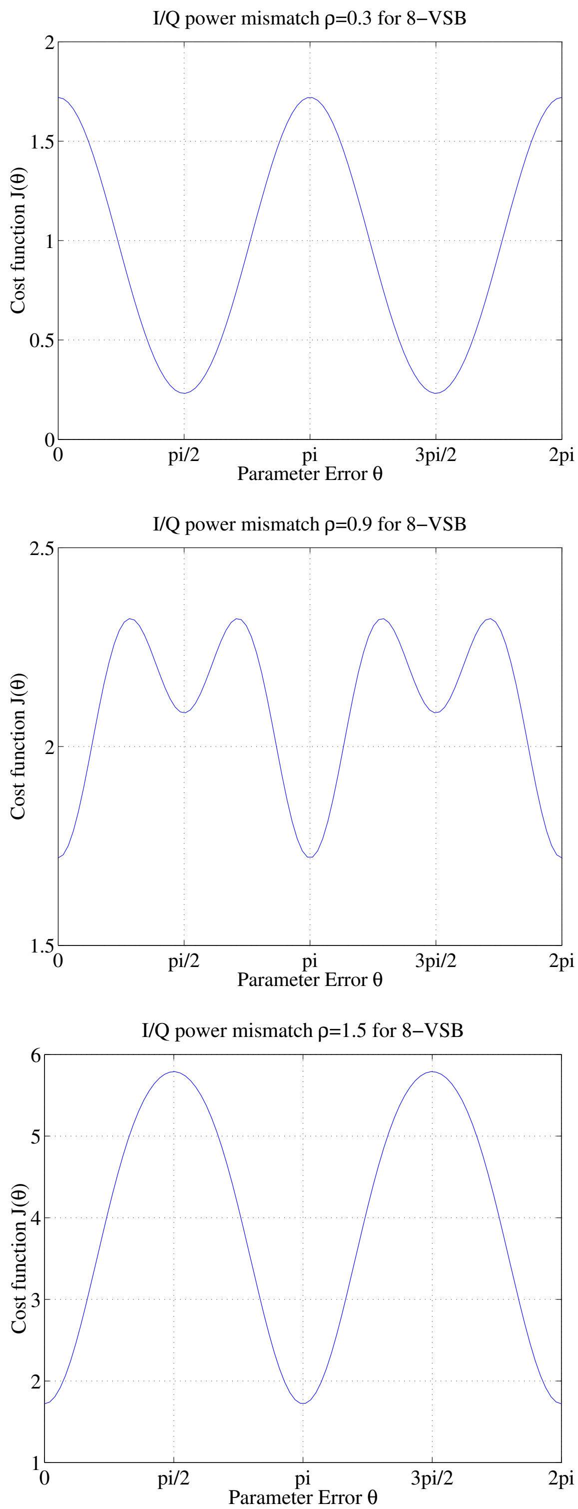

Figure 3.4: J_{ISI} for 8-VSB in the presence of I/Q power mismatch

3.4.2 In-phase and Quadrature Dependency

For QAM-type signals, due to the advantageous pre-processing by a blind equalizer, ISI is not a hindrance, but the source sequence may have inherent in-phase and quadrature dependencies. For example, in modified QAM constellations the source still has identical in-phase and quadrature components, but fails to satisfy part ii) of Assumption 3.2. Instead,

$$E\left\{{s_R}^2{s_I}^2\right\} \neq E\left\{{s_R}^2\right\} E\left\{{s_I}^2\right\} = m_2^2.$$

In this scenario, the DMD cost function (3.8) becomes

$$J_{dep} = \frac{m_2^2}{2}\left(\frac{3E\left\{{s_R}^2{s_I}^2\right\}}{m_2^2} - \kappa_s\right)\sin^2 2\theta + C,$$

where C denotes a constant term. When $E\left\{{s_R}^2{s_I}^2\right\} < m_2^2\kappa_s/3$, the sign of the $\sin^2 2\theta$ term in (3.30) changes to negative. Thus, the local minima of the cost function are located at undesirable values at $\theta = \pi/4, 3\pi/4$, while local maxima occur at the desirable values $\theta = 0, \pi/2$.

For example, the V.29 constellation (shown in Figure 3.5-a and used in the V.29 modem standard) satisfies this condition. For unit power V.29 sources

$$\begin{aligned} m_2 &= 1, && (3.30)\\ m_4 &= 4 \cdot \frac{5 \cdot 29}{3^5} \approx 2.39, && (3.31)\\ \kappa_s &= m_4 \approx 2.39, && (3.32)\\ E\left\{s_R^2 s_I^2\right\} &= \frac{2^3 \cdot 41}{3^6} \approx 0.45, && (3.33)\\ E\left\{s_R^2 s_I^2\right\} &< \frac{\kappa_s}{3} \approx 0.80. && (3.34) \end{aligned}$$

Therefore, when using a constellation such as V.29, the value of θ which minimizes the cost $J(\theta)$ of (3.30) is offset from the projection onto the real axis by 45 degrees.

Hence when applying the DMD to such a constellation, this offset can be accounted for *a priori*. Alternatively, it is possible to change the sign of the stepsize in the algorithm, effectively searching for the direction which maximizes the dispersion rather than minimizing it.

3.5 Tracking Ability of the DMD

In many applications, the phase offset may drift over time due to the frequency offset of the carrier loop. This section investigates the tracking ability of the DM-derotator in the presence of a linear phase offset under the ideal situations and assumptions of section 3.2.

Assume the phase offset is drifting linearly at a rate Ω, i.e. the true phase offset at the k-th update is given by $\Phi + k\Omega$. Define

$$\theta_k := \Phi + k\Omega - \phi_k,$$

the deviation of the estimated parameter of the DM-derotator ϕ_k from the true phase offset. From the update equation (3.2) (again without loss of generality, let $\gamma = 0$)

$$\begin{aligned}
\theta_{k+1} &= \theta_k + \Omega - \mu\Re(ye^{-i\phi_k})^2\Re(ye^{-i\phi_k})\Im(ye^{-i\phi_k}) \\
&= \theta_k + \Omega - \mu\Re(se^{i\theta_k})^2\Re(se^{i\theta_k})\Im(se^{i\theta_k}).
\end{aligned}$$

By taking the ensemble average of the above non-linear dynamic system under Assumptions 3.1 and 3.2,

$$\begin{aligned}
E\left\{\theta_{k+1}\right\} &= E\left\{\theta_k\right\} + \Omega + \mu E\left\{\Re(se^{i\theta_k})^2\Re(se^{i\theta_k})\Im(se^{i\theta_k})\right\} \\
&= E\left\{\theta_k\right\} + \Omega + \mu\frac{m_2^2}{2}E\{\sin 2\theta_k\left[(\eta_{s_R} + \eta_{s_I})\sin^2\theta_k - \eta_{s_R}\right]\}.
\end{aligned}$$

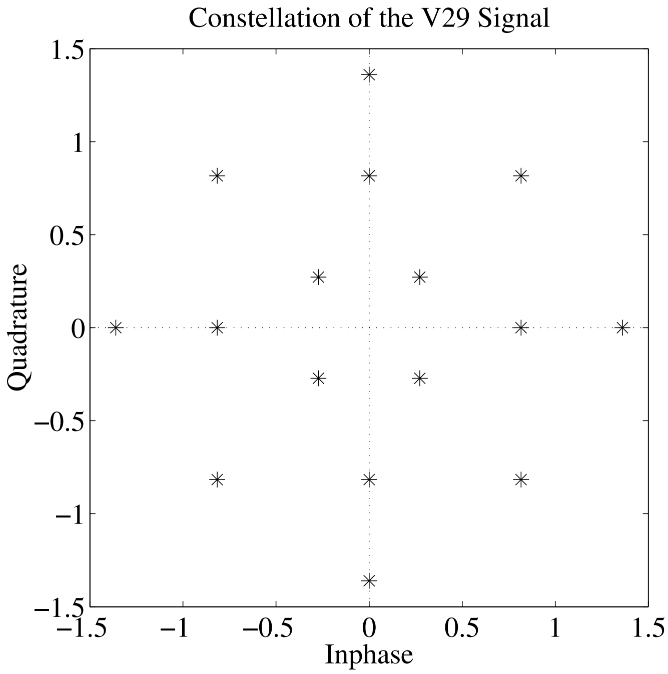

a) V29 Constellation

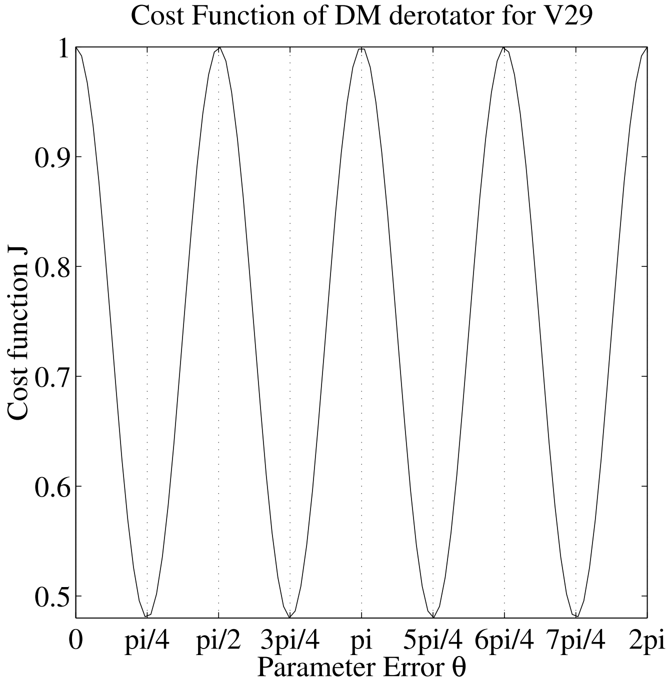

b) Cost function

Figure 3.5: The DMD cost function for V29 signal

Assume a steady state of the above system as illustrated in Figure 3.6-a) so that

$$\lim_{k\to\infty} E(\theta_{k+1}) = \lim_{k\to\infty} E(\theta_k), \tag{3.35}$$

and further assume that Ω is small enough to validate the first order approximation in the expectation term in (3.35). Then

$$\lim_{k\to\infty} E\{\sin 2\theta_k \left[(\eta_{s_R} + \eta_{s_I})\sin^2\theta_k - \eta_{s_R}\right]\} \tag{3.36}$$

$$\approx \lim_{\kappa\to\infty} E\left\{2\theta_k \left[(\eta_{s_R} + \eta_{s_I})(\theta_k)^2 - \eta_{s_R}\right]\right\} \tag{3.37}$$

$$\approx -2\eta_{s_R} \lim_{\kappa\to\infty} E\left\{\theta_k\right\}. \tag{3.38}$$

Using this first order approximation gives

$$\lim_{k\to\infty} E(\theta_k) \approx \frac{\Omega}{\mu m_2^2 \eta_{s_R}}.$$

For example, for a unit power QPSK source ($\eta_s = 2$ and $m_2^2 = 1$), $\Omega = 1 \times 10^{-4}$(radian), and $\mu = 1 \times 10^{-3}$, the steady state parameter error, $\lim_{k\to\infty} E(\theta_k)$, given by the above formula is 0.05. This agrees well with simulation results for small Ω (Figure 3.6-a). Figure 3.6-b shows the steady state parameter errors for various Ω and μ. For $\mu = 0.001$ and 0.002 the simulation results of the steady state parameter error agree with the approximation values given in (3.39) for Ω in the range between 2×10^{-5} and 2×10^{-4}. However, for $\mu = 0.0005$ the steady state parameter error deviates from the approximation values for large Ω, which shows the limit of the validity of the "small Ω assumption" in (3.39).

3.6 Conclusion

We have presented analysis of a blind adaptive phase correction algorithm based on dispersion minimization. We have derived a general cost function under acceptable

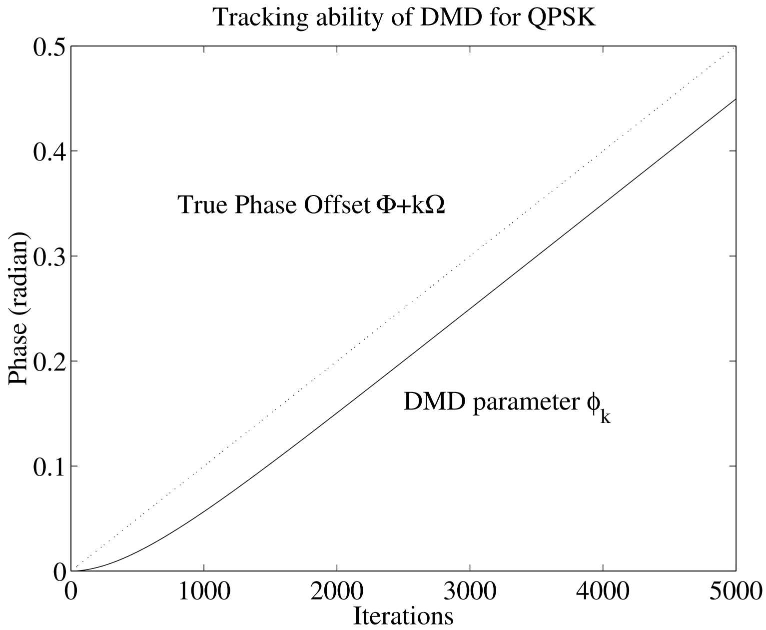

a) Tracking trace of DMD parameter

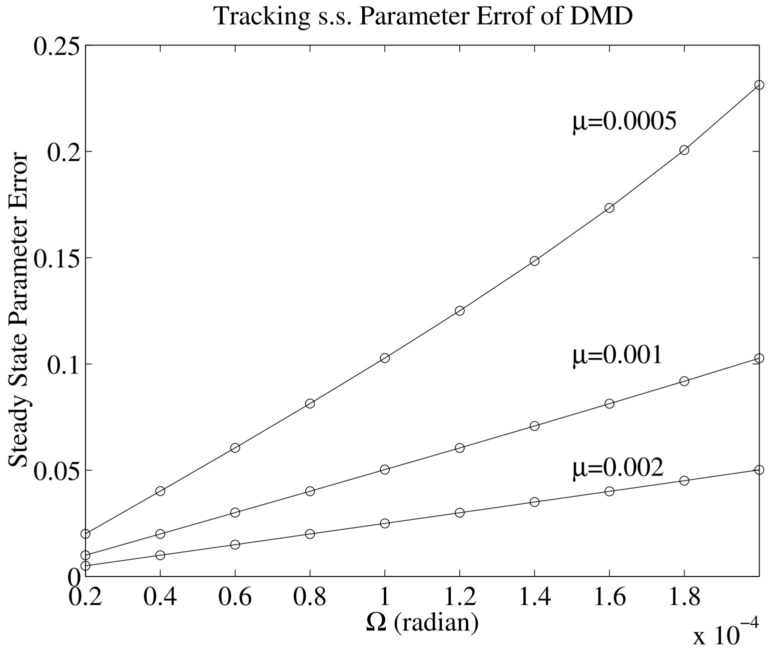

b) $\lim_{k\to\infty} E\left\{\theta_k\right\}$ for various Ω and μ

Figure 3.6: Tracking ability of DMD for QPSK

assumptions in the absence of ISI and confirmed that the DM-derotator works as expected for QAM and VSB sources. We have extended the analysis to a number of situations of practical significance, such as in the presence of ISI, to non-conventional source signals, and investigated the tracking ability of the algorithm.

Appendix for Chapter 3

3.A Proofs

Proof 3.A.1 (Statistical properties of digital VSB)

For a digital VSB signal

$$s_I[k] = \sum_{n=-\infty}^{\infty} h[n] s_R[k-n], \tag{3.39}$$

where h is the discrete Hilbert transform filter given by [OS98]

$$h[n] = \begin{cases} 2\dfrac{\sin^2(\pi n/2)}{\pi n} & \text{for } n \neq 0 \\ 0 & \text{for } n = 0 \end{cases}.$$

First,

$$\begin{aligned} E\left\{{s_R}^2[k]{s_I}^2[k]\right\} &= E\left\{{s_R}^2[k]\sum_n h[n]^2 {s_R}^2[k-n]\right\} & (3.40)\\ &\quad +E\left\{s_R[k]^2\sum_{n\neq n'} h[n]h[n']s_R[k-n]s_R[k-n']\right\} & (3.41)\\ &= \sum_{n\neq 0} h[n]^2 E\left\{{s_R}^2[k]{s_R}^2[k-n]\right\} + h[0]E\left\{{s_R}^4[k]\right\} & (3.42)\\ &= \sum_{n\neq 0} h[n]^2 E\left\{{s_R}^2[k]\right\} E\left\{{s_R}^2[k-n]\right\} & (3.43)\\ &= E\left\{{s_R}^2[k]\right\}\sum_{n\neq 0} h[n]^2 E\left\{{s_R}^2[k-n]\right\} & (3.44)\\ &= E\left\{{s_R}^2[k]\right\} E\left\{{s_R}^2[k]\right\} \|h\|^2 & (3.45)\\ &= E\left\{{s_R}^2[k]\right\} E\left\{{s_R}^2[k]\right\}, & (3.46) \end{aligned}$$

which establishes Assumption 3.2 *(i)*. The derivation has used the i.i.d property of $\{s_R\}$, $h[0] = 0$, and $\|h\| = 1$. Furthermore,

$$\begin{aligned} E\left\{s_R[k]s_I[k]\right\} &= \sum_{n\neq 0} h[n]E\left\{s_R[k]s_R[k-n]\right\} + h[0]E\left\{s_R[k]^2\right\} & (3.47)\\ &= 0. & (3.48) \end{aligned}$$

Similarly, it is not difficult to check that

$$E\left\{{s_R}^2[k]s_I[k]\right\} = E\left\{{s_R}^3[k]s_I[k]\right\} = E\left\{s_R[k]{s_I}^2[k]\right\} = E\left\{s_R[k]{s_I}^3[k]\right\} = 0,$$

$$E\left\{{s_R}^2[k]\right\} = E\left\{{s_I}^2[k]\right\},$$

which satisfies Assumption 3.2 *(ii), (iii)*.

In order to calculate the kurtosis of $\{s_I\}$, first consider a given channel c and source $\{s\}$. The kurtosis of $\{\mathrm{c} \star s\}$ is given by

$$\kappa_{\mathrm{c}\star\mathrm{s}} = 3 - \kappa_c \eta_s, \tag{3.49}$$

where $\kappa_c = (\sum_n \mathrm{c}^4[n])/\|\mathrm{c}\|^4$. The derivation is as follows

$$\begin{aligned} E\left\{(\mathrm{c}\star\mathrm{s}[k])^4\right\} &= E\left\{\left(\sum_n \mathrm{c}[n]\mathrm{s}[k-n]\right)^4\right\} && (3.50)\\ &= \sum \mathrm{c}^4[n]E\left\{\mathrm{s}[k-n]\right\} + 3\sum_{n\neq n'} \mathrm{c}^2[n]\mathrm{c}^2[n']E\left\{\mathrm{s}^2[k-n]\right\}E\left\{\mathrm{s}^2[k-n']\right\} && (3.51)\\ &= m_4\sum \mathrm{c}^4[n] + 3m_2^2(\|\mathrm{c}\|^4 - \sum \mathrm{c}^4[n]) && (3.52)\\ &= 3m_2^2\|\mathrm{c}\|^4 - (m_2^2 - m_4)\sum \mathrm{c}[n]^4, && (3.53) \end{aligned}$$

where we have used the algebraic fact that

$$\sum_{n\neq n'} \mathrm{c}^2[n]\mathrm{c}^2[n'] = \|\mathrm{c}\|^4 - \sum \mathrm{c}^4[n]. \tag{3.54}$$

On the other hand,

$$E\left\{(\mathrm{c}\star\mathrm{s}[k])^2\right\} = m_2\|\mathrm{c}\|^2. \tag{3.55}$$

Therefore,

$$\begin{aligned} \kappa_{\mathrm{c}\star\mathrm{s}} &= \frac{E\left\{E\left\{(\mathrm{c}\star\mathrm{s}[k])^4\right\}\right\}}{E\left\{(\mathrm{c}\star\mathrm{s}[k])^2\right\}^2} = \frac{3m_2^2\|\mathrm{c}\|^4 - (3m_2^2 - m_4)\sum \mathrm{c}[n]^4}{m_2^2\|\mathrm{c}\|^4} && (3.56)\\ &= 3 - \kappa_c\eta_s. && (3.57) \end{aligned}$$

Using this formula and the fact that for the discrete Hilbert transform filter, $\|h\|^2 = 1$, and

$$\sum_{n=\infty}^{\infty} h[n]^4 = \sum_{n=1}^{\infty} \frac{2 \cdot 2^4}{\pi^4 (2n-1)^4} = \frac{1}{3}, \tag{3.58}$$

which uses the summation formula [Jol61],

$$\sum_{n=1}^{\infty} \frac{1}{(2n-1)^4} = \frac{\pi^4}{3 \cdot 2^5}, \tag{3.59}$$

we finally have

$$\kappa_{s_I} = 3 - \frac{1}{3}(3 - \kappa_{s_R}) = 2 + \frac{\kappa_{s_R}}{3}. \tag{3.60}$$

■

Proof 3.A.2 (Dynamics of the DMD cost function for VSB in the presence of ISI)

The derivation of the DMD cost function in the presence of ISI yields (from (3.21)),

$$\frac{\partial J_{ISI}}{\partial \theta} = -2m_{R2}^2(6\rho - \kappa_{r_I}\rho^2 - \kappa_{r_R}) \sin 2\theta \left\{ \sin^2\theta - \frac{3\rho - \kappa_{r_R}}{6\rho - \kappa_{r_I}\rho^2 - \kappa_{r_R}} \right\}. \tag{3.61}$$

Define the following two terms which can change the dynamics of the cost function:

$$Q_1 = \frac{3\rho - \kappa_{r_R}}{6\rho - \kappa_{r_I}\rho^2 - \kappa_{r_R}}, \tag{3.62}$$

$$Q_2 = 6\rho - \kappa_{r_I}\rho^2 - \kappa_{r_R}. \tag{3.63}$$

Now we tabulate the ranges of ρ which change the signs of Q_1 and Q_2. After solving a series of quadratic equations, we summarize

Cases		Range of ρ
1) $Q_1 < 0$	1-a) $Q_2 > 0$	$(3 - \sqrt{D})/\kappa_{r_I} < \rho < \kappa_{r_R}/3^*$
	1-b) $Q_2 < 0$	$(3 + \sqrt{D})/\kappa_{r_I} < \rho$
2) $0 < Q_1 < 1$	2-a) $Q_2 > 0$	$\kappa_{r_R}/3 < \rho < \kappa_{r_I}/3$
	2-b) $Q_2 < 0$	ϕ
3) $Q_1 > 1$	3-a) $Q_2 > 0$	$3/\kappa_{r_I} < \rho < (3 + \sqrt{D})/\kappa_{r_I}$
	3-b) $Q_2 < 0$	$0 < \rho < (3 - \sqrt{D})/\kappa_{r_I}$

$$* : (3 - \sqrt{D})/k_{r_I} < \kappa_{r_R}/3 \text{ always holds.}$$

where $D = 9 - \kappa_{r_R}\kappa_{r_I}$. From the second derivative,

$$\frac{\partial^2}{\partial\theta^2} J_{ISI} \quad = \quad -4m_2^2 Q_2 \cos 2\theta \left\{\sin^2\theta - Q_1\right\} - 2m_2^2 Q_2 \sin^2 2\theta, \tag{3.64}$$

we can observe that in case 2) for the stationary points $\left\{\theta | \sin^2\theta = Q_1\right\}$

$$\frac{\partial^2}{\partial\theta^2} J_{ISI}|_{\theta=\pm\sin^{-1}\sqrt{Q_2}} = -2m_2^2 Q_2 \sin^2(2\sin^{-1}\sqrt{Q_1}) < 0, \tag{3.65}$$

and so $\left\{\theta | \sin^2\theta = Q_1\right\}$ are local maxima. For a one dimensional cost function, this implies that any stationary point located between two consecutive elements in $\left\{\theta | \sin^2\theta = Q_1\right\}$ must be a local minimum. Therefore, $\{\theta | \sin 2\theta = 0\}$ are local minima for case 2). For cases 1-a) and 3-b), the cost function behaves like a non-uniformly distorted $\cos 2\theta$ and has local maxima at $\theta = 0, \pi$ and local minima at $\theta = \pi/2, 3\pi/2$. Similarly, for cases 1-b) and 3-a) the cost function yields local maxima at $\theta = \pi/2, 3\pi/2$ and local minima at $\theta = 0, \pi$. ■

Chapter 4

Blind Carrier Frequency Offset Estimation for OFDM Systems based on Higher Order Statistics

We develop a new blind carrier frequency offset correction scheme for OFDM systems based on fourth order statistics. The proposed algorithm does not require the transmission of known signals and performs perfect frequency offset estimation and recovery under a certain condition on the channel which is satisfied for OFDM channels in practical situations. The global convergence of this algorithm to a unimodal solution can be shown to be independent of the channel ISI. Simulation results and the connection to other algorithms, such as a Maximum Likelihood(ML) approximation and dispersion minimization, are presented.

4.1 Introduction

In OFDM systems, the importance of synchronization goes beyond the conventional concept in single carrier systems as an optimal conversion from the IF analog signal to the baseband digital signal. Proper synchronization in multicarrier systems is required to maintain orthogonality of subchannels before equalization and detection. Destruction of orthogonality of subcarriers results in inter channel interference (ICI) and inter symbol interference (ISI), and consequently degrades overall system performance. Therefore, preserving the orthogonality of the subchannels is considered a central task of signal processing for multicarrier systems just as equalization is for single carrier systems [PP99].

Carrier frequency offset is one of the critical synchronization parameters in preserving orthogonality [PBM95] and numerous techniques have been developed for this task. Most existing carrier frequency offset recovery schemes rely on training sequences [LSM97], [LR96], [Moo94], [SC97], [LLG01]. However, these approaches inevitably reduce the achievable information rate and, in addition, require reliable signal-to-noise ratio (SNR) performance of the receiver which might not be feasible in the initial acquisition stage [CVC01]. To avoid this loss, several methods that do not require pilot symbols or training sequences have been proposed. These non-data aided approaches either exploit the cyclic prefix structure [DA95], [VdBSB97], [B01] or feedback from the FFT output. The feedback schemes can be further divided into an ML approximation approach [DC93], [MD01] or estimation-based approach using the second order statistics [TLZ00], [BPG02]. However, the methods using the cyclic prefix structure exhibit serious performance degradation in the presence of multipath channels. In fact, this problem occurs in most existing non-data aided methods. For example, ML approximation approaches are derived under the assumption of an ideal additive white Gaussian noise (AWGN) channel. Although simulation results promise acceptable performance for certain multipath channels [MD01], no justification of its use for multipath channels has been attempted. An ESPRIT based algorithm in [TLZ00], one of the second order statistics approaches, has an estimation ambiguity problem when the channel roots are located at null carriers. Another second order statistics approach, exploiting the existence of null subcarriers in most OFDM standards [BPG02], overcomes the performance dependency on the multipath channels without ambiguity. However, this algorithm is vulnerable to undesirable interference in the null subcarriers, which motivated the existence of null subcarriers.

In this chapter, we propose a robust blind frequency offset algorithm with channel independent performance which does not rely on null subcarriers. Instead, the proposed algorithm uses the fourth order statistics of the FFT output and, thus, overcomes drawbacks of other existing blind methods. Exploitation of higher order statistics has proven to be beneficial for blind equalization in single carrier system [Hay94], [JSE$^+$98]. Our approach can be interpreted as an extension of blind equalization techniques in single carrier systems to OFDM system in order to minimize ICI caused by inaccurate frequency offset. In Section 4.2, the system model for a discrete time OFDM system is introduced and ICI due to frequency offset is formulated. Section 4.3 proposes a frequency estimation algorithm based on the second power of the output energy and investigates its global convergence. A condition on the channels for which the algorithm succeeds is derived, and it is shown that all conventional OFDM channels satisfy the condition. In Section 4.4 several connections to other approaches, such as ML approximations, are mentioned. Section 4.5 presents simulation results and concludes.

4.2 System Model

Consider a discrete time baseband OFDM system as illustrated in Figure 4.1, where $\mathbf{s}_l = [s_{0,l} \cdots s_{N-1,l}]^T$ denotes l-th block of N samples from an identically independently distributed (i.i.d.) source data drawn from a finite alphabet set. $\mathbf{s}_l$ is transformed via an inverse discrete Fourier Transformation (IDFT) and a cyclic-prefix of length L ($[s_{N-L} \cdots s_{N-1}]^T$) is inserted. Then, it is transmitted through a multipath channel with impulse response $\mathbf{c} = [c_0 \cdots c_{N_c-1}]^t$ and additive white complex circular Gaussian noise $w(k)$, which is assumed to be uncorrelated with the source signal. $r(k)$ denotes the received signal and $\mathbf{x}_l = [x_{0,l} \cdots x_{N-1,l}]^T$ denotes the block of data after removal of the cyclic-prefix. $\mathbf{x}_l$ is now processed by a discrete Fourier Transformation (DFT) and finally the output signal $\mathbf{y}_l = [y_{0,l} \cdots y_{N-1,l}]^T$ is produced. Under the assumption that channel length does not exceed the cyclic prefix interval (i.e. $N_c \leq \mathrm{L} + 1$) and symbol synchronization is properly done, the insertion and removal operation of the cyclic prefix between enforces the channel convolution matrix C of $\mathbf{c}$ in the following relation between the source data $\mathbf{s}_l$ and the pre-DFT data $\mathbf{x}_l$

$$\mathbf{x}_l = CD^H \mathbf{s}_l + \mathbf{w}_l \tag{4.1}$$

to become a circulant matrix, i.e.

$$C = \begin{pmatrix} c_0 & c_1 & c_2 & \cdots & c_{N_c-1} & 0 & \cdots & 0 \\ 0 & c_0 & c_1 & c_2 & \cdots & c_{N_c-1} & 0 & \cdots \\ & & \ddots & & \ddots & & \ddots & \\ c_2 & \cdots & c_{N_c-1} & 0 & \cdots & 0 & c_0 & c_1 \\ c_1 & c_2 & \cdots & c_{N_c-1} & 0 & \cdots & 0 & c_0 \end{pmatrix} \tag{4.2}$$

where D denotes the DFT matrix and $\mathbf{w}_l$ denotes a vector of i.i.d. white complex circular Gaussian noises.

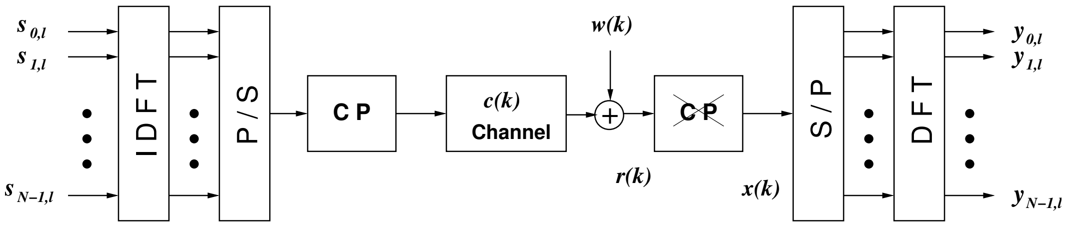

Figure 4.1: Discrete-time Multicarrier system model

In the absence of carrier frequency offset, the input-output relation for the source $\mathbf{s}_l$ and the output $\mathbf{y}_l$ can be written as

$$\mathbf{y}_l = DCD^H\mathbf{s}_l + D\mathbf{w}_l.$$

As a circulant matrix, C can be uniquely factorized as $C = D^H \Lambda D$, where Λ is a diagonal matrix, of which diagonal elements represent the DFT of the channel $\mathbf{c}$ [Dav94]. Therefore, the DFT operation diagonalizes the channel matrix and as a result we have orthogonal subchannels

$$\mathbf{y}_l = \Lambda\mathbf{s}_l + D\mathbf{w}_l. \tag{4.3}$$

However, in the presence of frequency offset ν normalized to the symbol rate (i.e. $-1/2 < \nu < 1/2$), the received signal $r(k)$ is multiplied by $e^{j2\pi\nu k/N}$ and the pre-DFT data is written as

$$\mathbf{x}_l = e^{j2\pi\nu l\frac{L+N}{N}} F_\nu C D^H \mathbf{s}_l + e^{j2\pi\nu l\frac{L+N}{N}} F_\nu \mathbf{w}_l, \tag{4.4}$$

where F_ν is a diagonal matrix representing frequency offset, defined as

$$F_\nu[k,k] = e^{j2\pi\nu\frac{k}{N}} \quad (-N/2 < \nu < N/2). \tag{4.5}$$

Notice that the block-by-block phase term $e^{j2\pi\nu l(L+N)/N}$ goes away as $\nu = 0$. Since the proposed algorithm in this chapter uses the fourth power of the output, which is invariant under block-by-block phase changes, without loss of generality, we ignore the phase term $e^{j2\pi\nu l(L+N)/N}$. Thus, the input-output relation can be written as

$$\begin{aligned}\mathbf{y}_l &= DF_\nu CD^H\mathbf{s}_l + DF_\nu\mathbf{w}_l \\ &= DF_\nu D^H\Lambda\mathbf{s}_l + DF_\nu\mathbf{w}_l.\end{aligned}$$

Due to the non-trivial F_ν, $DF_\nu D^H$ cannot be reduced to a diagonal matrix. In fact, the matrix formula, $DF_\nu D^H$, suggests that $\mathbf{y}_l$ is a discrete-time-sinc interpolation of $\Lambda\mathbf{s}_l$ with respect to the time delay ν/N. Therefore, the ICI introduced by F_ν can be quantified by an interpolation filter, i.e. in component-wise form

$$y_{n,l}(\nu) = \Lambda_n s_{n,l} I_0(\nu) + \sum_{m\neq n} \Lambda_m s_{m,l} I_{m-n}(\nu) + w_{n,l}, \tag{4.6}$$

where $I_k(\nu)$ denotes the k-th sinc-interpolation filter tap with respect to ν, which is given by

$$I_k(\nu) = \frac{1}{N}\sum_{l=0}^{N-1} e^{2\pi j\frac{l}{N}(k+\nu)} = \frac{\sin(\pi(k+\nu))}{N\sin(\pi(k+\nu)/N)} e^{\pi j\frac{N-1}{N}(k+\nu)}. \tag{4.7}$$

In (4.6), $w_{n,l}$ denotes the n-th component of $DF_\nu\mathbf{w}_l$. Because D is a unitary matrix and $\mathbf{w}_l$ is a circular complex Gaussian signal, $\{w_{n,l}\}$ is still white Gaussian, $(E\left\{w_{n,l}^* w_{n,k}\right\} = \sigma_w^2\delta(l-k))$, and uncorrelated with other subchannel noise components $(E\left\{w_{n,l}^* w_{m,l}\right\} = 0$ for $m \neq n)$.

The magnitudes of the interpolation filter impulse response $I_k(\nu)$ characterize the effect of ν on ICI. For example, observe that $|I_k(\nu)| = \delta(k)$ if and only if $\nu = 0$. In the following we summarize useful properties of I_k to develop our frequency offset correction algorithm in next section.

Property 4.1 We observe the following two properties of $I_k(\nu)$

$$i)\quad \sum_{k=0}^{N-1} |I_k(\nu)|^2 = 1, \tag{4.8}$$

$$ii)\quad \sum_{k=0}^{N-1} |I_k(\nu)|^4 = 1 - \frac{2}{3}\left(1 - \left(\frac{1}{4}\right)^{\log_2 N}\right)\sin^2(\pi\nu), \tag{4.9}$$

where in $ii)$, without loss of much generality, we assume N is a power of 2. (For a general case, the coefficient term of $\sin^2(\pi\nu)$ will be modified accordingly.)

Proof: See Proof 4.A.1 in the appendix of this chapter.

4.3 Frequency Estimation Algorithm

Consider the carrier frequency offset recovery scheme in the presence of unknown offset ν_0 illustrated in Figure 4.2. The output of the FFT is fed back to the synchronization device to produce estimate $\hat{\nu}$ of ν_0, and correct frequency offset symbol-by-symbol by multiplying by $e^{-j2\pi\hat{\nu}k/N}$ for $k = 0, ...N-1$. With this scheme perfect phase offset recovery is achieved when the parameter error, $\nu = \hat{\nu} - \nu_0$, goes to zero. We will now develop the algorithm in detail.

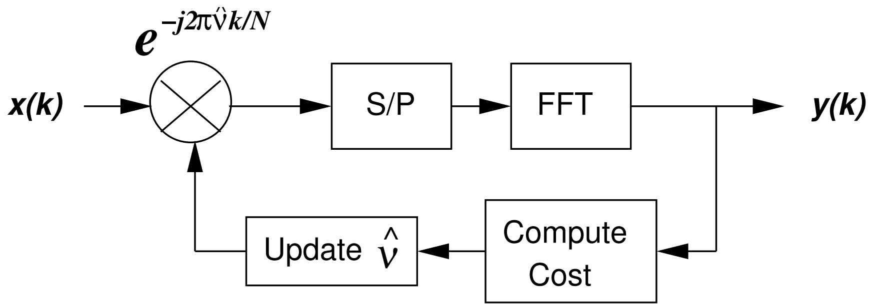

Figure 4.2: Block diagram of the proposed Carrier Frequency Offset Synchronization

4.3.1 Cost Function

Property 4.1 says that $\sum_k I_k^4(\nu)$ is a unimodal function of ν, while $\sum_k I_k^2(\nu)$ is constant. Hoping we to exploit this property, we consider the following cost function based on the fourth order statistics of the output in order to minimize ICI terms in (4.6) and consequently correct frequency offset

$$J(\nu) = \sum_{n=0}^{N-1} E\left\{|y_n(\nu)|^4\right\}. \tag{4.10}$$

Expansion of the expectation will reveal the character of this cost function:

Theorem 4.1 Consider the diagonal channel frequency response as a vector, i.e.

$$H = [\Lambda[0,0]\cdots\Lambda[N-1,N-1]]^T, \tag{4.11}$$

and let ν denote the parameter error of the carrier frequency offset estimator. Then we have,

$$i) \quad \sum_{n=0}^{N-1} E\left\{|y_n(\nu)|^2\right\} = \|H\|^2 + \sigma_w^2, \tag{4.12}$$

$$ii) \quad \sum_{n=0}^{N-1} E\left\{|y_n(\nu)|^4\right\} = \|H\|^4\kappa_s\kappa_H + 2\kappa_w\|H\|^2\sigma_w^2 + \kappa_w\sigma_w^2 - \frac{2\|H\|^4}{3}((\kappa_w+\kappa_s)\kappa_H - \kappa_w)(1-(\frac{1}{4})^{log_2 N})\sin^2(\pi\nu). \tag{4.13}$$

Proof: : See Proof 4.A.2 in the end of this chapter.

Theorem 4.1 says that the proposed cost function (4.10) is a sinusoidal function of ν with coefficient

$$-\frac{2\|H\|^4}{3}((\kappa_w+\kappa_s)\kappa_H - \kappa_w)(1-(\frac{1}{4})^{log_2 N}). \tag{4.14}$$

All terms in the coefficient in (4.14) are constant, but κ_H. Depending on the value of κ_H, the sign of (4.14) changes. Thus, (4.13), and equivalently the proposed cost function (4.10), has a unimodal minimum at $\nu = 0$ when

$$\kappa_\Lambda < \frac{\kappa_w}{\kappa_w + \kappa_s}, \tag{4.15}$$

(for example, Figure 4.3 illustrates the cost function for an ideal channel) and a unimodal maximum at $\nu = 0$ otherwise. Since for most communication sources $1 \le \kappa_s < \kappa_w$, it is enough to check if

$$\kappa_\Lambda < \frac{1}{2} \tag{4.16}$$

holds for OFDM channels in order to satisfy (4.15) and justify minimization of the cost function (4.10).

Due to the assumption that channel length N_c is less than the cyclic prefix length L (which is less than the DFT size N), the length N vector Λ is given by interpolation of a length N_c vector and consequently the "peakyness" of Λ is limited by the percentage of the cyclic prefix length. The following property states a bound on κ_H with respect to the cyclic prefix length.

Property 4.2 Suppose $\mathbf{c}$ is a length K vector and $\mathbf{y}$ is the output of an N-point DFT, $\mathbf{y} = D[c_0 \cdots c_{K-1}\, 0 \cdots 0]^T$. When $N = KM$ for an integer M, the kurtosis of $\mathbf{y}$ is bounded by $1/M$, i.e.

$$\kappa_{\mathbf{y}} \le \frac{1}{M}. \tag{4.17}$$

Proof: Proof 4.A.3 in the appendix of this chapter.

According to Property 4.2, κ_Λ does not exceed $1/2$ with a cyclic prefix length less then 50% of the symbol length. Usually the cyclic prefix length does not exceed 25% of the symbol length, and consequently the minimization of the cost function (4.10) is an appropriate strategy for correction of the carrier frequency offset.

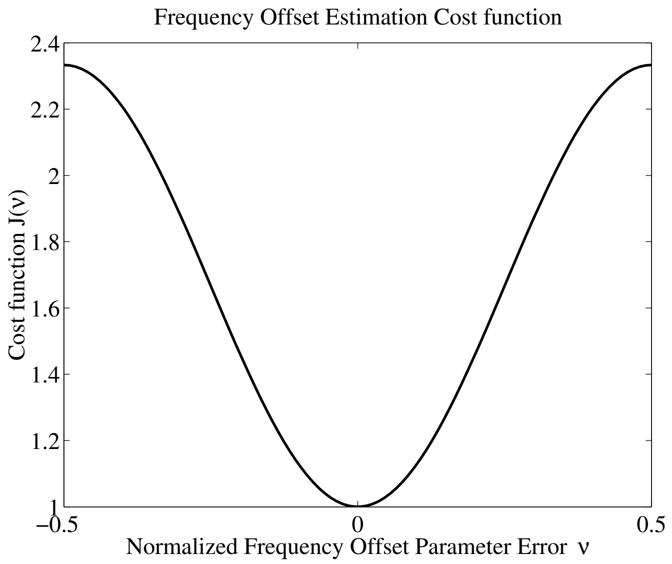

Figure 4.3: Frequency offset estimation cost function for ideal channel

4.3.2 Estimation Algorithm

We use a stochastic descent algorithm [TJL01] of the cost function (4.10) to obtain the carrier frequency offset estimate $\hat{\nu}$. The estimate is updated symbol by symbol by minimizing the instantaneous cost function, $\sum_n |y_{n,l}(\nu_0 - \hat{\nu}_k)|^4$, i.e.

$$\begin{aligned} \hat{\nu}_{k+1} &= \hat{\nu}_k - \frac{\mu}{4}\frac{\partial}{\partial \hat{\nu}} \sum_n |y_{n,l}(\nu_0 - \hat{\nu}_k)|^4 && (4.18) \\ &= \hat{\nu}_k - \mu \sum_n |y_{n,l}(\nu_0 - \hat{\nu}_k)|^2 \,\mathrm{Real}\left\{ y^*_{n,l}(\nu_0 - \hat{\nu}_k)\frac{\partial}{\partial \hat{\nu}} y_{n,l}(\nu_0 - \hat{\nu}_k)\right\} && (4.19) \\ &= \hat{\nu}_k + \mu \sum_n |y_{n,l}(\nu_0 - \hat{\nu}_k)|^2 \,\mathrm{Real}\left\{ y^*_{n,l}(\nu_0 - \hat{\nu}_k) z_{n,l}(\nu_0 - \hat{\nu}_k)\right\} && (4.20) \end{aligned}$$

,where

$$\mathbf{z}_l(\hat{\nu}_k) = D\frac{\partial}{\partial \hat{\nu}} F_{\hat{\nu}_k}\mathbf{x}_l, \quad \text{and } D\frac{\partial}{\partial \hat{\nu}} F_{\hat{\nu}_k}[m,m] = j2\pi\frac{m}{N}e^{j2\pi\hat{\nu}_k\frac{m}{N}}, \tag{4.21}$$

and μ is the step size. Therefore, one additional FFT is required in order to calculate $\mathbf{z}_l$ for the update. [MD01] circumvents this problem by introducing the following rough approximation of $\frac{\partial}{\partial \nu}\mathbf{y}_l$

$$\frac{\partial}{\partial \nu} y_{n,l}(\nu) \approx \frac{1}{2}(y_{n,l}(\nu+1) - y_{n,l}(\nu-1)) \tag{4.22}$$

$$\approx \frac{1}{2}(y_{n+1,l}(\nu) - y_{n-,l}(\nu)). \tag{4.23}$$

using the fact that $y_{n,l}(\nu+k) = y_{n+k,l}(\nu)$ in the absence of noise. In section 4.5 it will be shown that the performance of these two updates are almost the same.

4.4 Connection To the Other Algorithms

4.4.1 ML approximations

In [DC93], [MD01] the log-likelihood function for ν under the assumption of an ideal AWGN channel ($\Lambda_k = 1$) has been approximated by

$$\Gamma(\nu) = \sum_{n=0}^{N-1} \ln(1 + \frac{1}{\sigma_w^4} |y_{n,l}(\nu)|^2). \tag{4.24}$$

In [MD01] the authors attempt to directly maximize (4.24), while in [DC93] minimization of a simpler approximation, $\sum_n |y_{n,l}(\nu)|^2$, is proposed using the first order approximation, $\ln(1+x) \approx x$. However, as Theorem 4.1 indicates this quantity is constant and not a function of ν. Depending on the implementation of an OFDM system, symbol shaping may be used, and in such a case the output energy might not be constant. But still the difference from a constant cost function would be too fragile to be used for robust frequency offset estimation. Using a further finer approximation, $\ln(1+x) \approx x - \frac{x^2}{2}$, we have

$$\Gamma(\nu) \approx \frac{1}{\sigma_w^4} \sum_n |y_{n,l}(\nu)|^2 - \frac{1}{2\sigma_w^8} \sum_n |y_{n,l}(\nu)|^4 . \tag{4.25}$$

From this equation, one can interpret the approach proposed in this chapter, maximizing fourth power (4.20), as a refined closed approximation of ML-approximation for the ideal channel case. This relation provides partial explanation of the successful simulation results for multipath channels of the ML approximation algorithm in [MD01], which was developed under an AWGN channel assumption.

4.4.2 Constant Modulus Algorithm

An OFDM system can be viewed as a multi-input multi-output (MIMO) system and the distortion caused by the inaccuracy in synchronization can be modelled as a MIMO channel. In this framework, removal of ICI and ISI can be interpreted as a source separation problem. The Constant Modulus Algorithm (CMA) is a popular algorithm used for blind equalization and also source separation [JSE+98], [Car98]. Assuming an appropriate frequency domain equalizer (FEQ), minimizing the following CM cost function will attempt to reduce ICI and ISI caused by the carrier frequency offset.

$$\begin{aligned} J(\nu) &= \sum_n \beta_n E\left\{(|y_{n,l}|^2 - \gamma_n)^2\right\} && (4.26) \\ &= \sum_n \beta_n E\left\{|y_{n,l}|^4\right\} - 2\sum_n \beta_n \gamma_n E\left\{|y_{n,l}|^2\right\} + \sum_n \gamma_n^2, && (4.27) \end{aligned}$$

where $\{\beta_n\}$ is a set of weighting factors and the $\{\gamma_n\}$ are constants determined by source statistics and the frequency domain channel (H) [JSE+98]. Since the second power term, $\sum_n E\left\{|y_{n,l}|\right\}^2$, is a constant, minimizing the proposed cost function (4.10) is equivalent to minimizing CMA for $\beta_n = 1$ and $\gamma_n = 1$ in (4.27).

4.5 Simulation Results and Conclusion

Simulations have been run under the following conditions.

i) The symbols $\mathbf{s}_l$ are QPSK, i.e. $\kappa_s = 1$.

ii) An OFDM symbol consists of 64 samples.

iii) The cyclic prefix is 16 samples long (25% of symbol length).

iv) There 12 Null subcarriers.

v) The channel has 16 paths, with random phase and exponential power delay profile, i.e.,

$$E\left|c[k]\right|^2 = e^{-k/3}. \tag{4.28}$$

vi) The signal to noise ratio (SNR) is 30dB.

Figure 4.4 confirms the global convergence of this algorithm with respect to the stochastic gradient update as in (4.20). Parameter errors corresponding to different initializations converge to zero for the ideal channel in 30dB SNR. Figure 4.5 compares the two updates considered in Section 4.3.2 for a non ideal channel in 30dB SNR. For a multipath channel without FEQ the algorithm suffers from high excess MSE and thus small step size is required for reliable steady state performance. Thus, parameter trajectories in Figure 4.5 exhibit slow convergence. A gear shifting step size technique can be used in order to improve convergence speed during the transient period. Notice that the performance difference between the exact update of (4.10) and the approximated update of (4.23) is quite modest.

In conclusion, the proposed carrier frequency recovery algorithm based on the fourth power maximization performs perfect carrier frequency estimation and correction independently from the initialization. We have characterized the channels for which the fourth power maximization strategy works and shown that OFDM channels in the practical situation of less then 50% cyclic prefix satisfy the condition. In the absence of multipath channel, this fourth power minimization algorithm

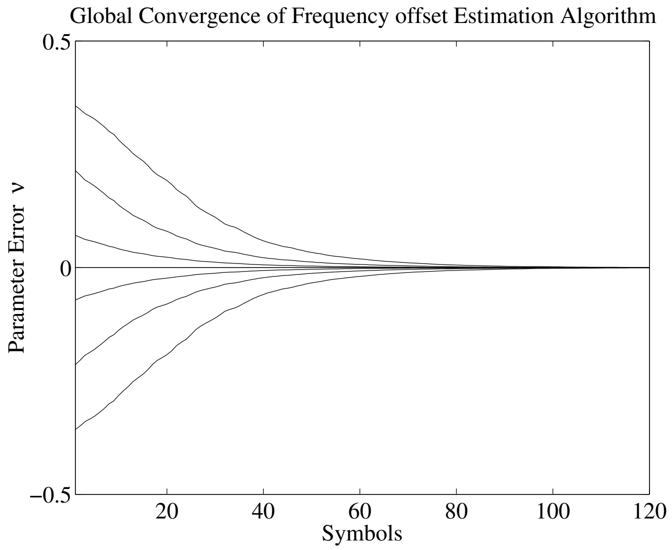

Figure 4.4: Global Convergence of Parameter Error

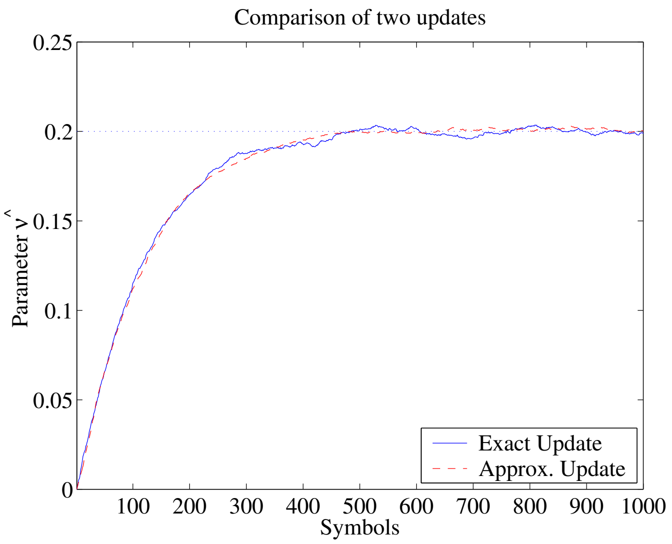

Figure 4.5: Comparison of exact update vs. approximated update

can be viewed as a ML approximation or an algorithm based on a conventional high order statistics MIMO source separation approach such as CMA. Open questions remain regarding performance analysis in the presence of Doppler shifts and multipath spread longer than the cyclic prefix.

Appendix for Chapter 4

4.A Proofs

Proof 4.A.1 (of Property 4.1)

The property $i)$ can be proven by either a direct approach or by using Parseval's Theorem [OS98] as done in this proof. For a DFT input $x(\nu) = [1\ e^{2\pi\nu/N} \cdots e^{2\pi(N-1)\nu/N}]$, the output power is given by $\|D\mathbf{x}(\nu)\|^2 = N\sum I_k^2(\nu)$. On the other hand, $\|\mathbf{x}(\nu)\|^2 = N$. From Parseval's Theorem, or D being a unitary matrix, we have

$$N\sum_k |I_k(\nu)|^2 = N. \tag{4.29}$$

For the property $ii)$, we assume that N is power of 2. From $\sin(\pi + x) = -\sin(x)$, we have

$$\sum_k |I_k(\nu)|^4 = \frac{\sin^4(\pi\nu)}{N^4}\sum_{k=0}^{N-1}\frac{1}{\sin^4(\pi k/N + \pi\nu/N)}. \tag{4.30}$$

Since N is even, we can pair the elements of $\{k/N \mid k = 0, ..., N-1\}$ into $\{k/N,\ k/N + 1/2 \mid k = 0, ..., N/2-1\}$, which leads us to

$$\begin{aligned}\sum_k |I_k(\nu)|^4 &= \frac{\sin^4(\pi\nu)}{N^4}\sum_{k=0}^{N/2-1}\frac{1}{\sin^4(\pi k/N + \pi\nu/N)} + \frac{1}{\cos^4(\pi k/N + \pi\nu/N)}\\ &= \frac{\sin^4(\pi\nu)}{N^4}\sum_{k=0}^{N/2-1} 2^4\frac{1 - 2\sin^2(\pi k/N + \pi\nu/N)}{\sin^4(\pi k/N + \pi\nu/N)},\end{aligned}$$

where we used $\sin(\pi/2 + x) = \cos(x)$ and some other trigonometry identities. Successively repeating the above maneuver $\log_2 N$ times gives the final form

$$\sum_{k=0}^{N-1} |I_k(\nu)|^4 = \frac{\sin^4(\pi\nu)}{N^4}N^4\frac{1 - \frac{2}{3}(1 - (\frac{1}{4})^{\log_2 N})\sin^2(\pi\nu)}{\sin^4(\pi\nu)} \tag{4.31}$$

$$= 1 - \frac{2}{3}(1 - (\frac{1}{4})^{\log_2 N})\sin^2(\pi\nu). \tag{4.32}$$

■

Proof 4.A.2 (of Theorem 4.1)

Let $\bar{y}_n$ denote the signal part of y_n, i.e., $y_n = \bar{y}_n + w_n$. Since the source s_n and noise w are uncorrelated, for each subchannel we have

$$E\left\{|\bar{y}_n(\nu) + w_n|^4\right\} = E\left|\bar{y}_n\right|^4 + 2\kappa_w E\left|\bar{y}_n\right|^2 \sigma_w^2 + E\left\{w_n^4\right\}. \tag{4.33}$$

From the i.i.d. property of the source, we have

$$E\left|\bar{y}_n(\nu)\right|^2 = \sum_k \left|H_{(k-n)}\right|^2 \left|I_k(\nu)\right|^2, \tag{4.34}$$

$$E\left|\bar{y}_n(\nu)\right|^4 = \kappa_s \sum_k \left|\Lambda_{(k-n)}\right|^4 \left|I_k(\nu)\right|^4 + \kappa_w \sum_{k\neq m} \left|H_{(k-n)}\right|^2 \left|H_{(m-n)}\right|^2 \left|I_k(\nu)\right|^2 \left|I_m(\nu)\right|^2, \tag{4.35}$$

where the subscript $(k-n)$ denotes $k-n \mod N$. The cost function can now be written as

$$\sum_n E\left\{|\bar{y}_n(\nu) + w_n|^4\right\} = \sum_n E\left\{|\bar{y}_n|^4\right\} + \sigma_w^2 \sum_n E\left\{|\bar{y}_n(\nu)|^2\right\} + N\kappa_w\sigma_w^2. \tag{4.36}$$

Notice that

$$\sum_n E\left\{|\bar{y}_n(\nu)|^2\right\} = \sum_k |H_k| \sum_k |I_k(\nu)|^2 = \|H\|^2, \tag{4.37}$$

which proves part $i)$ and

$$\begin{aligned}
\sum_n E\left|\bar{y}_n(\nu)\right|^4 &= \kappa_s \sum_k |H_k|^4 \sum_k |I_k(\nu)|^4 + \kappa_w \sum_{k\neq m} |H_k|^2 |H_m|^2 \sum_{k\neq m} |I_k(\nu)|^2 |I_m(\nu)|^2 \\
&= \left(\kappa_s \sum_k |H_k|^4 - \kappa_w \sum_{k\neq m} |H_k|^2 |H_m|^2\right) \sum_k I(k)^4 + \kappa_w \sum_{k\neq m} |H_k|^2 |H_m|^2 \\
&= \|H\|^4 \left((\kappa_s + \kappa_w)\kappa_H - \kappa_w\right) \sum_k |I_k(\nu)|^4 + \kappa_w \sum_{k\neq m} |H_k|^2 |H_m|^2 \\
&= \|H\|^4 \left((\kappa_s + \kappa_w)\kappa_H - \kappa_w\right) \sum_k I_k(\nu)^4 + \kappa_w \|H\|^4 (1-\kappa_H),
\end{aligned} \tag{4.38}$$

where, we have used the relation

$$1 = \left(\sum_k |I_k(\nu)|^2 \right)^2 = \sum_k |I_k(\nu)|^4 + \sum_{k \neq m} |I_k(\nu)|^2 \, |I_m(\nu)|^2 \tag{4.39}$$

Combining (4.38) and Property 4.1-*ii*) proves part *ii*). ■

Proof 4.A.3 (of Property 4.2)

Let D_N denote the N-point DFT and $\mathbf{y} = D_N[c_0 \cdots c_{K-1} \ 0 \cdots 0]^T$ for a length K vector $\mathbf{x}$ ($N = MK$). Without loss of generality, we assume $\|\mathbf{c}\| = 1$ and hence $\|\mathbf{y}\| = 1$. Recall that the DFT matrix is given by

$$D_N[l, m] = \frac{1}{\sqrt{N}} W^{(l-1)(m-1)}, \tag{4.40}$$

where $W = e^{j2\pi/N}$ [OS98]. By exploiting the structure of D_N, we have

$$[y_m, \ y_{m+M}, \cdots, y_{m+(K-1)M}]^T = \frac{1}{\sqrt{M}} D_K F_{W^m} \mathbf{c}, \text{ for } m = 0, ..., M-1, \tag{4.41}$$

where F_{W^m} is a diagonal matrix given by $F[k, k] = W^{km}$. Since the maximum kurtosis of $D_K F_{W^m} \mathbf{c}$ is 1 when $\mathbf{c} = 1/\sqrt{K}[1, \ W^m, \cdots, W^{(K-1)m}]^H$ and $\|D_K F_{W^m} \mathbf{c}\|^4 = \|\mathbf{c}\|^4 = 1$, we have $\|D_K F_{W^m} \mathbf{x}\|_4^4 \leq 1$ and consequently

$$\sum_{k=0}^{K-1} |y_{m+kM}|^4 \leq \frac{1}{M^2}. \tag{4.42}$$

Therefore, from $\|\mathbf{y}\| = 1$ we have

$$\kappa_{\mathbf{y}} = \sum_{n=0}^{N-1} |y_n|^4 = \sum_{m=0}^{M-1} \sum_{k=0}^{K-1} |y_{m+kM}|^4 \leq \frac{M}{M^2} = \frac{1}{M}. \tag{4.43}$$

■

Chapter 5

Characterization and Adaptive Equalization of FSK Signals under Multipath Distortion

Conventionally, multipath channel characterization and equalization are considered mostly for linear modulation schemes where equalization has been modelled as a linear deconvolution problem. In this chapter, we characterize the non-linear distortion of frequency-shift keying (FSK) signals due to a multipath channel as a linear time varying channel. The dynamic range of time variation of this time-varying channel model is small for a mild multipath channel and large for a severe multipath channel. This characterization justifies the use of a decision directed adaptive linear equalizer for FSK signals after frequency demodulation in order to mitigate the distortion due to a multipath channel.

5.1 Introduction

Modern digital communication systems utilize various DSP techniques in order to enhance receiver performance. Digital filtering for channel equalization is perhaps the most successful example, where an adaptive filter mitigates inter symbol interference of linearly modulated signals such as QAM. For linearly modulated signals the distortion due to a multipath channel is well modelled by a time invariant linear filter. Hence, equalization is basically achieved by deconvolution of the baud spaced or fractionally spaced sampled received signal [TXK94]. However, for non-linear modulation schemes such as FSK the multipath distortion cannot be modelled as a time invariant linear filter, and a simple linear equalization scheme for this distortion is considered not feasible.

In this chapter, we show that adaptive linear filtering can be justified as an effective means of mitigating the multipath distortion of FSK signals by modelling this non-linear distortion as a time varying linear channel in the absence of channel noise. The coefficients of this time varying channel model are contributed by the magnitude of the multipath channel coefficients (time invariant quantity) and phase terms of the multipath channel and FSK signals (time variant quantity). Thus, the time span of this time-varying channel model is the same as the time span of the multipath channel on FSK signals, and the dynamic range of the time variation depends on the severity of the multipath channel. Decision-directed LMS (DD-LMS) can be applied in order to equalize the short-term time average channel of a modestly time varying channel model.

For a more severe multipath channel additional blind adaptive equalization such as via CMA [TA83] can be applied directly on the pre-demodulated FSK signal in order to reduce the severity of the multipath channel, as done experimentally in

[RH98].

5.2 Multipath Distortion in FSK system

5.2.1 Review of a FSK system

We consider a continuous phase FSK (CPFSK) scheme [Pro95]. The discrete PAM sequence $\{s_n\}$ is converted to a continuous time signal $v(t)$ by a pulse shaping filter $g(t)$ with baud interval T

$$v(t) = \sum s_n g(t - nT). \tag{5.1}$$

Then $v(t)$ is integrated and frequency modulated

$$\psi(t) := \int_{-\infty}^{t} v(\tau) d\tau \tag{5.2}$$

$$u(t) := e^{-j2\pi[j\beta\psi(t)+j\zeta_0]}, \tag{5.3}$$

where β is a constant called the modulation index. Without loss of generality, we assume $\beta = 1$ and the phase offset $\zeta_0 = 0$ henceforth. Assuming a linear channel $\mathbf{c}$ and an absence of channel noise, the received signal is represented as

$$r(t) = \mathbf{c}(t) \star \mathbf{u}(t), \tag{5.4}$$

where $\star$ denotes convolution. Suppose that the multipath delays of $\mathbf{c}(t)$ are integer multiples of a constant t_0, i.e.

$$\mathbf{c}(t) = \sum_{i=0}^{i=N_c} \rho_i e^{j\phi_i} \delta(t - it_0), \tag{5.5}$$

where ρ_i and ϕ_i denote the magnitude and phase respectively.

In the receiver, the received signal $r(t)$ is demodulated by extracting an estimate of $\psi(t)$ as the phase of $r(t)$ and differentiating

$$\hat{\psi}(t) = \angle r(t), \tag{5.6}$$

$$\hat{v}(t) = \frac{d}{dt}\hat{\psi}(t). \tag{5.7}$$

Finally, the output of the receiver is given by

$$\hat{s}_n = \hat{v}(t)|_{t=nT}. \tag{5.8}$$

5.2.2 Time Varying Filtering Model of Multipath Distortion

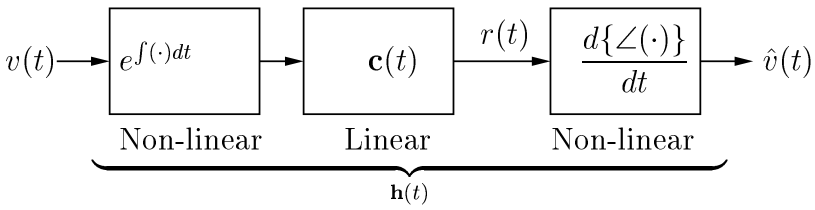

Figure 5.1: Block Diagram

Figure 5.1 illustrates the block diagram of the FSK system described in the previous section. Now we establish a mathematical model h(t) for the effect of the multipath channel $\mathbf{c}(t)$ on the relation between the pulse shaped source signal $v(t)$ in (5.1) and the demodulated received signal $\hat{v}(t)$ in (5.7). From

$$r(t) = \sum_{i=0}^{N_c} \rho_i e^{j(\psi(t-it_0)+\phi_i)}, \tag{5.9}$$

define

$$r_X(t) := \sum \rho_i \cos(\psi(t-it_0)+\phi_i), \tag{5.10}$$

$$r_Y(t) := \sum \rho_i \sin(\psi(t-it_0)+\phi_i). \tag{5.11}$$

Then from (5.6)

$$\hat{\psi}(t) = \tan^{-1}\left(\frac{r_Y(t)}{r_X(t)}\right), \tag{5.12}$$

and from (5.7)

$$\begin{aligned}
\hat{v}(t) &= \frac{d}{dt}\tan^{-1}\left(\frac{r_Y(t)}{r_X(t)}\right) && (5.13)\\
&= \frac{1}{1+\frac{r_Y(t)^2}{r_X(t)^2}}\left(\frac{\dot{r}_Y(t)}{r_X(t)} - \frac{r_Y(t)}{r_X(t)^2}\dot{r}_X(t)\right) && (5.14)\\
&= \frac{1}{\|r(t)\|^2}\left(r_X(t)\dot{r}_Y(t) - r_Y(t)\dot{r}_X(t)\right), && (5.15)
\end{aligned}$$

where $\dot{r}_X(t)$ and $\dot{r}_X(t)$ are time derivatives of r_X and r_Y respectively, i.e.

$$\begin{aligned}
\dot{r}_X(t) &= -\sum \rho_i \sin(\psi(t-it_0)+\phi_i)v(t-it_0), && (5.16)\\
\dot{r}_Y(t) &= \sum \rho_i \cos(\psi(t-it_0)+\phi_i)v(t-it_0). && (5.17)
\end{aligned}$$

Define a discrete time varying linear filter $\mathrm{h}(t)$ via its components

$$\begin{aligned}
\mathrm{h}(t)_i \;:=\; & \frac{\rho_i}{|r(t)|^2}[r_X(t)\cos(\psi(t-it_0)+\phi_i)\\
& +r_Y(t)\sin(\psi(t-it_0)+\phi_i)]. && (5.18)
\end{aligned}$$

Then, $\hat{v}(t)$ can be expressed as

$$\hat{v}(t) = \mathrm{h}^T(t)\cdot\mathbf{v}(t), \tag{5.19}$$

where $\mathbf{v}(t)$ is a vector drawn from $v(t)$ defined as

$$\mathbf{v}(t) = [v(t)\cdots v(t-it_0)\cdots v(t-iN_c)]. \tag{5.20}$$

When $\hat{v}(t)$ is sampled at $T_s = t_0$, (5.19) reveals a linear time-varying channel model of the FSK distortion between $\{\hat{v}(t)|_{t=kt_0}\}$ and $\{v(t)|_{t=kt_0}\}$ via $\mathrm{h}(t)$.

5.2.3 Properties of time-varying channel model

Now we have a time varying linear model for the multipath distortion of frequency modulation schemes. Here, we examine two properties of $\mathrm{h}(t)$, which help to characterize the distortion of FSK signals due to a multipath channel.

Property 5.1

i) $\sum \mathrm{h}(t)_i = 1$ as long as $|r(t)| \neq 0$. Thus, $\mathrm{h}(t) \neq 0$, unless $\mathbf{c}(t) = 0$.

ii) Denote

$$\varphi_{ik}(t) := \psi(t - it_0) - \psi(t - kt_0) + \phi_i - \phi_k, \tag{5.21}$$

then $\mathrm{h}(t)$ can be compactly described by $\{\rho_i\}$, the magnitude coefficients of the channel, and the phase terms $\{\ \cos(\varphi_{ik}(t))\ \}_{i,k=1,\ldots,N_c}$, i.e.,

$$\begin{aligned} \mathrm{h}(t)_i &= \frac{\rho_i}{|r(t)|^2} \sum_k \rho_k \cos(\varphi_{ik}(t)) && (5.22) \\ &= \rho_i \frac{\sum_k \rho_k \cos(\varphi_{ik}(t))}{\sum_i \sum_k \rho_i \rho_k \cos(\varphi_{ik}(t))}. && (5.23) \end{aligned}$$

Proof: The proof of i) follows from using (5.10) and (5.11) in (5.18) to reveal

$$\begin{aligned} \sum_i \mathrm{h}(t)_i &= \frac{1}{|r(t)|^2} \Big(r_X(t) \sum \rho_i \cos(\psi(t - it_0) + \phi_i) \\ &\qquad + r_Y(t) \sum_i \rho_i \sin(\psi(t - it_0) + \phi_i) \Big) \\ &= \frac{1}{|r(t)|^2} [r_X(t) r_X(t) + r_Y(t) r_Y(t)] = 1. && (5.24) \end{aligned}$$

as long as $|r(t)| \neq 0$. Since $\sum \mathrm{h}_i(t) = 0$ is a necessary condition for $\mathrm{h}(t) = 0$, $\mathrm{h}(t) \neq 0$ unless $\mathbf{c}(t) = 0$. The proof of ii) follows from trigonometric identities. ∎

Although $\sum \mathrm{h}_i(t) = 1$, it is possible that individual $|\mathrm{h}_i(t)| \to \infty$ when $\|r(t)\| \to 0$ via destructive interference. However, such destructive interference rarely occurs for non-fading channels. Therefore, we assume $\|r(t)\|^2 > 0$ and $\mathrm{h}_i(t)$ are reasonably bounded values.

Since $\mathrm{h}(t)$ is a function of $\{\cos(\varphi_{ik}(t))\}$, the time variation of $\mathrm{h}(t)$ is determined by the time variation of $\{\cos(\varphi_{ik}(t))\}$ and their contribution to $\mathrm{h}(t)$ through $\{\rho_i\rho_k\}$. On the other hand, we have

$$\varphi_{ik}(t) = \int_{\tau=t-it_0}^{\tau=t-kt_0} v(\tau)d\tau + \phi_i - \phi_k. \tag{5.25}$$

Since $v(\tau)$ is generated by an i.i.d. source sequence $\{s_n\}$, $\cos(\varphi_{ik}(t))$ is also observed to behave like a random source independent from t_0 when $t_0 > T$ (recall that T is the baud interval). Thus, the main factor which determines time variation of $\mathrm{h}(t)$ is the scale factor $\rho_i\rho_k$ in the contribution of the random factor $\cos(\varphi_{ik}(t))$ to $\mathrm{h}(t)$.

Property 5.2 Let us consider channels satisfying a condition that the amplitude of one tap, denote its index as i_c, dominates that of all other taps. Explicitly, the products of any two other taps $\{\rho_l\rho_m\}_{i_c\neq l,m}$ are considered ignorable in comparison with the main tap ρ_{i_c} so that

$$(\rho_{i_c} - \sum_{k\neq i_c}\rho_k)^2 \approx \sum_k \rho_k^2 - \sum_{k\neq l}\rho_k\rho_l. \tag{5.26}$$

For such channels the dynamic range of $\mathrm{h}(t)$ is large for a severe multipath channel and small for a mild multipath channel.

Proof: Applying the following bound

$$\begin{aligned}\sum_k \rho_k^2 - \sum_{k\neq l}\rho_k\rho_l &\leq \sum_i\sum_k \rho_i\rho_k\cos(\varphi_{ik}(t)) \\ &\leq \sum_k \rho_k^2 + \sum_{k\neq l}\rho_k\rho_l, \end{aligned} \tag{5.27}$$

and the following approximation justified by the assumption that $\{\rho_l\rho_m\}_{i_c\neq l,m}$ are ignorable in comparison with the main tap ρ_{i_c}

$$\sum_k \rho_k^2 - \sum_{k\neq l} \rho_k\rho_l \approx (\rho_{i_c} - \sum_{k\neq i_c} \rho_k)^2 \tag{5.28}$$

to (5.22) yields

$$\frac{\rho_{i_c}^2 - \rho_{i_c}\sum_{k\neq i_c}\rho_k}{(\rho_{i_c}+\sum_{k\neq i_c}\rho_k)^2} \leq \mathrm{h}(t)_{i_c} \leq \frac{\rho_{i_c}^2 + \rho_{i_c}\sum_{k\neq i_c}\rho_k}{(\rho_{i_c}-\sum_{k\neq i_c}\rho_k)^2}. \tag{5.29}$$

From (5.29), we can observe that as a channel becomes severe ($\rho_{i_c} - \sum_{k\neq i_c}\rho_k \to 0$), the upperbound of $\mathrm{h}(t)_i$ dramatically increases. ■

As illustrated in property 5.2, our use of the label of multipath severity implies that the magnitude of secondary path gains approach that of the largest.

5.2.4 Example: Two tap channel case

Consider a two-tap multipath channel $\mathbf{c}$ described by

$$\mathbf{c}(t) = \delta(t) + \rho e^{j\phi}\delta(t-t_0). \tag{5.30}$$

From (5.3)-(5.4), as in (5.9),

$$\alpha_0 = 1 + \rho\cos(\varphi(t)), \tag{5.31}$$

$$\alpha_1 = \rho^2 + \rho\cos(\varphi(t)), \tag{5.32}$$

$$\|r(t)\|^2 = 1 + 2\rho\cos(\varphi(t)) + \rho^2, \tag{5.33}$$

and

$$\mathrm{h}(t) = [\frac{1+\rho\cos(\varphi(t))}{1+2\rho\cos(\varphi(t))+\rho^2}\ \frac{\rho^2+\rho\cos(\varphi(t))}{1+2\rho\cos(\varphi(t))+\rho^2}]. \tag{5.34}$$

Relating (5.30) to (5.5), $\rho_0 = 1$, $\phi_0 = 0$, $\rho_1 = 1$, and $\phi_1 = \phi$, such that from (5.21)

$$\varphi(t) = \psi(t) - \psi(t-t_0) - \phi. \tag{5.35}$$

Notice that a destructive interference occurs when the two taps have the same magnitude with opposite phase ($\rho = 1$ and $\varphi = \pi$), such that $|\mathrm{h}_0| \to \infty$ and $|\mathrm{h}_1| \to \infty$. This simple two tap channel model yields a tighter bound on $h_0(t)$ than (5.29) (Recall that $\mathrm{h}_1 = 1 - \mathrm{h}_0$)

$$\frac{1}{1+\rho} \leq \mathrm{h}_0(t) \leq \frac{1}{1-\rho}. \tag{5.36}$$

Again as ρ approaches 1, the range of $\mathrm{h}_0(t)$ expands dramatically. Assuming that $\mathrm{h}_0(t)$ varies uniformly, the mean value of $\mathrm{h}_0(t)$ is

$$E\left\{\mathrm{h}_0(t)\right\} = \frac{2}{1-\rho^2}. \tag{5.37}$$

In Figure 5.2, we compare the time variation of h_0 for a severe multipath ($\rho = 0.5$) and a mild multipath ($\rho = 0.2$) when $\phi = 0$, which confirms the following theoretical prediction

$$\begin{aligned} &0.67 \leq \mathrm{h}_0 \leq 2 && \text{for } \rho = 0.5, \\ &0.83 \leq \mathrm{h}_0 \leq 1.25 && \text{for } \rho = 0.2. \end{aligned} \tag{5.38}$$

5.3 Equalization

Now we consider equalization of FSK signals based on the channel modelling developed in the preceding section.

5.3.1 Blind Adaptive Post-D and Pre-D filter

Figure 5.3 and Figure 5.4 illustrate blind adaptive equalization schemes for CPFSK presented in [RH98]. Figure 5.3 shows a equalizer using DD-LMS, which is referred to as a post-D filter. Notice that as a result of the time-varying channel model

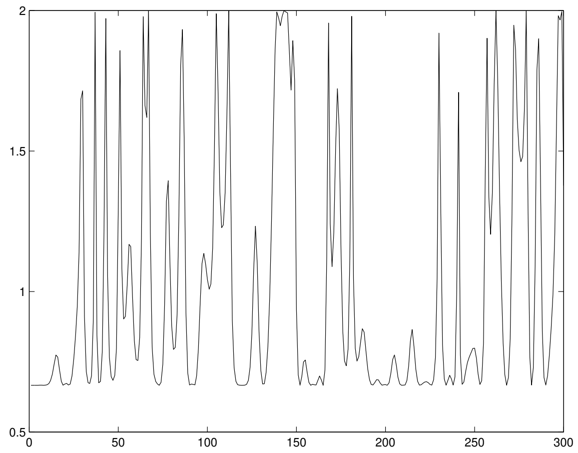

a) Severe Case $\rho = 0.5$

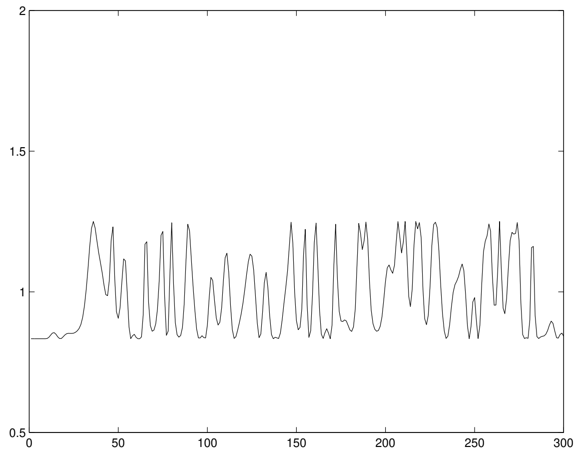

b) Mild Case $\rho = 0.2$

Figure 5.2: Time variation of h_0

(5.19) the length of the post-D filter permitting perfect equalization is the same as that of a conventional T/2 linear equalizer for a linear channel [JSE+98].

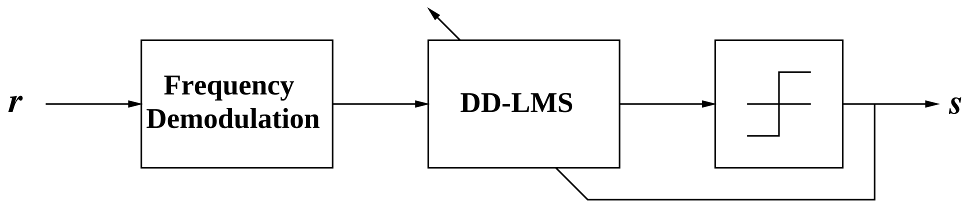

Figure 5.3: Post-D filter

For severe multipath channels, in order to deal with fast time variation of h(t), CMA equalization can be applied to the received FM signal before demodulation (which is referred to as a pre-D filtering). However, CMA requires an i.i.d. source for successful equalization [JSE+98], while the transmitter output FSK signal, $\{u(t)|_{t=nT_S}\}$, is not an i.i.d. source in general (since it is generated through an integration operator). Nonetheless, we can reasonably well approximate the FM transmitter output $\{u(t)|_{t=nT_S}\}$ as an i.i.d. source for a reasonable modulation index β used in practice [Pro95]. Although the pre-D CMA filter may not achieve perfect equalization for the FSK signal, it can mitigate enough multipath distortion so that a post-D DD-LMS algorithm can equalize h(t).

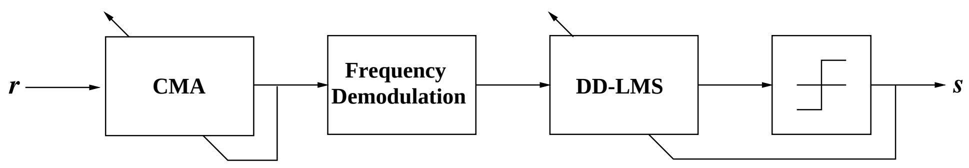

Figure 5.4: Pre-D filter & Post-D filter

5.3.2 Simulation Results

We now examine the performance of DD-LMS for the two tap channel model considered in section 2.3. Channels A and B are two tap channels with the delay $t_0 = 2T$ ($T_s = T/2$, where T is baud interval) and $\rho = 0.2$ and $\rho = 0.5$ respectively. We used raised cosine pulse shaping for 2-level FSK. In the absence of noise, the variance of recovery error due to multipath distortion is -19dB and -14dB respectively. Figure 5.5 illustrates the performance gain of the T/2 post-D DD-LMS filter of length 10 in the presence of noise (SNR 4-20 dB) with the step size $\mu = 0.001$. For more realistic simulation results refer to [RH98], [CMRJ00].

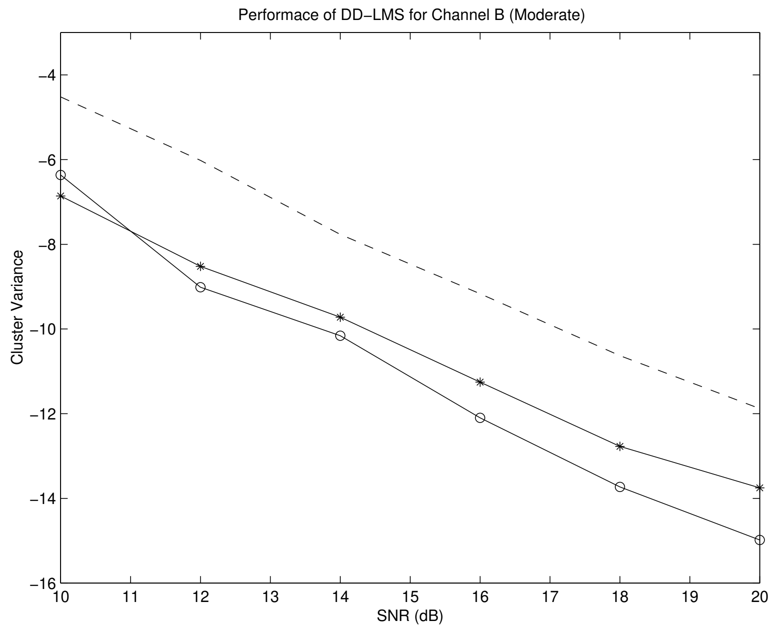

A) For $\rho = 0.2$ (moderate)

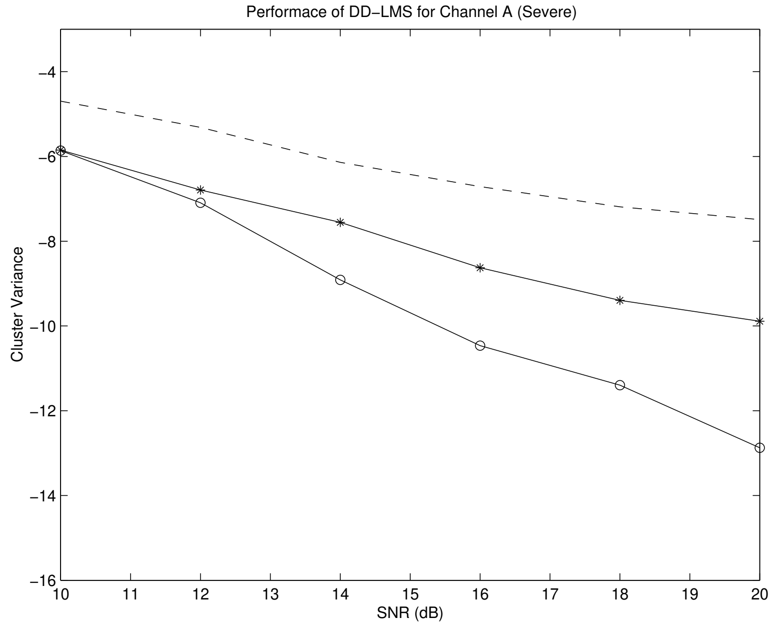

B) For $\rho = 0.5$ (severe)

Dotted line : Without Adaptation

Solid line with * : stepsize=1×10^{-3}

Solid line with o : stepsize=2×10^{-2}

Figure 5.5: Performance of Post-D DD-LMS

Chapter 6

Concluding Remarks

6.1 Summary

We have addressed issues of blind parameter estimation for data acquisition in digital communication systems. Blind adaptive estimation of synchronization parameters based on dispersion minimization was considered from chapter two to chapter five and blind adaptive equalization methods were studied for a particular non-linear modulation scheme in chapter six.

In chapter two, we considered blind timing phase offset recovery for a single carrier system. The timing offset recovery problem was formulated as a channel optimization problem with respect to the output MSE in the presence of a finite length equalizer. In order to achieve the goal blindly, we took a dispersion minimization approach as an approximation of the MMSE approach. A geometrical interpretation of estimating DM-timing offset provided intuition on the MSE performance trade-off of DM-timing. More detailed, but somewhat heuristic, analysis was carried out to quantify the MSE performance of DM-timing for the single sensor case. We classified two types of channels: clustered and sparse. For the clustered channels, the deviation of DM-timing from MMSE-timing is relatively small regardless of the severity of the multipath, which implies that DM-timing may exhibit near MMSE performance. On the other hand, for the sparse channels, deviation is related to the severity of the multipath; the more severe the multipath is, the poorer the MSE performance. For the single sensor case, we derived conditions under which the DM-timing algorithm produces a unique DM-solution.

In chapter three, we presented an analysis of the performance and behavior of a blind adaptive carrier phase offset recovery scheme based on dispersion minimization, named here the DM-derotator. The stationary points of the DM-derotator for a variety of source signals including digital VSB and QAM were classified. VSB signals, or in general, sources with different statistics for the real and the imaginary components, were shown to have undesirable local minima. Initialization, or re-initialization, strategies were discussed for VSB signals. The analysis was extended to a variety of situations which reflect possible impairments in a realistic system; including (*i*) its behavior in the presence of Inter Symbol Interference, (*ii*) its behavior when there are statistical dependencies between the in-phase and quadrature components, and (*iii*) its tracking ability.

In chapter four, we developed a blind carrier frequency offset correction scheme for OFDM systems. Although the algorithm is based on fourth order statistics of the OFDM output, we showed that it can be viewed as a dispersion minimization approach for OFDM systems. It was shown that this algorithm overcomes a major drawback in most existing blind carrier frequency offset recovery algorithms: channel dependency. A condition for an OFDM system under which this algorithm converges to the correct frequency offset was derived, and the condition was seen to be met by virtually all practical systems.

In chapter five, the non-linear nature of the effect of multipath on a non-linear modulation scheme, CPFSK, was characterized and its mitigation method considered. The nonlinear distortion was modelled as a time varying filtering, the dynamic range of which depends on the severity of the multipath channel; the more severe the multipath channel, the wider the range of variation. A blind adaptive method, DD-LMS, was applied in examples to estimate the averaged value of the variation, and mitigate the distortion.

6.2 Future Direction

In this dissertation, we have applied existing adaptive blind estimation techniques for well defined synchronization parameters. We have covered the most important synchronization parameters considered essential in current receiver architectures. However, for future receiver architectures, it is possible that proper recovery from RF impairments will emerge as an important signal processing task for the synchronization stage along with the synchronization parameters we have considered here.

Modelling a RF impairment, such as Inphase-Quadrature mismatch, joint Inphase-Quadrature timing offset optimization, phase noise, or non-linear distortion due to power amplifier, as a manageable estimation problem, and finding robust and efficient solutions is likely to be an important task for design of the next generation receivers. In this case, the adaptive blind approach based on dispersion minimization considered in this thesis would be a strong candidate to resolving such RF impairment problems. Research in this direction promises significant practical contributions to future receiver design.

Bibliography

[Abi95] A. A. Abidi. Direct-conversion radio transceivers for digital communications. *IEEE Trans. Solid-State Circuits*, December 1995.

[Abi99] A. A. Abidi. Cmos wireless transceivers: the new wave. *IEEE Comm. Magazine*, pages 119–124, August 1999.

[Ari92] S. Ariyavisitakul. A decision feedback equalizer with time-reversal structure. *IEEE J. Sel. Areas Communication*, pages 599–613, April 1992.

[AS72] M. Abramowitz and C. A. Stegun. *Handbook of Mathematical Functions with Formulas, Graphs, and Mathematical Tables, 9th printing.* Dover, 1972.

[B01] B. Bölcskei. Blind estimation of symbol timing and carrier frequency offset in wireless OFDM systems. *IEEE Trans. Communication*, 49(6):988–998, June 2001.

[BGR80] A. Benveniste, M. Goursat, and G. Ruget. Robust identification of a nonminimum phase system: Blind adjustment of a linear equalizer in data communications. *IEEE Trans. Automatic Control*, pages 385–399, June 1980.

[BPG02] S. Barbarossa, M. Pompili, and G. B. Giannakis. Channel-independent synchronization of orthogonal frequency division multiple access systems. *IEEE J. Sel. Areas Communication*, pages 474–486, February 2002.

[Car98] J. Cardoso. Blind signal separation: statistical principles. *Proc. IEEE*, pages 2009–2025, October 1998.

[CBSJ01] W. Chung, J. Balakrishnan, W. Sethares, and C. R. Johnson, Jr. Timing recovery based on dispersion minimization. *Proceedings of the 2001 Conference on Information Sciences and Systems*, March 2001.

[CJ02] W. Chung and C.R. Johnson, Jr. Blind carrier frequency offset estimation for ofdm systems based on higher order statistics. *Conference on Information Sciences and System*, March 2002.

[CJR02] W. Chung, C.R. Johnson, Jr., and M. J. Ready. Characterization of multipath distortion of fsk signals. *IEEE Signal Processing Lett.*, pages 26–29, January 2002.

[CMRJ00] W. Chung, R. K. Martin, M. Ready, and C.R. Johnson, Jr. Blind adaptive equalizer for fsk systems based on a characterization of multipath on the fsk signals. *Conference on Information Sciences and System*, March 2000.

[Com00] Advanced Television Systems Committee. ATSC Digital Television Standard (Doc. A/53). Technical report, (www.tsc.org), March 2000.

[CSJ00] W. Chung, W. A. Sethares, and C. R. Johnson, Jr. Blind adaptive phase offset correction. *IEEE GLOBECOM 2000*, November 2000.

[CVC01] Y. Choi, P. J. Voltz, and F. A. Cassara. ML Estimation of carrier frequency offset for multicarrier signals in rayleigh fading channels. *IEEE Trans. Vehicular Technology*, pages 644–655, March 2001.

[DA95] F. Daffara and O. Adami. A new frequency detector for orthogonal multicarrier transmission techniques. *Proc. IEEE Vehicular Technology Conf.*, pages 804–809, 1995.

[Dav94] P.J. Davis. *Circulant Matrices.* Chelsea Publishing, 1994.

[DC93] F. Daffara and A. Chouly. Maximum likelihood frequency detectors for orthogonal multicarrier systems. *Proc. ICC'93*, pages 766–771, June 1993.

[Don81] D.L. Donoho. On minimum entropy deconvolution. *Applied Time Series Analysis II*, pages 565–608, 1981.

[ECHS00] T.J. Endres, R.A. Casas, S.N. Hulyalkar, and C.H. Strolle. On sparse equalization using mean-square-error and constant modulus criteria. *Conference on Information Science and System*, March 2000.

[Fra80] L.E. Franks. Carrier and bit synchronization in data communication - A tutorial review. *IEEE Trans. Communication*, August 1980.

[GLS96] F. Guglielmi, C. Luschi, and A. Spalvieri. Joint clock recovery and baseband combining for the diversity radio channel. *IEEE Trans. Communication*, pages 114–117, January 1996.

[God78] D. N. Godard. Passband timing recovery in all-digital modem receiver. *IEEE Trans. Communication*, 26, May 1978.

[God80] D. N. Godard. Self-recovering equalization and carrier tracking in a two-dimensional data communication system. *IEEE Trans. Communication*, pages 1867–1875, 1980.

[GT99] M. Gu and L. Tong. Geometrical characterization of constant modulus receivers. *IEEE Trans. Signal Processing*, October 1999.

[GW81] R. D. Giltin and S. B. Weinstein. Fractionally spaced equalization: an improved digital transversal equalizer. *Bell Syst. Tech. J.*, pages 301–321, 1981.

[Hay94] S. Haykin. *Blind Deconvolution.* Prentice Hall, 1994.

[HT01] H. Holma and A. Toskala. *WCDMA for UMTS.* John Wiley & Sons Inc., 2001.

[Jol61] L.B.W. Jolley. *Summation of Series.* Dover Publications, 1961.

[JSE+98] C. R. Johnson, Jr., P. Schniter, T. J. Endres, J. D. Behm, D. R. Brown, and R. A. Casas. Blind equalization using the constant modulus criterion: A review. *Proc. IEEE*, 86:1927–1950, October 1998.

[Kay93] S.M. Kay. *Fundamentals of Statistical Signal Processing.* Prentice Hall, 1993.

[Kob71] H. Kobayashi. Simultaneous adaptive estimation and decision algorithm for carrier-modulated data transmission systems. *IEEE Trans. Communication*, pages 268–280, June 1971.

[Kun97] S.Y. Kung. Independent component analysis in hybrid mixture: KuicNet learning algorithms and numerical analysis. *Proc. Intl. Symposium on Multimedia Information Processing*, December 1997.

[LLG01] J. Li, G. Liu, and G.B. Giannakis. Carrier frequency offset estimation for OFDM-based WLANs. *IEEE Signal Processing Lett.*, pages 80–82, March 2001.

[LR96] M. Luise and R. Reggianini. Carrier frequency acquisition and tracking for OFDM systems. *IEEE Trans. Communication*, 44, March 1996.

[LSM97] U. Lambrette, M. Speth, and H. Meyr. OFDM robust frequency synchronization by single carrier training data. *IEEE Commun. Lett.*, pages 46–48, March 1997.

[Luc65] R.W Lucky. Automatic equalization for digital communications. *Bell Syst. Tech. J.*, pages 547–588, 1965.

[Lyo75] D. L Lyon. Timing recovery in synchronous equalized data communication. *IEEE Trans. Communication*, pages 269–274, February 1975.

[Mac98] O. Macchi. *Adaptive Processing.* John Wiley & Sons Inc., 1998.

[Maz75] J.E. Mazo. Optimum timing phase for an infinite equalizer. *Bell Syst. Tech. J.*, pages 189–201, January 1975.

[MD97] U. Mengali and A. N. D'Andrea. *Synchronization Techniques for Digital Receivers.* Plenum Press, 1997.

[MD01] M. Morelli and A. N. D'Andrea. Feedback frequency synchronization for OFDM applications. *IEEE Commun. Lett.*, 5(1):28–30, January 2001.

[MM76] K.H. Mueller and M Muller. Timing recovery in digital synchronous data receivers. *IEEE Trans. Communication*, May 1976.

[MMF98] H. Meyr, M. Marc, and S. A. Fechtel. *Digtial Communication Receivers.* John Wiley & Sons Inc., 1998.

[Moo94] P. Moose. A technique for orthogonal frequency division multiplexing frequency offset correction. *IEEE Trans. Communication*, pages 2908–2914, October 1994.

[OS98] A. V. Oppenheim and R. W. Shafer. *Discrete-Time Signal Processing.* Prentice Hall, 1998.

[PBM95] T. Pollet, M. Bladel, and M. Moeneclaey. BER sensitivity of OFDM systems to carrier frequency offset and wiener phase noise. *IEEE Trans. Communication*, 43:191–193, February 1995.

[Poo98] H. V. Poor. *An Introduction to Signal Detection and Estimation.* Springer, 1998.

[PP97] A. Paulraj and C. Papadias. Space Time Processing for Wireless Communications. *IEEE Singal Processing Magazine*, 46(5):49–83, November 1997.

[PP99] T. Pollet and M. Peeters. Synchronization with DMT modulation. *IEEE Communications Magazine*, 37(4):80–86, April 1999.

[Pro95] J. Proakis. *Digital Communications.* McGraw-Hill, 1995.

[RFT98] F. Rashid-Farrokhi and L. Tassiulas. Joint optimal power control and beamforming in wireless networks using antenna array. *IEEE Trans. on Communications*, 46(10):1313–1324, October 1998.

[RH98] M.J. Ready and J. Harp. Performance improvements achieved by equalizing intermediate rate fsk signals. *Asilomar Conference, Pacific Grove, CA*, pages 379–383, November 1998.

[Sal73] J Salz. Optimal mean-square decision feedback equalization. *Bell Syst. Tech. J.*, pages 1341–1373, October 1973.

[Sam70] P. A. Samuelson. *Economics.* McGraw Hill, 1970.

[SC97] T. Schmidl and D. Cox. Robust frequency and timing synchronization for OFDM. *IEEE Trans. Communication*, 45(12):1613–1621, December 1997.

[SCG91] J.J. Shynk, C.K. Chan, and R.P. Gooch. Comparative performance study of several blind equalization algorithms. *SPIE, San Diego, CA*, 1991.

[Sch95] W.F. Schreiber. Advanced television systems for terrestrial broadcasting: Some problems and proposed solutions. *Proc. IEEE*, pages 958–981, June 1995.

[Sha48] C. E. Shannon. A mathematical theory of communication. *Bell Syst. Tech. J.*, pages 379–423, July 1948.

[SJ00] P. Schniter and C. R. Johnson, Jr. Bounds for the MSE performance of constant modulus estimators. *TIT*, pages 2544–2560, November 2000.

[TA83] J. R. Treichler and B.G. Agee. A new approach to multipath correction of constant modulus signals. *IEEE Trans. Signal Processing*, April 1983.

[TCE+01] A. Touzni, R.A. Casas, T.J. Endres, C.H. Strolle, and S. Hulyalkar. Phase recovery based on minimization of single-axis constant modulus criterion: Performance analysis. *Conference on Information Sciences and System*, March 2001.

[TF88] G.B. Thomas and R. L Finney. *Calcuus and Analytic Geometry.* Addison Wesley, 1988.

[TJL01] J. R. Treichler, C. R. Johnson, Jr., and M. G. Larimore. *Theory and Design of Adaptive Filters.* Prentice Hall, 2001.

[TLZ00] U. Tureli, H. Liu, and M. Zoltowski. OFDM blind carrier offset estimation: ESPRIT. *IEEE Trans. Communication*, 48:1459–1461, September 2000.

[TSC98] V. Tarokh, N Seshadri, and N.R. Calderbank. Space-time codes for high data rate wireless communication: performance criterion and code construction. *IEEE Trans. Information Theory*, pages 744–765, March 1998.

[TXK94] L. Tong, G. Xu, and T. Kaliath. Blind channel identification and equalization using second-order statistics: A time-domain approach. *IEEE Trans. Information Theory*, 40:340–349, March 1994.

[VdBSB97] J.J. Van de Beek, M. Sandell, and P.O. Borjesson. ML estimation of time and frequency offset in OFDM systems. *IEEE Trans. Communication*, pages 1800–1805, July 1997.

[Ver86] S. Verdu. Minimum probability of error for asynchronous gaussian multiple-access channels. *IEEE Trans. Information Theory*, pages 85–96, January 1986.

[Wid70] B. Widrow. *"Adaptive filters," in Aspects of Network and System Theory.* Rinehart and Winston, 1970.

[ZTJ98] H. Zeng, L. Tong, and C.R. Johnson, Jr. Relationships between CMA and wiener receivers. *IEEE Trans. Information Theory*, pages 1523–1538, July 1998.